CLOSED/SEMI-CLOSED FORM SOLUTIONS FOR FACE/CORE DEBONDS IN SANDWICH BEAMS

A Dissertation
Presented to
The Academic Faculty

By

Siddarth Niranjan Babu

In Partial Fulfillment
of the Requirements for the Degree
Doctor of Philosophy in the
School of Aerospace Engineering

Georgia Institute of Technology

May 2022

CLOSED/SEMI-CLOSED FORM SOLUTIONS FOR FACE/CORE DEBONDS IN SANDWICH BEAMS

Thesis committee:

Prof. George A. Kardomateas, Advisor
School of Aerospace Engineering
Georgia Institute of Technology

Dr. Claudio V. Di Leo
School of Aerospace Engineering
Georgia Institute of Technology

Dr. Julian J. Rimoli
School of Aerospace Engineering
Georgia Institute of Technology

Prof. David McDowell
School of Mechanical Engineering
Georgia Institute of Technology

Dr. Graeme J. Kennedy
School of Aerospace Engineering
Georgia Institute of Technology

Date approved: Apr 22, 2022

To my parents,

Niranjan Babu and Saraswathi

ACKNOWLEDGMENTS

First, I would like to express my sincere gratitude to my advisor Prof. George Kardomateas for his guidance, support and encouragement. His advice on both research and my career have been invaluable. His patience, motivation, and immense knowledge has helped in all the time of research and writing of this thesis. He has been a really positive influence on my career and personality.

I would like to thank my committee members Dr. David L. McDowell, Dr. Julian J. Rimoli, Dr. Graeme J. Kennedy and Dr. Claudio V. Di Leo for their help and valuable suggestions. Their courses and questions during Ph.D. qualifiers have helped me build a strong foundation to pursue my research.

Special thanks to Dr. Dewey H. Hodges for being a part of my thesis proposal committee. I am grateful for his support and valuable feedback. His courses and books were a great source to gain knowledge. I have also learnt a lot from him while working as a teaching assistant.

The financial support of the Office of Naval Research, the interest and encouragement of the Grant Monitor, Dr. Y.D.S Rajapakse, and the teaching assistanships provided by the School of Aerospace Engineering are gratefully acknowledged. In addition, I would also like to thank Dr. Mitchel Walker, Dr. Jechiel Jagoda, Dr. Stephen Ruffin and all administrative staff of School of Aerospace Engineering for their continued support during my time at Georgia Tech. I would also like to thank all AE faculty and staff their help and support.

I am thankful to my friends and colleagues who made this work possible. I would also like to thank Komahan Boopathy, Sivabalan Mani, Yuan Zhangxian and Ruthvik Chandrasekaran for their companionship over the years. The times spent with them on and off campus made my time at Georgia Tech fun and enjoyable.

Finally, I would like to thank my family for their unconditional love, encouragement and support. I am always thankful to them for all their sacrifices. They are always there to help me when I need them or when I'm going through tough times.

TABLE OF CONTENTS

Acknowledgments iv

List of Tables ix

List of Figures xi

Chapter 1: Introduction and Background 1

1.1 Motivation 1

1.2 Literature Review 3

1.2.1 Effects of Transverse Shear 5

1.2.2 Crack Face Contact 7

1.2.3 Crack Face Friction 9

1.3 Research Goals 10

Chapter 2: Elastic Foundation Analysis of Double Cantilever Beam 12

2.1 Using Timoshenko Beam Theory 15

2.1.1 Displacement Fields 15

2.1.2 Governing Equations 18

2.1.3 Boundary Conditions 26

2.2 Fracture Parameters 31

2.2.1 Energy Release Rate 31

2.2.2 Mode Partitioning 38

2.3 Results and Discussion 39

2.4 Conclusion 47

Chapter 3: Elastic Foundation Analysis of Single Cantilever Beam 48

3.1 Using Timoshenko Beam Theory 49

3.1.1 Displacement Field 49

3.2 Governing Equations 50

3.2.1 Bonded Section of the beam: $0 \leq x \leq l$ 51

3.2.2 Debonded Section of the beam: $-a \leq x \leq 0$ 55

3.3 Boundary Conditions 57

3.4 Energy Release Rate 61

3.4.1 J-Integral 61

3.4.2 Rate of Energy Released by the springs 63

3.5 Mode Partitioning 64

3.6 Results and Discussion 65

3.7 Conclusion 70

Chapter 4: Crack face contact model - Tensionless Foundation 71

4.1 Governing equations 72

4.1.1 Cracked section 73

4.1.2 Bonded section 77

4.2 Boundary and Continuity Conditions 80

4.3 Energy Release Rate 90
4.4 Mode Partitioning 96
4.5 Results and Discussion 98
4.6 Conclusion 102

Chapter 5: Crack face contact model - with Friction 103
5.1 Governing Equations 104
5.1.1 Cracked section 104
5.1.2 Bonded section 110
5.2 Boundary Conditions 112
5.3 Energy Release Rate 121
5.4 Mode Partitioning 124
5.5 Results and Discussion 124
5.6 Conclusion 126

Chapter 6: Conclusions and Future Work 127
6.1 Conclusions 127
6.2 Future Work 132

References 133

LIST OF TABLES

2.1 DCB: Energy Release Rates - Al face & Al foam core 41

2.2 DCB: Mode Partitioning Values - Al face & Al foam core 42

2.3 DCB: Energy Release Rates and Mode Partitioning for an Orthotropic core . 43

2.4 DCB: Energy Release Rates and Mode Partitioning - Small crack (a/L = 1%) 44

2.5 DCB: Energy Release Rates and Mode Partitioning - Small crack (a/L=4%) 45

2.6 DCB: Effect of Core Stiffness (a = 200mm) 45

3.1 SCB: Material Properties 65

3.2 SCB: Energy release rate and mode partitioning - Al Face & Al Foam Core 67

3.3 SCB: Energy release rate and mode partitioning - Al Face & H100 Core . . 67

3.4 SCB: Effect of Core Stiffness for V_d=0.5 Nt, M_d=0. Debond length a=200mm 68

3.5 SCB: Effect of Core Stiffness for V_d=0.5 Nt, M_d=100Nmm. Debond length a=200mm 68

3.6 SCB: Results for a smaller debond length, a=20mm. Aluminium Foam (7 GPa) Core 69

3.7 SCB: Results for a smaller debond length, a=20mm. H100 (0.13 GPa) Core 69

4.1 ENF: Energy Release Rate Values - Al Foam Core 99

4.2 ENF: Energy Release Rate Values - Soft Core 100

5.1 ENF friction: Energy Release Rate Values - Al Foam Core 124

LIST OF FIGURES

2.1 Sandwich beam 12

2.2 Sandwich Beam Cross Section 13

2.3 Sandwich section geometry and applied loading configuration 14

2.4 Timoshenko Beam Theory assumption: Transverse shear strain = $\frac{dw}{dx} - \phi$ . . 15

2.5 Elastic Foundation in the Bonded Section of the beam 19

2.6 Double Cantilever Beam specimen with external moments and shear loads . 27

2.7 J-Integral Path 32

3.1 Single Cantilever Beam Specimen 48

3.2 Support Reaction on the substrate 51

3.3 Shear distribution in the Substrate: Bonded section SCB 52

3.4 Shear distribution in the Substrate: Debonded section SCB 56

3.5 J-Integral path - SCB specimen 61

3.6 FEA Mesh - SCB Beam 65

4.1 End-Notched Flexure Specimen 72

4.2 Tensionless Foundation in ENF Specimen 73

4.3 Coordinate System in the ENF specimen 74

4.4 Zero-area path for J-Integral Calculation - ENF 90

4.5 ENF sandwich specimen with pre-meshed crack 99

5.1 Tensionless Foundation with crack face friction in ENF Specimen 103

5.2 Beam Element in the Debonded Face - Region I 105

5.3 Beam Element in the Substrate - Region I 106

5.4 Zero-area path for J-Integral Calculation - ENF 122

SUMMARY

The Elastic Foundation Analysis (EFA) is one of the approaches that could be used to analyze a face/core debond in a closed form. It can be used to model the effects of the core and bottom face on the top face in sandwich composites. A sandwich beam is considered with an elastic foundation introduced in the bonded section of the beam between the top face sheet and the substrate (core and the bottom face). Sandwich beams also have an issue unique, it has large transverse shear due to presence of weak core and to capture it, the governing equations of the beam for both the debonded section and the bonded section are derived based on the Timoshenko beam theory. The elastic foundation includes both the normal and the shear springs to account for the transverse displacements and section rotations of the beam sections. The model is comprehensive and includes both the deformation of the debonded part and the substrate.

In the elastic foundation approach, the closed form expressions for the modulus of the normal and rotational shear springs derived based on elasticity theory are used. It is shown that the model is applicable for both isotropic and orthotropic face and core materials.

Double Cantilever Beam (DCB) specimen with external shear loads and bending moments is chosen and the appropriate conditions are used to obtain the constant coefficients in general solutions from the governing equations. Closed form expressions for energy release rates are obtained using J-Integral approach. Another measure for the energy release rate in the context of the elastic foundation model is the energy stored in this differential spring element, which would be released by the differential crack propagation. Mode partitioning measure based on the physical meaning of the springs in the elastic foundation approach, which makes use of the axial and transverse displacements near the crack tip. The model presented provides closed form solutions that are quick and reliable.

In the Single Cantilever Beam (SCB) specimen with external shear loads on the debonded top face, the substrate part is restricted in the transverse displacement. The transverse shear

in the substrate is significant and to capture it, a linearly distributed shear reaction is considered on the fixed bottom edge of the SCB specimen. The elastic foundation approach is modified to restrict the transverse displacement of the substrate and capture the transverse shear. The governing equations are solved using the boundary and continuity conditions of the SCB specimen. Closed form expressions for the energy release rates and mode partitioning are obtained using similar approach to DCB specimen.

In the case of Mode-II fracture, the effects of crack face contact are usually neglected in most models presented in the literature. The elastic foundation model is extended here by introducing a tensionless spring foundation in the cracked region. A novel approach to include tensionless springs to capture the compressive stresses across the interface between the debonded face sheet and the substrate is used. Crack faces will have contact zones and the length of the contact region also needs to be solved. The End Notched Flexure (ENF) sandwich specimen is chosen to demonstrate Mode-II fracture and the governing equations are obtained using Euler-Bernoulli beam theory. Using appropriate boundary and continuity conditions, a system of non-linear equations are obtained. These are solved to find the solutions for the constant coefficients in the general solutions of the transverse displacement and the unknown length of crack face region. Further, the tensionless spring foundation model is extended further to also capture the effects friction in the crack face contact. The modified governing equations are obtained and are solved.

Expressions for energy release rates are obtained using J-Integral and J-Integral is modified to account for the energy lost due to the friction tractions.The solutions for mode partitioning are obtained using the axial and transverse displacements near crack tip. The model presented is simple and efficient and would not compromise the accuracy of the results when compared with finite element models or previous models(from literature).

CHAPTER 1
INTRODUCTION AND BACKGROUND

1.1 Motivation

Sandwich structures are used to obtain minimum weight with maximum specific stiffness in aerospace, marine, civil and wind turbine industries. A sandwich panel consists of two stiff metallic or composite thin face sheets separated by a low density thick core. Due to this configuration, sandwich structures usually have high bending stiffness and strength with little resultant weight penalty and high energy absorption capability. Face sheets need to be successfully bonded for the sandwich structures to have superior performance. Hence, the interface between the face and core is considered to be the weak link. Debonding may occur at the interface and such debonds can grow and eventually lead to complete failure of the structure. Generally, the main cause of failure is the lack of bonding or inadequate bonding, which will compromise the transfer of shear stress across the interface between face and core.

Fracture mechanics is the field of mechanics concerned with understanding and predicting failure. The energy release rate and the mode mixity of the face/core debonds are needed to assess the detrimental effects of the debonds. An issue unique to sandwich is the very large transverse shear due to its weak core. Due to complexities and possibilities of sandwich construction, energy release and mode mixity of interface debonds are mostly obtained using finite element analysis. Using finite element analysis to conduct damage tolerance and optimization design studies is difficult and time-consuming. There are higher order theories that can capture the effects of transverse shear and they are time consuming and difficult. Many FAA safety rules and inspection need simple closed form solution for sandwich beam. A simple analytical approach that can be used to obtain consistent results

for obtaining fracture parameters of the face/core debonds in sandwich composite beams would be really useful.

Therefore, there is a need for simple beam theory approach that can incorporate the effect of transverse shear. One such approach that could be used to analyse a face/core debonds and include effect of shear, is an elastic foundation approach with Timoshenko beam theory. Such that the elastic foundation incorporates both normal and rotational springs to capture the additional degree of freedom in Timoshenko beam theory. The elastic foundation approach should be comprehensive and unlike previous models, it should include the deformation of the substrate part. Closed form approach for obtaining energy release rate and mode mixity values are required, such they it gives consistent results.

Single Cantilever Beam (SCB) sandwich specimen are commonly used specimens for evaluating debond fracture toughness in mode I loading. In literature, previous models, even models based on the elastic foundation approach, ignored the transverse shear in the substrate and assumed it to be rigid. There is a need to extend the elastic foundation approach to capture the effect of transverse shear in substrate and obtain closed form expressions for the energy release rate and mode partitioning values.

Also the effects of contact in the debonded section are mostly neglected. But in Mode II/III fracture, it has been shown in literature that crack face contact is the reason for poor reproducibility of the values of mode II/III fracture toughness. In the contact region, there will be compressive stresses across the interface between the crack faces. The influence of contact in the debonded section is usually modeled using the finite element method. So, a quick and easy way to model contact and friction using simple beam theory and elastic foundation approach would be valuable to quickly and accurately estimate the values for energy release rate, mode mixity and contact region. By capturing all these effects, elastic foundation approach would provide an easy way to obtain simple and accurate results for face/core debonds in sandwich beams.

1.2 Literature Review

Sandwich structures have been well summarized and discussed in many books[1, 2, 3, 4]. Principal aspects of sandwich construction and assumptions on which it is based on is well defined in the book by Howard [1]. The book by Carlsson and Kardomateas [2] focuses on the structural behaviour and failure characteristics of sandwich materials and structures. In addition, it also covers the failure mechanisms and the associated fracture mechanics treatment.

Debonds in the sandwich beam are sensitive to compressive loading. These debonds are susceptible to buckling and subsequent rapid growth during the postbuckling phase. The problem is pertinent to design of such structures not only because this failure mode impairs the strength but also leads to substantial loss of stiffness. In sandwich structures, there is a large mismatch in elastic properties of the two faces and the core. Generally these structures are loaded in mixed mode (combined opening and shearing). And since fracture resistance depends on mode mixity and energy release rate, a reliable way for obtaining these values is needed. Experimental evaluation of fracture energy using sandwich specimens are presented in Ref.[5][6][7]. These experiments showed that the type of adhesive is important when failure occurs by interfacial crack propagation. Interfacial crack growth occured at the bondlayer/core interface which evidently is a critical zone. A Mixed Mode Beam (MMB) delamination test procedure was presented for a split unidirectional laminate by Reeders and Crews[8]. It was created by combining the mode I loading for the DCB test with that for the mode II ENF test. This approach provided delamination fracture toughness data over a wide range of G_I/G_{II} ratios using identical test specimens and procedures. Balaban and Tee[9] studied the effect of different variations in core densities and thicknesses on strain energy release rate(SERR) of the sandwich composite were evaluated experimentally, analytically and numerically.

In literature various models have been developed to study the debonding in beam struc-

tures. A simple analytical model based on potential energy of the system to predict stress intensity factors was developed by Zenkert[10]. Expressions for energy release rate are very useful and it was first derived by Yin and Wang[11] for a delaminated homogeneous composite. The expressions were then extended by Suo and Hutchinson[12] to a delaminated bimaterial. The sandwich configuration is, however, a trimaterial with two face sheets and a core in the middle. Closed form algebraic expressions for the energy-release rate and the mode mixity were obtained for a debonded sandwich by Kardomateas[13]. Similarly, fracture of a sandwich specimen loaded with axial forces and bending moments was analyzed by Ostergaard[14]. Saseendran et al.[15] further extended it for sandwich composite double-cantilever beam fracture specimen with the face sheets reinforced by stiff plates. Here, the expressions for the energy release rate and mode mixity phase angle for a reinforced double-cantilever beam loaded with uneven bending moments were derived using a superposition scheme and laminate beam theory. A laminated beam analysis was done by Carlsson et al.[16] to predict if the crack would propagate self-similarly, or if it would kink upwards or downwards although it cannot predict magnitude of the kink angle. The analysis could be used to design a DCB sandwich specimens to achieve a certain desired crack propagation path. Ratcliffe and Reeder[17] developed a procedure for sizing a single cantilever beam (SCB) that are used to characterize facesheet-core debonding in sandwich structure. The characterization is accomplished by measuring the critical strain energy release rate G_c. An analytical analysis based on LEFM to give energy release rates and mode mixity for both isotropic and orthopic materials were conducted in Ref.[18]. Crack root rotation is a measure of deviation from clamped boundary conditions of region in front of crack tip. The root rotation depends on the shear force and the bending moment acting at the crack tip. Such rotation significantly affects the compliance and energy-release rate[19]. In experiments[20, 21, 22], it has been shown that fracture energy can depend on the mode mixity. Hence, a complete analysis of the interface debonds require the determination of both the energy release rate and the mode mixity. In the all the discussed studies,

the effect of transverse shear deformation, crack face contact and crack face friction have all been neglected.

1.2.1 Effects of Transverse Shear

Studies have shown that the effects of shear provide additional terms to the general steady-state solutions and the shear component of the energy release rate contains a contribution from the interaction of the shear force with the compliance associated with the defromations at the crack tip [23, 24]. Various models have been developed to study and capture these effects. Morais and Pereiera [25] developed a modified beam theory and used it to predict the compliance and the total energy release rate G of glass/epoxy multidirectional specimens. Various layerwise theories were developed and used for bi-material beams. Interface cracks between two shear deformable elastic layers were studied [26, 27]. A method based on first-order shear deformable theory was developed to calculate the energy release rate and stress intensity factor for bi-layer structure. Deformation of crack tip was derived based on shear deformable bi-layer beam theory and the associated energy release rate was derived using J-Integral. Further, a novel interface deformable bi-layer beam theory accounting local effects at crack tip was developed by Qiao and Wang [28]. Two interface compliances were introduced to account for the effect of interface stress on the crack tip deformation, which can be referred to as elastic foundation effect.

Various numerical models have been developed to obtain energy release and compliance. In bimaterial crack problem, Li et al. [29] studied the effect of shear by a semi numerical approach. Similar semi-numerical approaches were used by Andrews [23] and Barbieri et al. [30] for homogeneous solid and symmetric sandwich specimen respectively. Sun and Pandey developed a model [31] based on an approximate 2-D elasticity solution, the flexibility of the joint of beam segments in cracked beam was explicitly derived. Numerical evaluation of energy release rate for various cracked specimens using modified beam model was done. These models have been shown to improve the accuracy of re-

sults for materials that have high stiffness value and are shown to be inaccurate when the materials are soft(low stiffness). Several models to model flexible core were developed to overcome this limitation. In 1992, Frostig et al. [32] proposed the High-Order Sandwich Panel Theory (HSAPT), in which the transverse compressibility and the shear effects of the core sheets are both included. It was then extended by including axial rigidity to obtain the Extended High-Order Sandwich Panel Theory (EHSAPT) by Phan et al. [33]. By comparison to the elasticity solution, the EHSAPT shows high accuracy in both displacement and stress distributions for a wide range of core materials. Odessa et al. [34, 35] formulated a unified nonlinear model with Extended High Order Sandwich Panel Theory (EHSAPT) for the analysis of the process of debonding between a face sheet and the core in sandwich panels. Mode-mixity is also an important parameter that is necessary to characterize face/core debonds. A different mode-mixity approach [36] based on extrapolation of crack flank displacement results of the Crack Surface Displacement Extrapolation (CSDE) method was presented for 2-D applications. It is a finite element based structural propagation model. It is able to simulate crack propagation in and out of a sandwich interface consisting of orthotropic bimaterials using fracture toughness distributions as input. A number of zigzag theories have been developed where the displacements have a piecewise variation through the thickness [37, 38]. Irularo et al.[38] modeled multilayered composite and sandwich plates as mixed cubic zigzag model. The in-plane displacements follow a piece-wise cubic distribution and the transverse displacement has a parabolic variation through thickness. These numerical models and approaches are difficult and time consuming. Hence, there is a need for simple analytical approach.

A simple beam theory approach that could be used to analyze a face/core debond, and include the effect of shear, is the elastic foundation approach. Elastic foundation analysis have been used for a long time to study crack propagation [39, 40, 41, 42, 39, 43]. It was used by Kanninen[39] to study the mid-thickness crack in double cantilever beam (DCB) specimen in a homogeneous material. Williams[40] extended it further by using

Timoshenko beam theory. Both used similar expressions for the stiffness of the elastic foundation. Li and Carlsson[42] analyzed the Tilted Sandwich Debond specimen using elastic foundation approach to predict its compliance. Elastic foundation analysis of force and moment - loaded single cantilever sandwich beam specimen was presented by Saseendran [44]. In these elastic foundation analyses, the substrate was assumed to be rigid and the effects of the end fixity at the bonded segment were not included. An important concern in elastic foundation analyses is the formula for the elastic foundation modulus. Kanninen [39] has used simple approximate formulas (accurate) for modulus. Kardomateas et al. [45] conducted a comprehensive study that resulted in a closed form expression for both the normal and shear spring stiffnesses. These formulas were derived based on both the elasticity solution and the extended high - order sandwich panel theory. A closed form expressions for the energy release rate and mode partitioning of face/core debonds in sandwich beams were obtained by Kardomateas et al.[43] using elastic foundation approach. Unlike earlier studies, it included the deformation of substrate part as well. It was then further extended and the closed form expressions for the case of Single Cantilever Beam(SCB) Specimen were obtained in Ref.[46]. But, these studies[43][46] used Euler-Bernoulli beam theory and were not able to capture the effects of transverse shear in sandwich beam.

1.2.2 Crack Face Contact

Initiation and growth of delamination is in many cases caused by interlaminar normal stress [47, 48, 49, 50]. However, interlaminar shear stresses may also cause delamination [51]. And to determine the interlaminar strength, End Notched Flexure(ENF) specimen is widely accepted. Experimental characterization of mode II fracture was done by Kageyama et al. [52]. Carlsson et al. [53] studied the ENF specimen and found that the interlaminar shear deformation may influence the evaluation of the interlaminar mode II fracture toughness. Corleto and Hogan [54] used simple modified beam theory analysis with elastic foundation to evaluate the mode II delamination fracture toughness. Thouless [24] developed ana-

lytical expressions for the energy-release rate and phase angle of ENF, End-Loaded Split (ELS) and 3-Point flexure specimens. It was derived based on steady-state energy balance and the effects of shear are added as an additional term to it. Lu et al. conducted a numerical study on a straight beam under transverse load and a curved beam under constant moment[55]. It uses orthotropic rescaling technique to solve the straight beam and thin beam theory to solve curved beam problem. A Cracked Sandwich Beam (CSB) specimen was presented as a candidate for shear fracture characterization of the bondline between facings and core in a sandwich[56]. A CSB specimen consists of a sandwich panel under three-point loading scheme. Experimental results of interfacial debonding with a global mode II loading scheme using CSB specimens[57]. Strain energy release rates of an CSB specimen were investigated using refined zigzag theory[58]. Comparisons of the refined zigzag theory solutions to first-order shear deformation theory(FSDT) and FEM solution were made.

Due to the bimaterial character of the face/core interface in a sandwich, the analysis of fracture must recognize the mixed mode loading and that the fracture toughness depends on the relative amount of Mode I and Mode II at the debond tip. The mixed mode bending (MMB) test has been used for measuring the mixed mode interlaminar fracture toughness of monolithic composite materials in Ref.[8, 59, 60]. Quispitupa[61] derived expressions for compliance and energy release rate for MMB using superposition analysis of solutions for the DCB and CSB specimens by applying a proper kinematic relationship for the specimen deformation combined with the loading. Mixed mode cyclic growth in foam core sandwich specimens have been examined using the MMB test priciple. A modified Paris-Erdogan law was found to represent the experimentally measured crack growth rate data in Ref.[62].

All these models neglect the interactions between crack faces and ignore the effects they have on the fracture parameters. This is part of the reason why there is poor reproducibility of the values of Mode II fracture toughness G_{IIC}.

Interaction between crack faces occur only when they are in contact and they are com-

pressive in nature. Tensile stresses cannot be transmitted across the interface between crack faces. The absence of tensile stresses in the cracked region is because the debonded face sheet lifts away from the substrate. Extending the elastic foundation to account for only compressive stresses can be done using Tensionless springs in the foundation. Weitsman [63] has worked on foundation that react in compression only. The model employed in the study involved only linear differential equations. And when a foundation is tensionless, the existence of gaps between the structure and the foundations introduces additional unknowns into the problem. It was further extended in several studies [64, 65] for beams resting on the tensionless foundation. Ma et al.[66] addressed the static response of infinite beam supported on a unilateral two-parameter Pasternak foundation and subjected to transverse loads. Using this approach, we can extend the Elastic foundation approach to capture the compressive stresses across the interface and can improve the accuracy of the results.

1.2.3 Crack Face Friction

Fracture surface interactions can significantly affect the energy release rates and stress intensity factors. Comninou and Dundurs [67] developed an analytical model for stick-slip behaviour of interface cracks. A numerical model called Boundary Element Method was used by Mantic et al. [68] to solve interface crack problems in composites including the effects of crack face contact. Davies et al. [69] showed that it is important to account for crack face contact when calculating Mode II fracture toughness. And that the main reason behind this, could be the effects of friction. Russel and Street [70] conducted a experimental loading-unloading cycling test and found that the error in G_{IIC} ignoring friction was around 2%. Further experiments conducted in Ref.[71, 72] concluded that friction accounted for about 2% to 5% of the measured values of G_{IIC} from their tests. A model estimating the magnitude of the frictional Mode II stress intensity factor was developed by Bian et al. [73]. Other models too predicted the reduction of Mode II stress intensity factors by fracture surface roughness [74, 75].

Cohesive Zone Modeling has been used to analyze fracture problems in composite materials. It is usually implemented in numerical methods and is used in investigation of fracture process in different material systems[76, 77, 78, 79, 80, 81, 82, 83, 84, 85, 86, 87]. Ouyang and Li[88] developed a Cohesive Zone Model (CZM) for the interface shear fracture of end notched flexure (ENF) specimen. Rabinovitch [89] developed a nonlinear analytical model that combines an extended high order multi-layer consideration of the strengthened beam with a cohesive interface modeling of its physical interfaces. Biel and Stigh[90] made a comparison of J-integral methods to experimentally determine cohesive laws in shear for adhesives. Further, a finite element model[91] with cohesive elements is used to determine the relationship between moment ratio and a stress based mode-mixity. It was found that almost any mode-mixity from pure Mode I to pure Mode II may be obtained by varying M1/M2. Other finite element models were presented to study the energy release rate of ENF specimen[92] [93, 94]. A finite element model based on virtual crack closure and compliance techniques was developed to calculate the strain energy release rate in Ref.[93]. Frictional effects were investigated by including the contact problem in the finite element model.

1.3 Research Goals

From the above discussions of the literature, these following things can be concluded:

- Most finite element tools and numerical approaches to obtains solutions for debonds in sandwich beam are mostly only applicable to isotropic material. For orthotropic materials, there is a need for extension of these tools.

- Closed form solutions have not been able to capture the transverse shear effects. Various assumptions are adopted in the literature for the elastic foundation analysis.

- There is poor reproducibility of Mode II fracture toughness values, this has been mainly attributed to contact effects. But, these contact effects are mostly neglected

in analytical approaches.

- Need a consistent and reliable analytical approach that can be used to quickly and accurately estimate the energy release rate and mode mixity values.

CHAPTER 2

ELASTIC FOUNDATION ANALYSIS OF DOUBLE CANTILEVER BEAM

Interface debonds are common cause for failure in sandwich structures. Due to the presence of a soft core, the effect of transverse shear is significant. In order to model the effects of the core & the bottom face on the top face in sandwich beams, the elastic foundation approach is used. The elastic foundation approach provides a way to obtain closed/near-closed form solution for debond problems in sandwich composite beams.

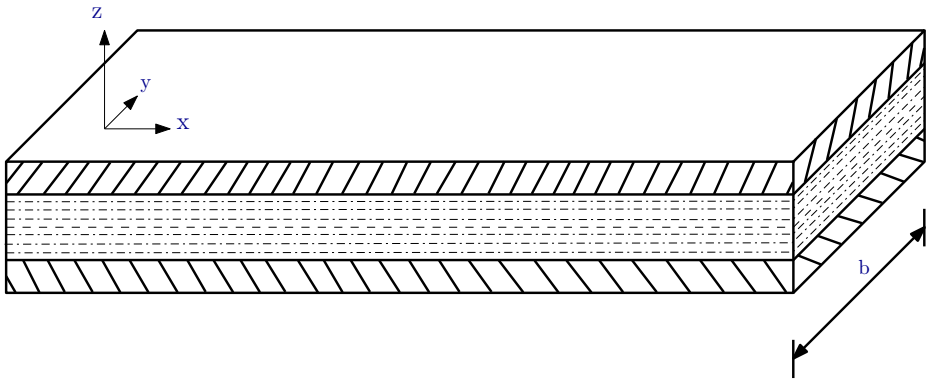

Figure 2.1: Sandwich beam

A tri-material sandwich beam consists of two face sheets bonded to a soft core as shown in Figure 2.1. The width of the beam is b. The top and bottom face sheets have thickness f_t & f_b, axial young's modulus E_{ft} & E_{fb} and shear modulus G_{ft} & G_{fb} respectively. The core is of thickness $2c$ with an axial young modulus of E_c and a shear modulus of G_c. The length of the cracked portion of the beam is a. As a plane problem, only the loading in x-z plane and the resulting displacements are considered.

The beam is broken down into different parts to conveniently represent them in the equations. The debonded top face sheet is denoted by "d", the substrate(core and the bottom face) part is denoted by "s" and the base(top, bottom face sheets and core) part is denoted by "b". It can be seen that only the Young's Modulus in axial direction (E_{11}) and Shear

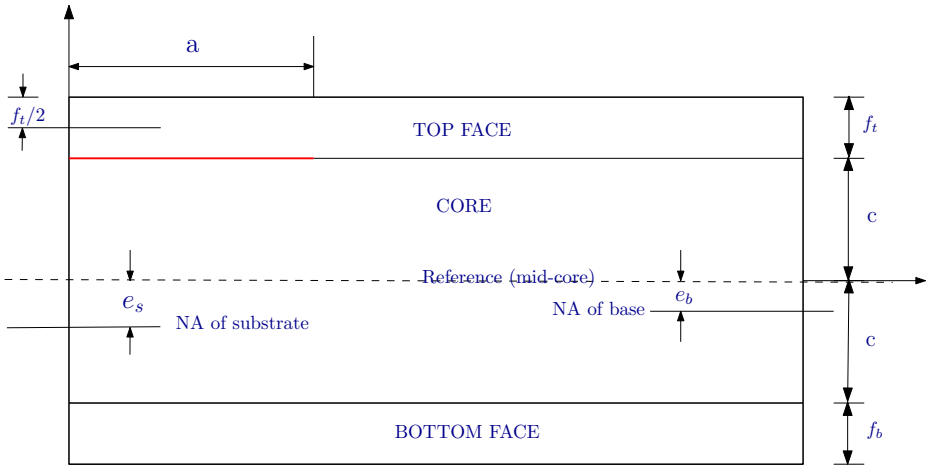

Figure 2.2: Sandwich Beam Cross Section

Modulus (G_{12}) appear in the beam theory formulation. Hence, this model can be used for either isotropic or orthotropic materials.

For a homogeneous beam, the neutral axis would be at the mid-thickness of the beam. Whereas, for the substrate part, the neutral axis is no longer at the geometrical mid-point of the section (Figure 2.2). With respect to a reference axis x through the middle of the core, the neutral axis of the substrate part is at a distance e_s.

$$e_s[E_c(2c) + E_{f_b} f_b] = E_{f_b} f_b(\frac{f_b}{2} + 2c) \tag{2.1}$$

and, the neutral axis of the base part is at a distance e_b

$$e_b[E_{f_t} f_t + E_c(2c) + E_{f_b} f_b] = E_{f_b} f_b\left(\frac{f_b}{2} + c\right) - E_{f_t} f_t\left(\frac{f_t}{2} + c\right) \tag{2.2}$$

The bending rigidity of the debonded face sheet is EI_d

$$(EI)_d = \frac{E_{f_t} b f_t^3}{12} \tag{2.3}$$

and the bending rigidity of the substrate is EI_s

$$(EI)_s = b\left[E_c\frac{2c^3}{3} + E_c(2c)e_s^2 + E_{f_b}\frac{f_b^3}{12} + E_{f_b}f_b\left(\frac{f_b}{2} + c - e_s\right)^2\right] \tag{2.4}$$

Similarly, the bending rigidity of base part is EI_b

$$\begin{aligned}(EI)_b \ = b\Bigg[&E_{f_t}\frac{f_t^3}{12} + E_{f_t}f_t\left(\frac{f_t}{2} + c + e_b\right)^2 + E_c\frac{2c^3}{3} + E_c(2c)e_b^2 \\ &+ E_{f_b}\frac{f_b^3}{12} + E_{f_b}f_b\left(\frac{f_b}{2} + c - e_b\right)^2\Bigg]\end{aligned} \tag{2.5}$$

The sandwich tri-material beam in Figure 2.3 has a debond of length a and an intact part of

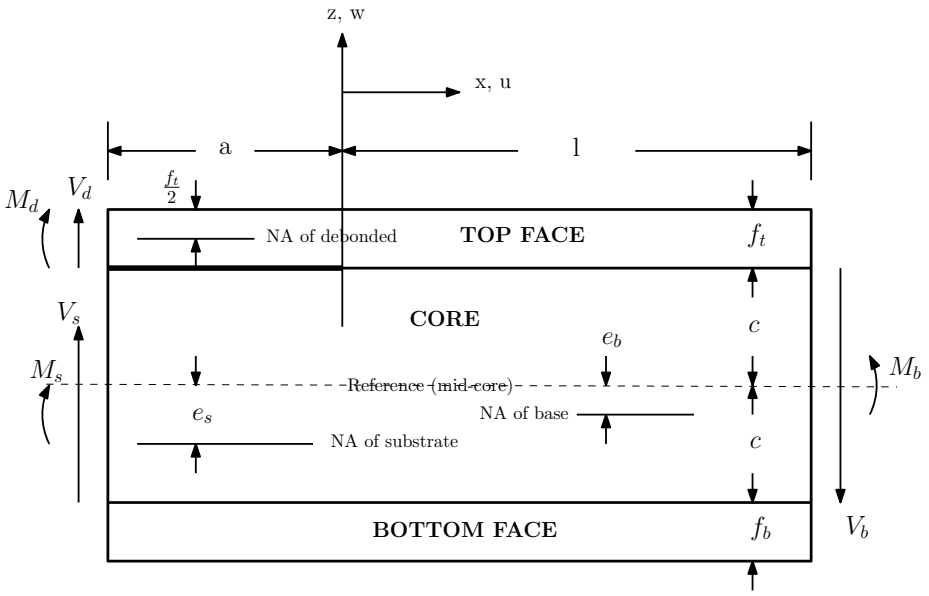

Figure 2.3: Sandwich section geometry and applied loading configuration

length l. The debonded part is loaded by a shear force V_d and a moment M_d; the substrate part is loaded by a shear force V_s and a moment M_s. The shear force and bending moment at the right end are V_b and M_b, respectively. Equilibrium of these forces and moments yields:

$$V_b = V_d + V_s; \qquad M_b = M_d + M_s + (V_d + V_s)(l + a) \tag{2.6}$$

It should be noted that the formulation and approach are applicable to both beams (plane stress) and wide panels (plane strain), but different moduli should be used for plane strain and plane stress problems. For plane strain, E should be replaced by E/(1-ν^2), where ν is Poisson's ratio. The coordinate system is set so that x = 0 is at the end if the debond, i.e., the debond is for negative x and the intact part for positive x (Fig. **??**). We denote by w, u, the transverse and axial displacements, respectively.

2.1 Using Timoshenko Beam Theory

2.1.1 Displacement Fields

The Timoshenko beam theory distinguishes between the angle of rotation of the beam cross-section, ϕ, and the slope of the neutral axis, dw/dx, as shown in Fig. Figure 2.4, which differ by the shear angle γ. The transverse displacement of the beam is 'w'. Hence, the displacement field is given by

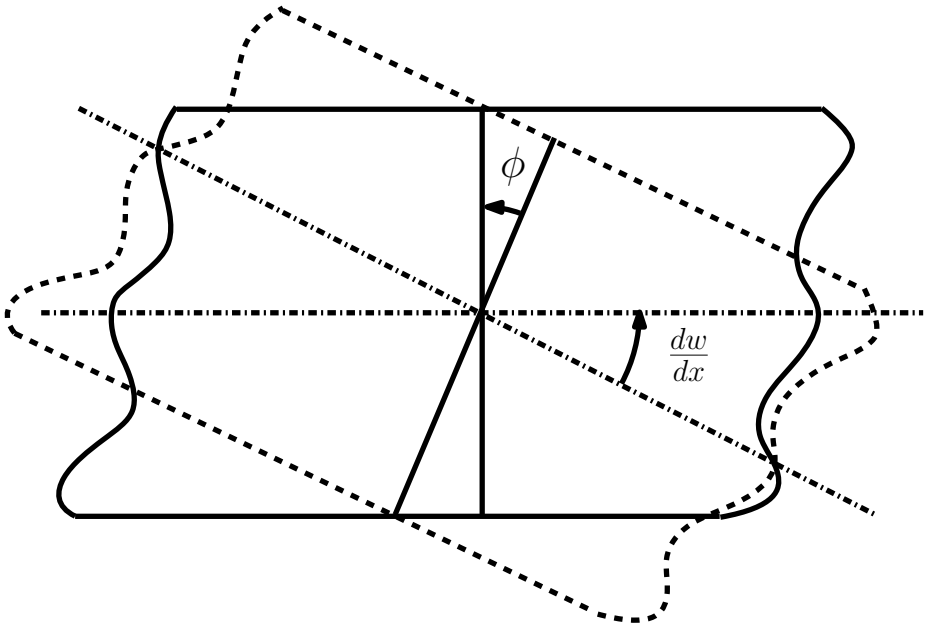

Figure 2.4: Timoshenko Beam Theory assumption: Transverse shear strain = $\frac{dw}{dx} - \phi$

$$u_x(x,z) = -z\phi; \tag{2.7}$$

$$u_z(x,z) = w \tag{2.8}$$

Strain Fields

Using the displacement field, the following relationship between the shear strain and the displacements is obtained:

$$\epsilon_{xx} = \frac{du_x}{dx} \tag{2.9}$$

$$\gamma_{xz} = \frac{du_x}{dz} + \frac{du_z}{dx} \tag{2.10}$$

Resulting in,

$$\epsilon_{xx} = -z\frac{d\phi}{dx} \tag{2.11}$$

$$\gamma_{xz} = \frac{dw}{dx} - \phi \tag{2.12}$$

Variational Formulation

From the principle of minimum potential, we know

$$\delta\pi = 0 \tag{2.13}$$

$$\delta(U+W) = 0 \tag{2.14}$$

Here, U is the strain energy and W is the work done. The first variation of the strain energy is given by

$$\delta U = \int_L \left[\left(\frac{dM}{dx} - V\right)\delta\phi - \frac{dV}{dx}\delta w\right]dx + [-M\delta\phi + V\delta w]_0^L \tag{2.15}$$

Assuming a distributed moment 'm' and a distributed transverse load 'q', we obtain the first variation of the external work as

$$\delta W = \int_L (m\delta\phi + q\delta w)dx \tag{2.16}$$

Using the above equation in the variation principle, we get the differential equations:

$$\frac{dM}{dx} - V + m = 0 \tag{2.17}$$

$$\frac{dV}{dx} - q = 0 \tag{2.18}$$

The beam has two portions along its length. There is an intact portion where beam is fully bonded and a debonded portion where there is a crack between the top face and the substrate. In the intact portion, an elastic foundation is assumed to be present between the top face and the substrate. Here, Timoshenko beam theory is used to better capture transverse shear effects. It introduces an additional degree of freedom and to capture it, we additionally use rotational shear springs in the elastic foundation as shown in Figure 2.5.

The elastic foundation load is a distributed load applied to both the debonded part and the substrate, creating a distributed load

$$q = -k_n w \qquad m = k_r \phi \tag{2.19}$$

Here, k_n is the stiffness of the normal springs and k_r is the stiffness of the rotational shear springs. It is important to have an accurate estimation of the elastic foundation stiffness values. In 2018, Kardomateas et. al[45] proposed solutions based on Extended High-Order Sandwich Panel theory which show very excellent agreement with the elasticity solutions. It also provided simple closed form expressions for normal and shear springs stiffness for the case of symmetric sandwich specimens. These stiffness expressions can be used for

both isotropic and orthotropic materials. Shear spring stiffness can be defined in two ways (k_s and k_r). One, using the displacements at the interface (k_s) and the other based on the section rotation of the beam (k_r). The simple stiffness expressions for the case of symmetric sandwich beams are:

$$k_n = b\frac{E_3^c}{c} \qquad k_s = b\frac{G_{13}^c}{c} \qquad k_r = bG_{13}^c\frac{f_t}{2} \tag{2.20}$$

In Timoshenko beam theory, the moment and shear are defined as

$$M = (EI)\frac{d\phi}{dx}; \qquad V = -(\kappa GA)\gamma; \qquad \gamma = \frac{dw}{dx} - \phi \tag{2.21}$$

For the debonded part and the substrate

$$M_d = (EI)_d\frac{d\phi_d}{dx}; \qquad V_d = -(\kappa GA)_d\gamma_d \tag{2.22}$$

$$M_s = (EI)_s\frac{d\phi_s}{dx}; \qquad V_s = -(\kappa GA)_s\gamma_d \tag{2.23}$$

2.1.2 Governing Equations

The governing equations of the sandwich beam with elastic foundation for the debonded part is,

$$-(EI)_d\frac{d^2\phi_d}{dx^2} - (\kappa GA)_d(\frac{dw_d}{dx} - \phi_d) + S(x)k_r(\phi_d - \phi_s) = 0 \tag{2.24}$$

$$(\kappa GA)_d(\frac{d^2w_d}{dx^2} - \frac{d\phi_d}{dx}) - S(x)k_e(w_d - w_s) = 0 \tag{2.25}$$

$$\tag{2.26}$$

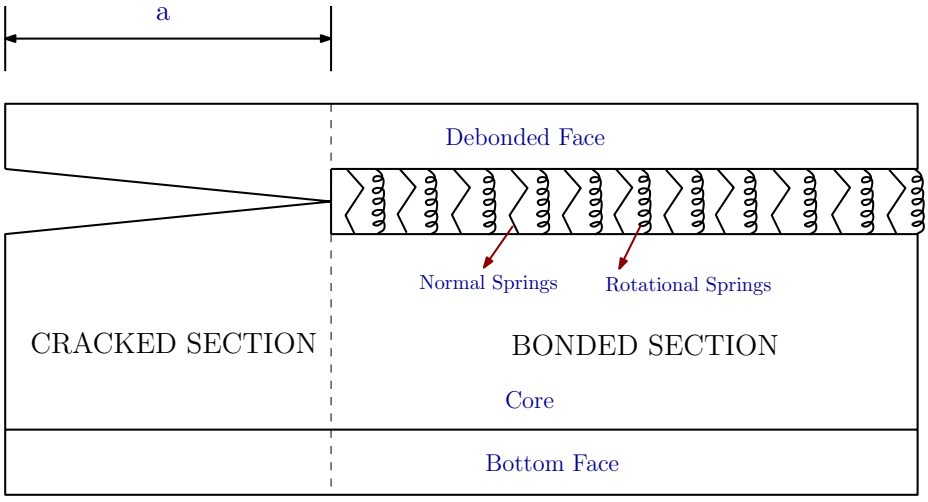

Figure 2.5: Elastic Foundation in the Bonded Section of the beam

and for the substrate,

$$-(EI)_s\frac{d^2\phi_s}{dx^2} - (\kappa GA)_s(\frac{dw_s}{dx} - \phi_s) + S(x)k_r(\phi_s - \phi_d) = 0 \tag{2.27}$$

$$(\kappa GA)_s(\frac{d^2w_s}{dx^2} - \frac{d\phi_s}{dx}) - S(x)k_e(w_s - w_d) = 0 \tag{2.28}$$

The governing equations of the beam are a homogeneous system of linear coupled 2^{nd} order differential equations. The function S(x) is a step function allowing to separate the portion of the beam where they are linked, x>0, and where they are not, x<0, i.e.,

$$S(x) = \begin{cases} 1 & \text{if x>0} \qquad \text{Bonded section} \\ 0 & \text{if x<0} \qquad \text{Cracked section} \end{cases} \tag{2.29}$$

Bonded section

In the bonded section, the governing equations are simplified to

$$w_d''''(x) - A[w_d''(x) - w_s''(x)] + B[w_d(x) - w_s(x)] = 0 \tag{2.30}$$

$$w_s''''(x) - C[w_s''(x) - w_d''(x)] + D[w_s(x) - w_d(x)] = 0 \tag{2.31}$$

where,

$$A = \left[\frac{k_n}{(\kappa GA)_d} + \frac{k_r}{(EI)_d}\right]; \qquad B = \left[\frac{k_n}{(EI)_d} + \frac{k_n k_r}{(EI)_d(\kappa GA)_d} + \frac{k_n k_r}{(EI)_d(\kappa GA)_s}\right]$$
$$C = \left[\frac{k_n}{(\kappa GA)_s} + \frac{k_r}{(EI)_s}\right]; \qquad D = \left[\frac{k_n}{(EI)_s} + \frac{k_n k_r}{(EI)_s(\kappa GA)_s} + \frac{k_n k_r}{(EI)_s(\kappa GA)_d}\right]$$

Here, the governing equations are fourth order coupled differential equations and are in terms of the transverse displacements of the debonded part and the substrate. These equations can be solved by taking the Laplace transform as shown next:

$$s^4 W_d(s) - As^2(W_d(s) - W_s(s)) + B(W_d(s) - W_s(s)) = 0 \tag{2.32}$$

$$s^4 W_s(s) - Cs^2(W_s(s) - W_d(s)) + D(W_s(x) - W_d(x)) = 0 \tag{2.33}$$

Solving Equation 2.32 we can obtain $W_s(s)$ in terms of $W_d(s)$,

$$W_s(s) = \frac{s^4 - As^2 + B}{B - As^2} W_d(s) \tag{2.34}$$

Using this relationship in Equation 2.33, we get

$$s^8 W_d(s) - (A + C)s^6 W_d(s) + (B + D)s^4 W_d(s) = 0 \tag{2.35}$$

Now taking inverse Laplace transform of the above equation results in,

$$w_d''''''''(x) - (A + C)w_d''''''(x) + (B + D)w_d''''(x) = 0 \tag{2.36}$$

This is an eighth-order linear homogeneous differential equation. Assuming a solution of

the form e^{rx}, results in the following equation:

$$r^8 - 2\lambda_1^2 r^6 + \lambda_2^4 r^4 = 0; \quad or \quad r^4(r^4 - 2\lambda_1^2 r^2 + \lambda_2^4) = 0 \tag{2.37}$$

Setting $\mu = r^2$, results in the quadratic equation

$$\mu^2 - 2\lambda_1^2 \mu + \lambda_2^4 = 0 \tag{2.38}$$

The discriminant of this quadratic equation is $\Delta = 4(\lambda_1^4 - \lambda_2^4)$ which means that there are three possibilities for the roots:

Case 1 : λ_1^2 - $\lambda_2^2 < 0$

When the discriminant is negative, the roots of the quadratic equation are complex conjugates as follows:

$$\mu_{1,2} = \lambda_1^2 + i\sqrt{\lambda_1^4 - \lambda_2^4} \tag{2.39}$$

This implies

$$r_{1,2,3,4} = \pm\sqrt{\lambda_1^2 \pm \sqrt{\lambda_1^4 - \lambda_2^4}} \qquad r_{5,6,7,8} = 0 \tag{2.40}$$

If we set

$$k_1 = real\left(\sqrt{\lambda_1^2 - \sqrt{\lambda_1^4 - \lambda_2^4}}\right) \;\; ; \;\; k_2 = im\left(\sqrt{\lambda_1^2 + \sqrt{\lambda_1^4 - \lambda_2^4}}\right) \tag{2.41}$$

then the general solutions for case 1 can be written as follows

$$\begin{aligned} w_d =& c_{1d}\cosh(k_1x)\cos(k_2x) + c_{2d}\sinh(k_1x)\cos(k_2x) + c_{3d}\cosh(k_1x)\sin(k_2x) \\ &+ c_{4d}\sinh(k_1x)\sin(k_2x) + c_{5d}x^3 + c_{6d}x^2 + c_{7d}x + c_{8d} \end{aligned} \tag{2.42}$$

$$\begin{aligned} w_s =& c_{1s}\cosh(k_1x)\cos(k_2x) + c_{2s}\sinh(k_1x)\cos(k_2x) + c_{3s}\cosh(k_1x)\sin(k_2x) \\ &+ c_{4s}\sinh(k_1x)\sin(k_2x) + c_{5s}x^3 + c_{6s}x^2 + c_{7s}x + c_{8s} \end{aligned} \tag{2.43}$$

Case 2 : λ_1^2 - λ_2^2 = *0*

When the discriminant is zero, the roots of the quadratic equation are real and equal as follows:

$$\mu_{1,2} = \lambda_1^2 \tag{2.44}$$

That implies

$$r_{1,2,3,4} = \pm\lambda_1 \; ; \qquad r_{5,6,7,8} = 0 \tag{2.45}$$

So, the solutions for this case 2 are as follows:

$$\begin{aligned} w_d =& c_{1d}x\cosh(k_1x) + c_{2d}x\sinh(k_1x) + c_{3d}\cosh(k_1x) + c_{4d}\sinh(k_1x) \\ &+ c_{5d}x^3 + c_{6d}x^2 + c_{7d}x + c_{8d} \end{aligned} \tag{2.46}$$

$$\begin{aligned} w_s =& c_{1s}x\cosh(k_1x) + c_{2s}x\sinh(k_1x) + c_{3s}\cosh(k_1x) + c_{4s}\sinh(k_1x) \\ &+ c_{5s}x^3 + c_{6s}x^2 + c_{7s}x + c_{8s} \end{aligned} \tag{2.47}$$

Case 3 : λ_1^2 - $\lambda_2^2 > 0$

When the discriminant is positive, the roots of the quadratic equation are real and dis-

tinct:

$$\mu_{1,2} = \lambda_1^2 \pm \sqrt{\lambda_1^4 - \lambda_2^4} \tag{2.48}$$

This implies:

$$r_{1,2,3,4} = \pm\sqrt{\lambda_1^2 \pm \sqrt{\lambda_1^4 - \lambda_2^4}}\,; \qquad r_{5,6,7,8} = 0 \tag{2.49}$$

The roots $r_{1,2,3,4}$ are real and distinct and the solution for the displacement field is as follows:

$$w_d = c_{1d}e^{r_1 x} + c_{2d}e^{r_2 x} + c_{3d}e^{r_3 x} + c_{4d}e^{r_4 x} + c_{5d}x^3 + c_{6d}x^2 + c_{7d}x + c_{8d} \tag{2.50}$$

$$w_s = c_{1s}e^{r_1 x} + c_{2s}e^{r_2 x} + c_{3s}e^{r_3 x} + c_{4s}e^{r_4 x} + c_{5s}x^3 + c_{6s}x^2 + c_{7s}x + c_{8s} \tag{2.51}$$

It is important to notice at this point that out of the three possible cases, the most useful case is the one where the discriminant is negative (Case 1). An extensive examination of material properties of most commonly used material combinations for sandwich composites (H100 core, Aluminum Foam, Aluminum Face and others) showed that and all these material combinations would lead to Case 1 with the displacement field given by eqns (8d) and (8e). Hence, we will be solving the debonded sandwich beam problem with the solutions (8d) and (8e) for the bonded section of the beam.

Solution for the Sandwich Beam in the Bonded section

For the bonded section of the beam, $0 \leq x \leq l$, substituting the displacement field Equation 2.42 into the differential equations Equation 2.24 to Equation 2.28 gives

$$Bw_s - Aw_s'' = w_d'''' - Aw_d'' + Bw_d \tag{2.52}$$

Using this relationship between w_d and w_s, we get

$$c_{1s} = F_1 c_{1d} + F_2 c_{4d}\ ; \qquad c_{2s} = F_1 c_{2d} + F_2 c_{3d} \tag{2.53}$$

$$c_{3s} = F_1 c_{3d} - F_2 c_{3d}\ ; \qquad c_{4s} = F_1 c_{4d} - F_2 c_{1d} \tag{2.54}$$

$$c_{is} = c_{id}\ ; \qquad i = 5, 6, 7, 8 \tag{2.55}$$

where,

$$F_1 = \frac{B^2 + A^2(k_1^2 + k_2^2)^2 + A(k_1^2 + k_2^2)^2(k_2^2 - k_1^2) + 2AB(k_2^2 - k_1^2) + B(k_1^4 - 6k_1^2k_2^2 + k_2^4)}{B^2 + 2AB(k_2^2 - k_1^2) + A^2(k_1^2 + k_2^2)^2} \tag{2.56}$$

$$F_2 = \frac{4Bk_1k_2(k_1^2 - k_2^2) - 2Ak_1k_2(k_1^2 + k_2^2)^2}{B^2 + 2AB(k_2^2 - k_1^2) + A^2(k_1^2 + k_2^2)^2} \tag{2.57}$$

The resulting substrate displacement is:

$$\begin{aligned} w_s =& (F_1 c_{1d} + F_2 c_{4d}) \cosh k_1 x \cos k_2 x + (F_1 c_{2d} + F_2 c_{3d}) \sinh k_1 x \cos k_2 x + \\ &+ (F_1 c_{3d} - F_2 c_{2d}) \cosh k_1 x \sin k_2 x + (F_1 c_{4d} - F_2 c_{1d}) \sinh k_1 x \sin k_2 x + \\ &+ c_{5d} x^3 + c_{6d} x^2 + c_{7d} x + c_{8d} \end{aligned} \tag{2.58}$$

The beam rotations ϕ_d and ϕ_s can be obtained using Equation 2.25 and Equation 2.28, which can be written as:

$$\frac{d\phi_d}{dx} = \frac{d^2 w_d}{dx^2} - \frac{k_n}{(\kappa GA)_d}(w_d - w_s)$$
$$\frac{d\phi_s}{dx} = \frac{d^2 w_s}{dx^2} - \frac{k_n}{(\kappa GA)_s}(w_s - w_d)$$

Substituting w_d and w_s in the above equation and then integrating, we get

$$\begin{aligned}\phi_d \;=\; & (M_1c_{2d}+M_2c_{3d})\cosh k_1x\cos k_2x+(M_1c_{1d}+M_2c_{4d})\sinh k_1x\cos k_2x+\\ & +(M_1c_{4d}-M_2c_{1d})\cosh k_1x\sin k_2x+(M_1c_{3d}-M_2c_{2d})\sinh k_1x\sin k_2x+\\ & +3c_{5d}x^2+2c_{6d}x+c_{\phi d} \qquad (2.59)\\ \phi_s \;=\; & (N_1c_{2d}+N_2c_{3d})\cosh k_1x\cos k_2x+(N_1c_{1d}+N_2c_{4d})\sinh k_1x\cos k_2x+\\ & +(N_1c_{4d}-N_2c_{1d})\cosh k_1x\sin k_2x+(N_1c_{3d}-N_2c_{2d})\sinh k_1x\sin k_2x+\\ & +3c_{5d}x^2+2c_{6d}x+c_{\phi_s} \qquad (2.60)\end{aligned}$$

where,

$$M_1 = \frac{F_2k_2k_n+k_1^3(\kappa GA)_d+k_1[(-1+F_1)k_n+k_2^2(\kappa GA)_d]}{(\kappa GA)_d(k_1^2+k_2^2)} \qquad (2.61)$$

$$M_2 = \frac{F_2k_1k_n+k_2[k_n-F_1k_n+(k_1^2+k_2^2)(\kappa GA)_d]}{(\kappa GA)_d(k_1^2+k_2^2)} \qquad (2.62)$$

$$N_1 = \frac{F_1k_1^3(\kappa GA)_s-F_2k_1^2k_2(\kappa GA)_s-F_2k_2[k_n+k_2^2(\kappa GA)_s]+k_1[k_n-F_1k_n+F_1k_2^2(\kappa GA)_s]}{(\kappa GA)_s(k_1^2+k_2^2)} \qquad (2.63)$$

$$N_2 = \frac{F_2k_1[-k_n+(k_1^2+k_2^2)(\kappa GA)_s]+k_2[(-1+F_1)k_n+F_1(k_1^2+k_2^2)(\kappa GA)_s]}{(\kappa GA)_s(k_1^2+k_2^2)} \qquad (2.64)$$

Debonded Section of the beam $-a \le x \le 0$

In the debonded section of the beam, there is no elastic foundation between the debonded face and the substrate. Hence, the governing equations are simplified to:

$$EI_d\phi_d'''+(\kappa GA)_d(w_d''-\phi_d')=0\;; \qquad (\kappa GA)_d(w_d''-\phi_d')=0 \qquad (2.65)$$

$$EI_s\phi_s'''+(\kappa GA)_s(w_s''-\phi_s')=0\;; \qquad (\kappa GA)_s(w_s''-\phi_s')=0 \qquad (2.66)$$

From the above equations

$$\phi_d''' = 0\ ; \qquad \phi_s''' = 0 \tag{2.67}$$

from which, we obtain the displacement field in the debonded section as follows:

$$w_d = e_{1d}x^3 + e_{2d}x^2 + e_{3d}x + e_{4d} \tag{2.68}$$

$$\phi_d = 3e_{1d}x^2 + 2e_{2d}x + e_{\phi_d} \tag{2.69}$$

$$w_s = e_{1s}x^3 + e_{2s}x^2 + e_{3s}x + e_{4s} \tag{2.70}$$

$$\phi_s = 3e_{1s}x^2 + 2e_{2s}x + e_{\phi_s} \tag{2.71}$$

It is important to note that in these solutions there are 20 coefficients, namely, the c_{id}, i = 1,2,..,8; and the c_{ϕ_j}, e_{ij}, $i = 1, 2, 3$, $j = d, s$. We need to solve for these unknown coefficients in order to determine the complete displacements and rotations of the beam sections.

2.1.3 Boundary Conditions

Double Cantilever Beam (DCB) specimen is widely used for measuring the fracture toughness in mode I,G_{Ic}, of composites. The specimen is under external bending moments and shear forces as shown in Figure 2.6.

At the crack tip, $x = 0$, the bending moments of the debonded face and the substrate can be obtained in terms of the external loads

$$M_d + V_d a = (EI)_d \phi_d'|_{x=0} = 2(EI)_d e_{2d} \tag{2.72}$$

$$M_s + V_s a = (EI)_s \phi_s'|_{x=0} = 2(EI)_s e_{2s} \tag{2.73}$$

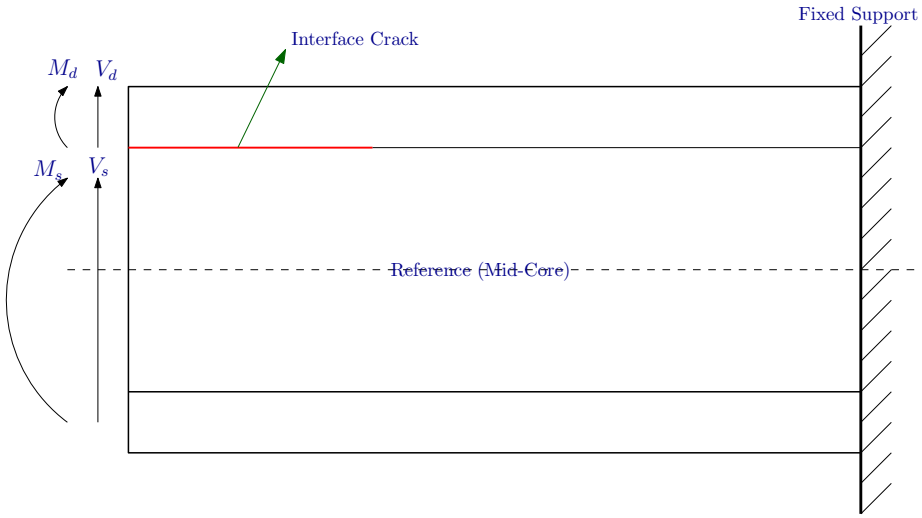

Figure 2.6: Double Cantilever Beam specimen with external moments and shear loads

which gives,

$$e_{2d} = \frac{M_d + V_d a}{2(EI)_d} \; ; \qquad e_{2s} = \frac{M_s + V_s a}{2(EI)_s} \tag{2.74}$$

Similarly, at the left end, x = -a, the bending moments of the debonded face and the substrate can be obtained in terms of the external loads

$$M_d = (EI)_d \phi_d'|_{x=-a} = (EI)_d(-6e_{1d}a + 2e_{2d}) \tag{2.75}$$

$$M_s = (EI)_s \phi_s'|_{x=-a} = (EI)_s(-6e_{1s}a + 2e_{2s}) \tag{2.76}$$

Using Equation 2.74 results in:

$$e_{1d} = \frac{V_d}{6(EI)_d} \; ; \qquad e_{1s} = \frac{V_s a}{6(EI)_s} \tag{2.77}$$

Also at the left end, $x = -a$, the shear forces on the debonded face and the substrate are

known from the applied external shear loads

$$V_d = -(\kappa GA)_d(w_d' - \phi_d)|_{-a} = -(\kappa GA)_d(e_{3d} - e_{\phi_d}) \tag{2.78}$$

$$V_s = -(\kappa GA)_s(w_s' - \phi_s)|_{-a} = -(\kappa GA)_s(e_{3s} - e_{\phi_s}) \tag{2.79}$$

In the polynomial part of the general solutions, it can be seen that the term c_{8d} produces no strain (since the strain in the Timoshenko beam theory is associated with the bending moment and shearing force, which in turn are expressed in terms of the first derivative of the displacement).

At the crack tip, $x = 0$, we also have continuity conditions across the debonded section and the bonded section of the beam *Displacement continuity*:

$$e_{4d} = c_{1d}\ ; \qquad e_{4s} = F_1 c_{1d} + F_2 c_{4d} \tag{2.80}$$

Beam rotation continuity:

$$e_{\phi_d} = M_1 c_{2d} + M_2 c_{3d} + c_{\phi d}\ ; \qquad e_{\phi s} = M_1 c_{2d} + M_2 c_{3d} + c_{\phi d} \tag{2.81}$$

Bending Moment continuity:

$$2e_{2d} = c_{1d}(k_1 M_1 - k_2 M_2) + c_{4d}(k_2 M_1 + k_1 M_2) + 2c_{6d} \tag{2.82}$$

$$2e_{2s} = c_{1d}(k_1 N_1 - k_2 N_2) + c_{4d}(k_2 N_1 + k_1 N_2) + 2c_{6d} \tag{2.83}$$

Shear Force continuity:

$$e_{3d} = c_{2d}k_1 + c_{3d}k_2 + c_{7d} \tag{2.84}$$

$$e_{3s} = c_{2d}(F_1 k_1 - F_2 k_2) + c_{3d}(F_2 k_1 + F_1 k_2) + c_{7d} \tag{2.85}$$

At the right end, $x = l$, the beam is clamped. So, the deflection of the debonded and the substrate part is zero:

$$\begin{aligned} w_d(l) = \; & c_{1d}\cosh k_1 l\cos k_2 l + c_{2d}\sinh k_1 l\cos k_2 x + c_{3d}\cosh k_1 l\sin k_2 l + \\ & + c_{4d}\sinh k_1 l\sin k_2 l + c_{5d}l^3 + c_{6d}l^2 + c_{7d}l + c_{8d} = 0 \end{aligned} \tag{2.86}$$

$$\begin{aligned} w_s(l) = \; & (F_1c_{1d} + F_2c_{4d})\cosh k_1 l\cos k_2 l + (F_1c_{2d} + F_2c_{3d})\sinh k_1 l\cos k_2 l + \\ & + (F_1c_{3d} - F_2c_{2d})\cosh k_1 l\sin k_2 l + (F_1c_{4d} - F_2c_{1d})\sinh k_1 l\sin k_2 l + \\ & + c_{5d}l^3 + c_{6d}l^2 + c_{7d}l + c_{8d} = 0 \end{aligned} \tag{2.87}$$

It is also important to note that the hyperbolic cosine and sine functions can quickly become very large numbers, unlike the hyperbolic tan function, and this would make the numerical solution fail, thus we divide by $\cosh k_1 l$, to obtain

$$\begin{aligned} & c_{1d}\cos k_2 l + c_{2d}\tanh k_1 l\cos k_2 x + c_{3d}\sin k_2 l + c_{4d}\tanh k_1 l\sin k_2 l + \\ & + (c_{5d}l^3 + c_{6d}l^2 + c_{7d}l + c_{8d})/\cosh k_1 l = 0 \end{aligned} \tag{2.88}$$

$$\begin{aligned} & (F_1c_{1d} + F_2c_{4d})\cos k_2 l + (F_1c_{2d} + F_2c_{3d})\tanh k_1 l\cos k_2 l + (F_1c_{3d} - F_2c_{2d})\sin k_2 l + \\ & + (F_1c_{4d} - F_2c_{1d})\tanh k_1 l\sin k_2 l + (c_{5d}l^3 + c_{6d}l^2 + c_{7d}l + c_{8d})/\cosh k_1 l = 0 \end{aligned} \tag{2.89}$$

Similarly, at the clamped end, the section rotation of the beam is zero:

$$\begin{aligned} \phi_d(l) = \; & (M_1c_{2d} + M_2c_{3d})\cos k_2 l + (M_1c_{1d} + M_2c_{4d})\tanh k_1 l\cos k_2 l + \\ & + (M_1c_{4d} - M_2c_{1d})\sin k_2 l + (M_1c_{3d} - M_2c_{2d})\tanh k_1 l\sin k_2 l + \\ & + (3c_{5d}l^2 + 2c_{6d}l + c_{\phi_d})/\cosh k_1 l = 0 \end{aligned} \tag{2.90}$$

$$\begin{aligned} \phi_s(l) = \; & (N_1c_{2d} + N_2c_{3d})\cos(k_2 l) + (N_1c_{1d} + N_2c_{4d})\tanh(k_1 l)\cos(k_2 l) + \\ & + (N_1c_{4d} - N_2c_{1d})\sin(k_2 l) + (N_1c_{3d} - N_2c_{2d})\tanh k_1 l\sin k_2 l + \\ & + (3c_{5d}l^2 + 2c_{6d}l + c_{\phi s})/\cosh k_1 l = 0 \end{aligned} \tag{2.91}$$

Also at the right end, $x = l$, the total bending moment and shear force are the sum of these created at the debonded part and the substrate part, i.e,

$$M_b = (EI)_d \phi'_d|_{x=l} + (EI)_s \phi'_s|_{x=l} \tag{2.92}$$

Similar to previous conditions, we again divide by $\cosh k_1 l$ to avoid numerical failure. This gives:

$$\begin{aligned}
\frac{M_b}{\cosh k_1 l} =& (EI)_d \Big[[c_{1d}(k_1 M_1 - k_2 M_2) + c_{4d}(k_1 M_2 + k_2 M_1)] \cos k_2 l + \\
&+ [c_{2d}(k_1 M_1 - k_2 M_2) + c_{3d}(k_1 M_2 + k_2 M_1)] \tanh k_1 l \cos k2l + \\
&+ [c_{3d}(k_1 M_1 - k_2 M_2) - c_{2d}(k_1 M_2 + k_2 M_1)] \sin k_2 l + \\
&+ [c_{4d}(k_1 M_1 - k_2 M_2) - c_{1d}(k_1 M_2 + k_2 M_1)] \tanh k_1 l \sin k_2 l \Big] + \\
&+ (EI)_s \Big[[c_{1d}(k_1 N_1 - k_2 N_2) + c_{4d}(k_1 N_2 + k_2 N_1)] \cos k_2 l + \\
&+ [c_{2d}(k_1 N_1 - k_2 N_2) + c_{3d}(k_1 N_2 + k_2 N_1)] \tanh k_1 l \cos k_2 l + \\
&+ [c_{3d}(k_1 N_1 - k_2 N_2) - c_{2d}(k_1 N_2 + k_2 N_1)] \sin k_2 l + \\
&+ [c_{4d}(k_1 N_1 - k_2 N_2) - c_{1d}(k_1 N_2 + k_2 N_1)] \tanh k_1 l \sin k_2 l \Big] + \\
&+ (EI_d + EI_s)(6c_{5d} l + 2c_{6d}) / \cosh k_1 l
\end{aligned} \tag{2.93}$$

and for the shear

$$V_b = -(\kappa GA)_d (w'_d - \phi_d)|_{x=l} - (\kappa GA)_s (w'_s - \phi_s)|_{x=l} \tag{2.94}$$

which gives,

$$\begin{aligned}
\frac{V_b}{\cosh k_1 l} = &- (\kappa GA)_d \Big[[c_{2d}(k_1 - M_1) + c_{3d}(k_2 - M_2)] \cos k_2 l + \\
&+ [c_{1d}(k_1 - M_1) + c_{4d}(k_2 - M_2)] \tanh k_1 l \cos k2l + \\
&+ [c_{4d}(k_1 - M_1) - c_{1d}(k_2 - M_2)] \sin k_2 l + \\
&+ [c_{3d}(k_1 - M_1) - c_{2d}(k_2 - M_2)] \tanh k_1 l \sin k_2 l + (c_{7d} - c_{\phi_d}) / \cosh k_1 l \Big] - \\
&- (\kappa GA)_s \Big[[c_{2d}(F_1 k_1 - F_2 k_2 - N_1) + c_{3d}(F_2 k_1 + F_1 k_2 - N_2)] \cos k_2 l + \\
&+ [c_{1d}(F_1 k_1 - F_2 k_2 - N_1) + c_{4d}(F_2 k_1 + F_1 k_2 - N_2)] \tanh k_1 l \cos k_2 l + \\
&+ [c_{4d}(F_1 k_1 - F_2 k_2 - N_1) - c_{1d}(F_2 k_1 + F_1 k_2 - N_2)] \sin k_2 l + \\
&+ [c_{3d}(F_1 k_1 - F_2 k_2 - N_1) - c_{2d}(F_2 k_1 + F_1 k_2 - N_2)] \tanh k_1 l \sin k_2 l + \\
&+ (c_{7d} - c_{\phi s}) / (\cosh k_1 l) \Big]
\end{aligned} \tag{2.95}$$

We can see that equations Equation 2.78-Equation 2.95 are a system of 16 linear algebraic equations. Here, in these equations, the unknowns c_{id}, $i = 1 \ldots 8$ and c_{ϕ_j}, e_{3j}, e_{4j}, e_{ϕ_j}, $j = d, s$ are coefficients in the general solutions. These 16 equations can be solved to obtain the solutions for remaining 16 unknown coefficients using simple a computer program.

2.2 Fracture Parameters

2.2.1 Energy Release Rate

Once we have solved the governing equations, the displacements and the section rotations of the beam section can be used to obtain the fracture parameters. The energy release rate is the instantaneous loss of potential energy per unit crack growth area. **J-Integral** The J-Integral represents a way to calculate the strain energy release rate. And the J-Integral is

defined by

$$J = \int_{\Gamma} W dz - T_i \frac{\partial u_i}{\partial x} ds \tag{2.96}$$

where $W = \int_0^{\epsilon} \sigma_{ij} d\epsilon_{ij}$ is the strain energy density. T_i and u_i are the components of the traction vector and the displacement vector, respectively. The integration path is shown in the Figure 2.7 ($\Gamma = BAA'FED'DCB$). On the horizontal segments of the path, there is no traction $\vec{T} = 0$ and dz = 0 so J = 0. Hence, only paths BA, $A'F$, ED' and $D'C$ contribute to J. On the vertical sides,

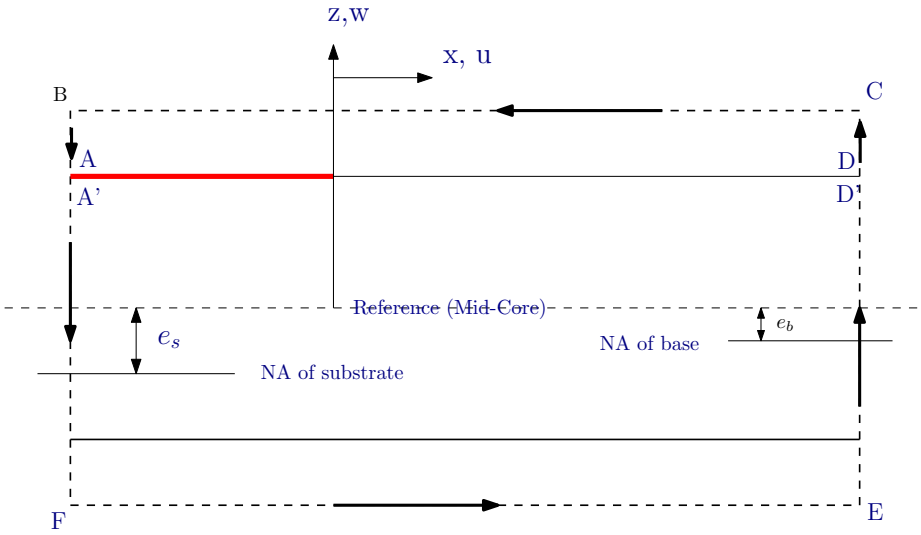

Figure 2.7: J-Integral Path

$$W = \frac{1}{2}(\sigma_{xx}\epsilon_{xx} + \sigma_{zz}\epsilon_{zz} + \tau_{xz}\gamma_{xz}) \; ; \quad T_i \frac{\partial u_i}{\partial x} = -\sigma_{xx}\epsilon_{xx} - \tau_{xz} w_{,x} \tag{2.97}$$

The equivalent shear modulus for the section should be derived by assuming the constituent sections are "springs in parallel", as shown in Kardomateas and Simitses [95]. For the debonded part, which is homogeneous, the equivalent shear modulus is:

$$G_d = G_{f_t} \tag{2.98}$$

For the substrate part which consists of the core and the bottom face:

$$\frac{2c+f_b}{G_s} = \frac{2c}{G_c} + \frac{f_b}{G_{f_b}} \tag{2.99}$$

For the base part

$$\frac{f_t+2c+f_b}{G_b} = \frac{f_t}{G_{f_t}} + \frac{2c}{G_c} + \frac{f_b}{G_{f_b}} \tag{2.100}$$

Regarding the shear correction factor, for a homogeneous section, κ = 6/5. Thus, for the debonded part:

$$\kappa_d = \frac{6}{5} \tag{2.101}$$

The shear correction factor for the substrate part can be found using the general asymmetric section formula in [45]:

$$\kappa_s = \frac{G_s b^2 (2c+f_b)}{4(EI)_s^2}\left(\frac{E_c^2}{G_c}q_2 - \frac{E_{f_b}^2}{G_- f_b}q_1\right) \tag{2.102}$$

where

$$q_1 = f_b(c-e_s+f_b)^4 + \frac{1}{5}[(c-e_s+f_b)^5 - (c-e_s)^5] - \\ - \frac{2}{3}(c-e_s+f_b)^2[(c-e_s+f_b)^3 - (c-e_s)^3] \tag{2.103}$$

$$q_2 = 2c(c+e_s)^4 + \frac{1}{5}[(c+e_s)^5 - (c-e_s)^5] - \frac{2}{3}(c+e_s)^2[(c-e_s)^3 - (c-e_s)^3] \tag{2.104}$$

The shear correction factor for the base part can again be taken from the Huang and Kardomateas [96] formula for a general asymmetric sandwich section. In terms of:

$$a_t = e_b + c + f_t\,; \quad b_t = e_b + c\,; \quad c_t = e_b + c + \frac{f_t}{2} \tag{2.105}$$

$$a_b = -e_b + c + f_b\,; \quad b_b = -e_b + c\,; \quad c_b = -e_b + c + \frac{f_b}{2} \tag{2.106}$$

and

$$d_i = \frac{E_{fi}^2}{E_c} f_i^2 c_i^2 + E_{fi} f_i c_i b_i^2 + \frac{E_c}{4} b_i^4 \tag{2.107}$$

the shear correction formula for the base part is given from:

$$\kappa_b = \frac{b^2(f_b + 2c + f_t)G_b}{EI_{eq}^2}(a_f + a_c) \tag{2.108}$$

where

$$a_f = \sum_{i=t,b} \frac{E_{fi}^2}{4G_i}\left[a_i^4 f_i - \frac{2}{3}a_i^2(a_i^3 - b_i^3) + \frac{1}{5}(a_i^5 - b_i^5)\right] \tag{2.109}$$

$$a_c = \frac{E_c}{G_c}\sum_{i=t,b}\frac{E_c}{20}(b_i^5 - e_b^5) - \left(E_c\frac{b_i^2}{2} + E_{fi}f_i c_i\right)\frac{1}{3}(b_i^3 - e_b^3) + d_i c \tag{2.110}$$

For a plane stress assumption, $\sigma_{zz} = 0$, and $\epsilon_{xx} = \sigma_{xx}/E$, therefore, when dz = -ds,

$$dJ = \frac{1}{2}\left(\sigma_{xx}\epsilon_{xx} + \sigma_{zz}\epsilon_{zz} + \tau_{xz}\gamma_{xz}\right)(-ds) - \left(-\sigma_{xx}\epsilon_{xx} - \tau_{xz}w_{i,x}\right)ds \tag{2.111}$$

or,

$$dJ = \frac{1}{2}\left(\frac{\sigma_{xx}^2}{E} - \kappa\frac{\tau_{xz}^2}{2G_{eq}} + 2\tau_{xz}w_{i,x}\right)ds \tag{2.112}$$

Similarly, when dz = ds,

$$dJ = \frac{1}{2}\Big(- \frac{\sigma_{xx}^2}{E} + \kappa\frac{\tau_{xz}^2}{2G_{eq}} - 2\tau_{xz}w_{i,x}\Big)ds \tag{2.113}$$

Notice that for a plane strain assumption, ϵ_{zz} = 0, we would have $\sigma_{zz} = \nu_{xz}\sigma_{xx}$, and $\epsilon_{xx} = (\sigma_{xx} - \nu_{zx}\sigma_{zz})/E = (1 - \nu_{zx}\nu xz)\sigma_{xx}/E$.

Therefore, again for a plane stress assumption:

On BA: $dz = -ds$,

$$\begin{aligned} J_{BA} &= \int_{-\frac{f_t}{2}}^{\frac{f_t}{2}} \left(\frac{1}{2E_d}\sigma_{xx}^2 - \frac{\kappa_d}{2G_{eq}}\tau_{xz}^2 + \tau_{xz}w_{i,x}|_{x=-a}\right)ds = \\ &= \int_{-\frac{f_t}{2}}^{\frac{f_t}{2}} \left(\frac{1}{2}E_d\frac{M_d^2 s^2}{(EI)_d^2} - \frac{\kappa_d}{2G_{eq}}\frac{V_d^2}{A_d^2} - \frac{V_d}{A_d}w_{d,x}|_{x=-a}\right)ds \end{aligned} \tag{2.114}$$

or,

$$J_{BA} = \frac{1}{2b^2}[\frac{12M_d^2}{E_d f_t^3} - \frac{\kappa_d V_d^2}{G_d f_t} - 2V_d b(3e_{1d}a^2 - 2e_{2d}a + e_{3d})] \tag{2.115}$$

On $A'F$: $dz = -ds$, and

$$J_{A'F} = \int_{A'F} \left(\frac{1}{2}E_d\frac{M_s^2 s^2}{(EI)_s^2} - \frac{\kappa_s V_s^2}{2G_s A_s^2} - \frac{V_s}{A_s}w_{s,x}|_{x=-a}\right)ds \tag{2.116}$$

or,

$$\begin{aligned} J_{A'F} =& \frac{M_s^2}{2(EI)_s^2}\Big[E_{f_b}f_b\Big[(c-e_s)(c-e_s+f_b) + \frac{f_b^2}{3}\Big] + 2E_c c\Big(\frac{c^2}{3} + e_s^2\Big)\Big] - \\ &- \frac{k_s V_s^2}{2G_s b^2(2c+f_b)} - \frac{V_s}{b}(3e_{1s}a^2 - 2e_{2s}a + e_{3s}) \end{aligned} \tag{2.117}$$

On EC: $dz = ds$, and,

$$J_{EC} = \int_{CE} \Bigg(- E_b \frac{M_b^2 s^2}{2(EI)_b^2} + \frac{\kappa_b V_b^2}{2G_b A_b^2} + \frac{V_b}{A_b}\phi_b|_{x=l} - \frac{V_b^2}{A_b(\kappa GA)_b} \Bigg) ds =$$
$$= - \frac{M_b^2}{2(EI)_b^2} \Bigg(E_{f_b} \int_{e_b-c-f_b}^{e_b-c} s^2 ds + E_c \int_{e_b-c}^{e_b+c} s^2 ds + E_{f_t} \int_{e_b+c}^{e_b+c+f_t} s^2 ds \Bigg) +$$
$$+ \frac{\kappa_b V_b}{2G_b A_b^2} \int_{e_b-c-f_b}^{e_b+c+f_t} ds + \frac{V_b}{A_b} \int_{e_b-c-f_b}^{e_b+c+f_t} \phi_b|_{x=l} ds - \frac{V_b^2}{A_b(\kappa GA)_b} \int_{e_b-c-f_b}^{e_b+c+f_t} ds \tag{2.118}$$

At $x = l$, we know from the boundary conditions that the section rotations ϕ_d and ϕ_s are zero. This also implies that $\phi_b = 0$. Therefore,

$$J_{EC} = - \frac{M_b^2}{2(EI)_b^2} \Bigg\{ E_{f_b} f_b \Big[(e_b - c)(e_b - c - f_b) + \frac{f_b^2}{3} \Big] + 2E_c c (\frac{c^2}{3} + e_b^2) + E_{f_t} f_t \Big[(e_b + c)(e_b + c + f_t) +$$
$$+ \left(\frac{\kappa_b V_b^2}{2G_b A_b^2} \right) (2c + f_t + f_b) - \frac{V_b^2}{b(\kappa GA)_b} \tag{2.119}$$

The strain energy release rate is the sum of these individual contributions (J_{BA}, $J_{A'F}$ and J_{EC}).

$$J = J_{BA} + J_{A'F} + J_{EC} \tag{2.120}$$

Hence, the energy release rate of the double cantilever beam specimen can be obtained

from the following expression:

$$
\begin{aligned}
J =& \frac{1}{2b^2}\left[\frac{12M_d^2}{E_d f_t^3} - \frac{\kappa_d V_d^2}{G_d f_t} - 2V_d b(3e_{1d}a^2 - 2e_{2d}a + e_{3d})\right] + \\
&+ \frac{M_s^2}{2(EI)_s^2}\Big\{E_{f_b} f_b\Big[(c - e_s)(c - e_s + f_b) + \frac{f_b^2}{3}\Big] + 2E_c c\Big(\frac{c^2}{3} + e_s^2\Big)\Big\} - \\
&- \frac{k_s V_s^2}{2G_s b^2(2c + f_b)} - \frac{V_s}{b}(3e_{1s}a^2 - 2e_{2s}a + e_{3s}) + \frac{\kappa_b V_b^2}{2G_b A_b^2}(2c + f_t + f_b) - \\
&- \frac{V_b^2}{b(\kappa GA)_b} + \frac{M_b^2}{2(EI)_b^2}\Big\{E_{f_b} f_b\Big[(e_b - c)(e_b - c - f_b) + \frac{f_b^2}{3}\Big] + \\
&+ 2E_c c(\frac{c^2}{3} + e_b^2) + E_{f_t} f_t\Big[(e_b + c)(e_b + c + f_t) + \frac{f_t^2}{3}\Big]\Big\}
\end{aligned}
\tag{2.121}
$$

Rate of Energy Released by the springs

In an elastic foundation approach, when the crack grows, it breaks the springs and, hence, it releases the energy stored in the broken springs. We can determine the released energy by finding the energy stored in the springs due to the deformations in the beam [9]. Let the differential spring length be da, the energy released by crack when it propagates by length da is the energy stored in this differential spring element:

$$
G_{spring} = \lim_{\delta a \to 0} \frac{1}{2\delta a} \int_0^{\delta a} \sigma_{zz}(r) \Delta w(\delta a - r) dr \tag{2.122}
$$

The normal spring stiffness is k_n and, therefore, the of energy released by the normal springs is given by:

$$
G_{spring,I} = \frac{1}{2} k_n [w_d(0) - w_s(0)]^2 = \frac{1}{2} k_n (e_{4d} - e_{4s})^2 \tag{2.123}
$$

Here, in the elastic foundation, we also have shear springs and k_r is the shear spring stiffness; thus the rate of energy released by the shear springs is given by:

$$
G_{spring,II} = \frac{1}{2} k_r (\phi_d(0) - \phi_s(0))^2 = \frac{1}{2} k_r (e_{\phi d} - e_{\phi s})^2 \tag{2.124}
$$

The total energy release rate obtained from the springs is,

$$G = G_{spring,I} + G_{spring,II} = \frac{1}{2}k_n(e_{4d} - e_{4s})^2 + \frac{1}{2}k_r(e_{\phi d} - e_{\phi s})^2 \tag{2.125}$$

Equation 2.125 can be used as another measure to find the energy release rate values. These values will next be compared with the J-Integral values and the ones from a finite element analysis.

2.2.2 Mode Partitioning

Mode mixity values are usually obtained using the complex stress intensity factor approach. This approach was used by Suo and Hutchinson [12] and Kardomateas *et al* [13]. Using this approach in [12] and [13] necessitated the estimation of stress intensity factor in terms of a single load-independent parameter (the parameter "ω"), which is numerically determined. The aim here is to obtain closed form expressions for the fracture parameter and thus, we use an alternate approach to obtaining mode partitioning. It makes use of the displacements near the beginning of the elastic foundation and was introduced by Kardomateas *et al* [43].

Notice that displacements as an alternative approach to determine mode mixity have been used in bi-material fracture mechanics by Berggreen *et al* [36]. However, the latter is based on the fracture mechanics singular field and thus it is different conceptually than the measure of mode partitioning, which is based on the elastic foundation model.

According to Timoshenko beam theory, the axial and transverse displacement distribution is given by Equation 2.8. Therefore, the displacements of the debonded part (notice that the positive slope is the counter-clockwise) in the limit are:

$$w_{d_o} = \lim_{x\to 0} w_d(x) = c_{1d} = e_{4d} \tag{2.126}$$

$$u_{d_o} = \frac{f_t}{2}\lim_{x\to 0}\phi_d(x) = \frac{f_t}{2}[(M_1 c_{2d} + M_2 c_{3d}) + c_{\phi_d}] = \frac{f_t}{2}e_{\phi d} \tag{2.127}$$

and the corresponding ones for the substrate part in the limit are:

$$w_{s_o} = \lim_{x \to 0} w_s(x) = (F_1 c_{1d} + F_2 c_{4d}) = e_{4s} \tag{2.128}$$

$$u_{s_o} = -(e_s + c) \lim_{x \to 0} \phi_s(x) = -(e_s + c)[(N_1 c_{2d} + N_2 c_{3d}) + c_{\phi_s}] = -(e_s + c) e_{\phi s} \tag{2.129}$$

In this case, the Timoshenko beam theory already accounts for transverse shear. So, the mode partitioning phase angle ψ_{EF}, based on the elastic foundation approach is defined from the relative crack flank opening and shearing displacements. It is defined so that $\phi_{EF} = 0$ if only transverse displacement occurs at the beginning of springs, x = 0 (pure Mode I) and $\phi_{EF} = 90^o$ if only axial displacement occurs at x = 0 (pure Mode II).

$$\psi_{EF} = \tan^{-1} \frac{\delta u}{\delta w} = \tan^{-1} \left(\frac{u_{d_o} - u_{s_o}}{w_{d_o} - w_{s_o}} \right) \tag{2.130}$$

or,

$$\psi_{EF} = \tan^{-1} [\frac{\frac{f_t}{2} e_{\phi d} + (e_s + c) e_{\phi s}}{e_{4d} - e_{4s}}] \tag{2.131}$$

In the elastic foundation model, a crack does not exist, instead we have beams connected by elastic springs. This mode partitioning is not the same conceptually as the mode mixity in a bi-material crack, which is based on the stress intensity factors from a fracture mechanics approach. But, as the results in the following section show, the two are very close in value.

2.3 Results and Discussion

We obtained results for a symmetrical sandwich beam with faces made out of isotropic Aluminum (Young's Modulus E_f = 70 GPa and Poisson's ratio ν_f = 0.3) and with made out of isotropic Aluminium Foam (Young's Modulus E_c = 7 GPa and Poisson's ratio ν_c = 0.32). We chose isotropic faces and core because we shall compare our results with the

commercial finite element code ABAQUS. In ABAQUS, the stress intensity factors (K_I and K_{II}) for an interfacial crack can be calculated only when the two materials are both isotropic and linearly elastic.

We chose a beam geometry, with face thicknesses f_t = f_b = 2 mm and core thickness $2c$ = 20mm. The total length of the beam was taken as L = 500mm. The beam has a debond between the top face and the core of length of a = 200mm.

For validation and comparison purposes, a double cantilever beam specimen and this material combination was modeled into ABAQUS. We create 2-D sandwich beam model with an interface crack. The crack is modeled using seam cracks. There are shear forces and bending moments at the left end, both on the face sheet and the substrate. We also have end boundary conditions at the right end. For the mesh in the beam, we mostly use second order 8-noded quad elements and few 6-noded triangle elements near the crack tip. These crack tip elements are also modeled using singular elements, where the midpoint is moved to one quarter side distance from the original midpoint position to the node. In the FEA model, we ignore the large deformation effects and perform a linear analysis. Here, we used isoparametric 8-node biquadratic plane stress (CPS8R) elements and few 6-node modified quadratic plane stress triangle elements (CPS6M) near the crack tip. The singular elements (CPS6M) were used near the crack tip in order to include stress singularity. Here, J-Integral and the stress intensity factor values are evaluated using a contour integral [14]. And, K_I and K_{II} are obtained using the interaction integral method. The mode mixity values from FEA can be obtained using the following relationship:

$$\psi_{FEA} = \tan^{-1}\left(\frac{K_{II}}{K_I}\right) \tag{2.132}$$

It should be noticed that ABAQUS has the option to calculate the energy release rates of modes I and II, G_I and G_{II}, respectively, through the virtual crack closure technique, however the values were widely varying depending on the mesh size at the crack tip. Same

oscillation of values has been observed at other studies of interfacial cracks [15]. Thus, the energy release rate components, G_I and G_{II}, cannot be used directly to estimate a related energy release rate based mode mixity from ABAQUS.

Table 2.1: DCB: Energy Release Rates - Al face & Al foam core

V_d (N)	V_s (N)	M_d (Nmm)	M_s (Nmm)	$J_{ref_{43}}$ (N/mm)	J_{EF} (N/mm)	J_{FEA} (N/mm)	G_{spring} (N/mm)
0.5	-0.5	100	-100	0.4381	0.4363	0.4356	0.4363
1.0	-1.0	50	-50	0.6920	0.6875	0.6859	0.6875
1.0	-1.0	100	100	0.9980	0.9827	0.9804	0.9817
10.0	-1.0	100	-100	48.6600	48.9263	48.3300	47.8958
1.0	-10.0	100	-100	0.8944	1.5328	1.1165	1.1083
0.5	0.0	0	0	0.1103	0.1114	0.1097	0.1084
0.0	-0.5	0	0	0.0003	0.0016	0.0003	$1.2\text{x}10^{-5}$
0.0	0.0	100	0	0.1070	0.1070	0.1070	0.1068

Table 2.1 shows the values of energy release rates obtained using the closed form expression (Equation 2.121) using the Timoshenko beam theory (J_{EF}). These values are obtained for a range of loading combination and are then compared with the J-Integral values from finite element analysis (subscript FEA). We are also comparing the energy release rate values with the results from elastic foundation model based on Euler-Bernoulli theory ($J_{ref_{43}}$) [43]. Here, we can see that the energy release rate values show very good agreement with the values from FEA. We can also notice that the results (J_{EF}) are better than the values from the other model ($J_{ref_{43}}$). This is mainly due to fact that the model here can better capture the effects of transverse shear when compared to the model based on Euler-Bernoulli beam theory.

In addition, Table 2.1 shows the values of the energy release by the springs. These values are very close to the J-Integral values in all the cases (even in the cases where the

substrate is heavily loaded). Notice that in load case 5 and 7, when the substrate is heavily loaded in shear, the J_{EF} values show a slight deviation the values from the finite element analysis. This is due to fact that the elastic foundation model using the Timoshenko beam theory is not able to fully capture the transverse shear effects. In fact, it has been shown in the literature [16] that in sandwich beams we need higher order theories to fully capture the transverse shear effect. It is also important to note that even for heavily shear loaded cases, the estimated G_{spring} values show close agreement with the J_{FEA} values.

Table 2.2: DCB: Mode Partitioning Values - Al face & Al foam core

V_d (N)	V_s (N)	M_d (Nmm)	M_s (Nmm)	$\psi_{ref_{43}}$ (deg)	ψ_{EF} (deg)	ψ_{FEA} (deg)
0.5	-0.5	100	-100	-26.70	-30.70	-28.50
1.0	-1.0	50	-50	-26.50	-30.59	-28.40
1.0	-1.0	100	100	-26.60	-30.70	-30.30
10.0	-1.0	100	-100	-26.80	-31.14	-30.80
1.0	-10.0	100	-100	-23.80	-26.59	-12.50
0.5	0.0	0	0	-26.90	-31.22	-31.20
0.0	-0.5	0	0	66.50	31.98	56.90
0.0	0.0	100	0	-27.00	-31.43	-31.50

Table 2.2 shows the mode partitioning measures for the same combination of loads. Here, we have defined the mode partitioning measure in the context of the elastic foundation analysis based on the Timoshenko beam theory (ψ_{EF}).

It should again be emphasized that in the elastic foundation approach, there is no crack as defined by the conventional fracture mechanics, i.e., there is no crack tip beyond which the top face and the core are bonded and have the same axial and transverse displacements. On the contrary, we have normal and shear springs at the interface and thus there is a gap between the top face and the core in the mathematical elastic foundation model. Therefore, we cannot use the mode mixity based on stress intensity factors and singular stress fields, as

is done in conventional fracture mechanics. Instead, we use the mode partitioning measure defined based on the transverse and axial displacements of springs at the tip (point where the springs start). Notice that in Table 2, the mode partitioning measure (ψ_{EF}) provides a good estimate of the mode mixity. Table 2.2 also shows the mode partitioning measure values obtained from previous mode (based on Euler-Bernoulli beam theory, $\psi_{ref_{43}}$). It can be seen that the mode partitioning measure from this model (ψ_{EF}) is consistently better than the values from obtained from previous model ($\psi_{ref_{43}}$). For all the loading cases, ψ_{EF} values closely follow the trend of ψ_{FEA}. Meanwhile, differences are observed in some cases and it is natural to expect that there will be cases of material combinations and/or loadings for which this simplified model may not be as accurate. Notice that for case 5, there is noticeable difference between the mode partitioning measure and mode mixity values. This is expected since the elastic foundation analysis uses a first order shear deformation theory to account for shear contribution, but this is expected to be inadequate in cases of large shear loading of the core.

Table 2.3: DCB: Energy Release Rates and Mode Partitioning for an Orthotropic core

V_d (N)	V_s (N)	M_d (Nmm)	M_s (Nmm)	$J_{ref_{43}}$ (N/mm)	J_{EF} (N/mm)	$\psi_{ref_{43}}$ (deg)	ψ_{EF} (deg)
0.5	-0.5	100	-100	0.6061	0.6203	33.06	41.00
1.0	-1.0	50	-50	0.9849	1.0224	33.60	40.38
1.0	-1.0	100	100	1.0988	1.1362	33.59	39.25
10.0	-1.0	100	-100	52.77	98.53	31.62	40.23
1.0	-10.0	100	-100	16.97	62.11	38.33	39.98
0.5	0.0	0	0	0.1186	0.2584	31.25	40.13
0.0	-0.5	0	0	0.0353	0.1737	41.33	39.63
0.0	0.0	100	0	0.1071	0.1070	32.09	40.14

The model presented here can be used for both isotropic and orthotropic cases. In Table 2.3, we obtained the results for a sandwich beam with orthotropic honeycomb core material. Its

Young's Modulus is E_1 = E_2 = 0.32 GPa, E_3 = 0.3 GPa, G_{23} = G_{31} = 48 MPa, G_{12} = 13 MPa and the Poisson's rations: ν_{12} = ν_{32} = ν_{31} = 0.25. The thickness of each face sheet is 2mm and the core thickness is 20mm. Using the elastic foundation model presented here, we obtained the energy release rate and mode partitioning values for this beam specimen. It interesting to note that this model can be quickly used to obtain results for orthotropic materials and can also be adapted for plane strain case. We cannot compare our results with the values from finite element analysis because it can calculate stress intensity factors $K_{I,II}$ for an interface crack only when the two materials are both isotropic and linear elastic. We have compared our results with the results from elastic foundation theory based on Euler-Bernoulli theory.

Table 2.4: DCB: Energy Release Rates and Mode Partitioning - Small crack (a/L = 1%)

V_d (N)	V_s (N)	M_d (Nmm)	M_s (Nmm)	J_{EF} (N/mm)	J_{FEA} (N/mm)	G_{spring} (N/mm)	ψ_{EF} (deg)	ψ_{FEA} (deg)
0.5	-0.5	100	-100	0.1161	0.1150	0.1162	-30.53	-30.02
1.0	-1.0	50	-50	0.0360	0.0354	0.0360	-29.62	-29.19
1.0	-1.0	100	100	0.1245	0.1224	0.1235	-31.20	-30.68
10.0	-1.0	100	-100	0.8429	0.3280	0.2997	-28.49	-27.30
1.0	-10.0	100	-100	0.6298	0.1242	0.1548	-27.61	-28.53
0.5	0.0	0	0	0.0017	0.0015	0.00012	-25.59	-23.49
0.0	-0.5	0	0	$1.6\text{x}10^{-3}$	$1.7\text{x}10^{-7}$	$5.8\text{x}10^{-6}$	-10.07	53.6
0.0	0.0	100	0.0	0.1070	0.1070	0.1068	-31.43	-30.86

Further, we obtained data for the case of a much smaller crack (Table 2.4), namely, for a crack length of a = 5mm (as opposed to a = 200mm). The energy release rate values (J_{EF}) from the elastic foundation model presented shows very good agreement with the values (J_{FEA}) from finite element analysis. Similarly, the mode partitioning measures (ψ_{EF}) also closely follow the same trend as the mode mixity from FEA. Again, we can

notice that there is some difference for loading case 5, it is mainly due to the shear loading the substrate. This is expected since the Timoshenko beam theory cannot fully capture the shear contribution from the substrate.

Table 2.5: DCB: Energy Release Rates and Mode Partitioning - Small crack (a/L=4%)

V_d (N)	V_s (N)	M_d (Nmm)	M_s (Nmm)	J_{EF} (N/mm)	J_{FEA} (N/mm)	G_{spring} (N/mm)	ψ_{EF} (deg)	ψ_{FEA} (deg)
0.5	-0.5	100	-100	0.1335	0.1334	0.1335	-28.49	-30.55
1.0	-1.0	50	-50	0.0571	0.0567	0.0571	-27.90	-29.87
1.0	-1.0	100	100	0.1615	0.1603	0.1605	-32.63	-31.16
10.0	-1.0	100	-100	1.6569	1.1340	1.076	-28.83	-29.84
1.0	-10.0	100	-100	0.6683	0.1665	0.1973	-23.31	-27.43
0.5	0.0	0	0	0.0029	0.0014	0.0012	-28.96	-29.56
0.0	-0.5	0	0	$1.6\text{x}10^{-3}$	$3.4\text{x}10^{-3}$	$6.3\text{x}10^{-6}$	54.84	-5.57
0.0	0.0	100	0	0.1070	0.1070	0.1068	-31.47	-31.43

We also obtained data for another case (Table 2.5), namely, for a crack length of a = 20mm. For load case 2 ($V_d = -V_s$ = 1.0 and $M_d = -M_s$ = 50.0), the model proposed here resulted in J_{EF} = 0.0571 Nt/mm whereas ABAQUS resulted in J_{FEA} = 0.0567 Nt/mm. Regarding the mode partitioning measure, the elastic foundation model resulted in ψ_{EF-T} = -29.87 deg whereas ABAQUS resulted in ψ_{FEA} = -27.8 deg. It can be seen that the energy release rate values obtained from this model is in agreement with the values from ABAQUS. Similarly, the mode partitioning values follow a similar trend to that of the mode mixity values from ABAQUS and there is only a slight variation in the value between them. Hence, it can be concluded that the accuracy of the elastic foundation model based on Timoshenko beam theory is not compromised when the crack lengths are smaller.

Table 2.6: DCB: Effect of Core Stiffness (a = 200mm)

E_f/E_c (N)	J_{EF-T} (N/mm)	J_{FEA} (N/mm)	ψ_{EF-T} (deg)	ψ_{FEA} (deg)
10	0.4363	0.4356	-30.7	-28.54
20	0.4390	0.4384	-24.72	-23.33
40	0.4430	0.4422	-18.86	-17.74
50	0.4447	0.4439	-16.90	-15.91
75	0.4486	0.4478	-13.09	-12.55
100	0.4521	0.4516	-10.24	-10.14
150	0.4586	0.4577	-5.64	-6.72
200	0.4645	0.4636	-1.92	-4.25
400	0.4861	0.4846	9.02	1.82

We also studied the effect of core stiffness on the fracture parameters. In Table 2.1 and Table 2.2, we studied a beam with Alumium Faces and Aluminum Foam core (E_f/E_c = 10). Here, Table 2.6 shows the energy release rate and mode partitioning values for various core materials (Al Foam core, H100 core etc.). In Table 2.6, it is interesting to note that the energy release rate values show very good agreement with the J-Integral values from ABAQUS for even soft core materials. Also, in all the cases, the mode partitioning measure values follow the same trend as that of the mode mixity values from the finite element analysis. But for very soft core materials ($E_f/E_c \geq 200$), we can notice that the mode partitioning values are slightly off and this is mainly due to use of first order shear deformation theory, which is inadequate at these very low core stiffnesses. Thus, to completely capture the transverse shear effects in very soft core materials, there is a need for higher order shear deformation theories.

2.4 Conclusion

Closed form expressions for the energy release rate and mode partitioning of face/core debonds in shear and moment loaded double cantilever sandwich beam specimen are derived. The beam is divided in four parts: two along its length, namely debonded part and bonded part and two along its thickness, namely debonded face and substrate, which includes the core and the bottom face. An elastic foundation approach based on the Timoshenko beam theory is pursued to obtain the governing equations. The model pursued here is comprehensive and includes the deformation of the substrate in the governing equations. The solutions are obtained such that these solutions are valid for both isotropic and orthotropic faces and core and can be applied for a general asymmetric sandwich beam (top and bottom faces not the same). The J - Integral approach is used here to obtain a closed form expression for the energy release rate and it shows excellent agreement with the corresponding values from a finite element analysis. A mode partitioning measure is defined based on the relative crack flank opening and shearing displacements. The results show that this mode partitioning values closely follow the traditional mode mixity values from finite element analysis.

CHAPTER 3

ELASTIC FOUNDATION ANALYSIS OF SINGLE CANTILEVER BEAM

In recent times, Single Cantilever Beam (SCB) test has gained attention as one of the best candidates for evaluating debond fracture toughness in mode I loading. The goal here is to employ an elastic foundation approach and the Timoshenko beam theory to derive closed form expressions for the energy release rate and mode partitioning of face/core debonds in Single Cantilever Beam (SCB) Sandwich Composite testing configuration. A SCB specimen of finite length is considered as having a "debonded" section where the debonded top face and the substrate are free and a "bonded" section where an elastic foundation is used between the top face and the substrate. The interaction between the top face and the substrate in the "bonded" section is modeled using both normal and rotational shear distributions to account for transverse and rotational degrees of freedom. The elastic foundation analysis used here is comprehensive, it includes the deformation of the substrate part and can also capture the shear deformation effects in the beam.

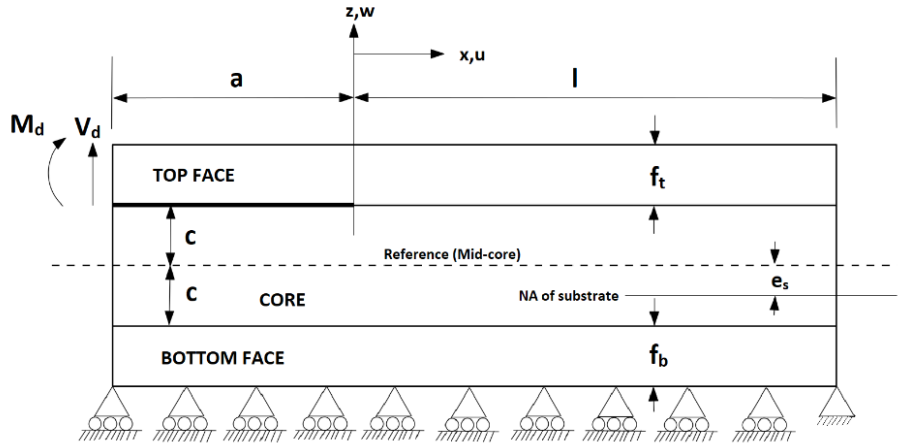

Figure 3.1: Single Cantilever Beam Specimen

The Single Cantilever Beam (SCB) specimen is again divided into different regions similar to the Double Cantilever Beam (DCB) specimen. Here, the debonded part is loaded

by a shear force V_d and a moment M_d and in the Single Cantilever Beam (SCB) specimen the substrate part is restricted in the transverse displacement. So there is no transverse displacement (w_s = 0) in the substrate part. The coordinate system is set so that x = 0 is at the end of the debond, i.e., the debond part for negative x and the intact part for positive x Figure 3.1. We denote the transverse and axial displacements using w and u, respectively.

3.1 Using Timoshenko Beam Theory

The Timoshenko beam theory distinguishes between the angle of rotation of the beam cross-section, ϕ, and the slope of the neutral axis, dw/dx, which differ by the shear angle γ. The displacement field is given by

3.1.1 Displacement Field

$$u_x(x,z) = -z\phi; \qquad u_z(x,z) = w \tag{3.1}$$

and the resulting shear strain is:

$$\gamma_{xz} = u_{x,z} + u_{z,x} = w_{,x} - \phi \tag{3.2}$$

Applying the variation principle, and integrating by parts, the strain energy $\delta U = \int\int\int(\sigma_{xx}\delta\epsilon_{xx} + \tau_{xz}\delta\gamma_{xz})dAdx$ leads to:

$$\delta U = \int_L \left[\left(\frac{dM}{dx} - V\right)\delta\phi - \frac{dV}{dx}\delta w\right]dx + [-M\delta\phi + V\delta w]|_0^L \tag{3.3}$$

Assuming a distributed moment, m, and a distributed transverse load, q, in the external work, we obtain the differential equations:

$$\frac{dM}{dx} - V + m = 0\ ; \quad \frac{dV}{dx} - q = 0 \tag{3.4}$$

And in the Timoshenko beam theory, the moment and shear are defined as:

$$M = (EI)\frac{d\phi}{dx}; \qquad V = -(\kappa GA)\gamma; \qquad \gamma = \frac{dw}{dx} - \phi \tag{3.5}$$

The elastic foundation load is a distributed load applied to both the debonded part and the substrate, creating a distributed load

$$q = -k_n w\ ; \qquad m = k_r \phi \tag{3.6}$$

Here, k_n is the stiffness of the normal springs and k_r is the stiffness of the rotational shear springs. It is important to have an accurate estimation of the elastic foundation stiffness values. In 2018, Kardomateas it et al [45] derived solutions based on Extended High-Order Sandwich Panel theory which shows excellent agreement with the elasticity theory. Elasticity theory solutions were also derived. They also provided simple closed form expressions for normal and shear springs stiffness for the case of symmetric sandwich specimens. These stiffness expressions can be used for both isotropic and orthotropic materials. Shear spring stiffness can be defined in two ways (k_s or k_r). One, using the displacements at the interface (k_s) and the other based on the section rotation of the beam (k_r). These expressions are as follows:

$$k_n = b\frac{E_3^c}{c} \qquad k_s = b\frac{G_{13}^c}{c} \qquad k_r = bG_{13}^c\frac{f_t}{2} \tag{3.7}$$

3.2 Governing Equations

Here, we can solve for the governing equations similar to what we did with the Double Cantilever Beam (DCB) specimen.

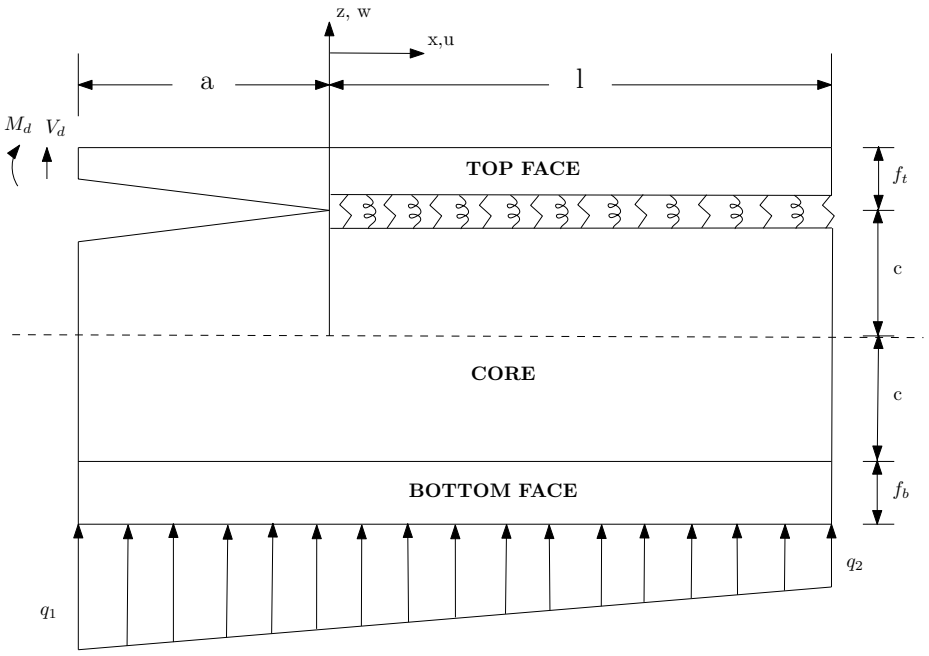

Figure 3.2: Support Reaction on the substrate

3.2.1 Bonded Section of the beam: $0 \leq x \leq l$

When we look at the top face sheet in the bonded section of the beam as in Figure 3.2, we get the following governing equations:

$$(EI)_d \frac{d^2\phi_d}{dx^2} + (\kappa GA)_d(\frac{dw_d}{dx} - \phi_d) - k_r(\phi_d - \phi_s) = 0 \tag{3.8}$$

$$-(\kappa GA)_d(\frac{d^2w_d}{dx^2} + \frac{d\phi_d}{dx}) - k_n(w_d) = 0 \tag{3.9}$$

And, in the substrate part of the SCB specimen, there is no transverse displacement and we are only interested in the transverse shear in the substrate. To obtain the shear forces acting on the substrate part, we will first consider a reaction on the fixed bottom edge as linearly distributed with q_1 and q_2, as the intensities of the linearly distributed reaction at the ends (as shown in Figure 3.2). Force equilibrium and moment equilibrium about the left end

would give us:

$$q_1 = -4\frac{V_d}{a+l} - 6\frac{M_d}{(a+l)^2}\ , \qquad q_2 = 2\frac{V_d}{a+l} + 6\frac{M_d}{(a+l)^2} \tag{3.10}$$

And, the shear force distribution along the bottom edge of the substrate would be

$$q_x(x) = \frac{q_2 - q_1}{a+l}x + \frac{q_2 a + q_1 l}{a+l}; \qquad -a \le x \le l \tag{3.11}$$

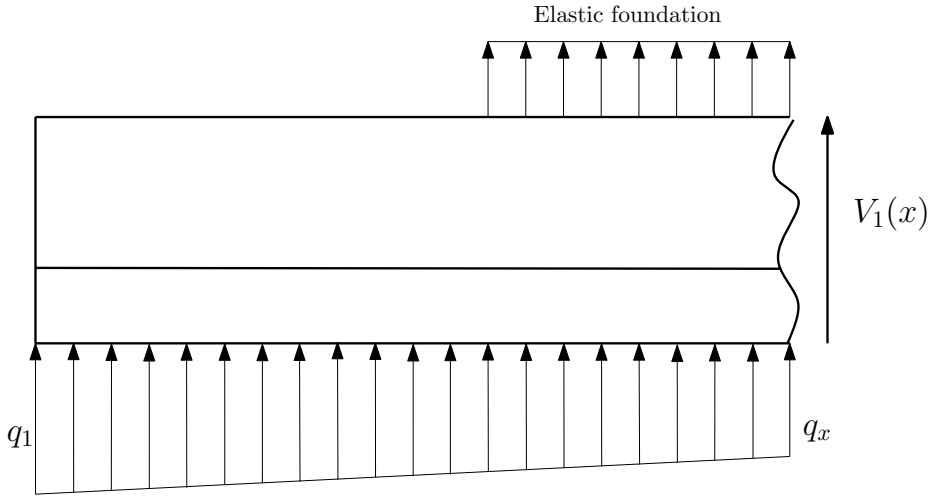

Figure 3.3: Shear distribution in the Substrate: Bonded section SCB

Now, using this reaction shear distribution and the spring force distribution, we can find the shear force at any point in the substrate part as shown in Figure 3.3

$$V_s + \int_{-a}^{x} q_x dx + \int_{0}^{x} k_n w_d dx = 0 \tag{3.12}$$

Differentiating the above equation, we get

$$\frac{dV_s}{dx} = -q_x - k_n w_d \tag{3.13}$$

$$\frac{d\phi_s}{dx} = \frac{q_x + k_n w_d}{(\kappa GA)_s} \tag{3.14}$$

We can differentiate Equation 3.8 and substitute Equation 3.9 & Equation 3.14 to obtain the governing equation for the top face sheet in terms of w_d

$$w_d''''(x) - A w_d''(x) + B w_d(x) = -\frac{k_r}{EI_d(\kappa GA)_s} q_x \tag{3.15}$$

where,

$$A = \left[\frac{k_n}{(\kappa GA)_d} + \frac{k_r}{(EI)_d}\right]; \qquad B = \left[\frac{k_n}{(EI)_d} + \frac{k_n k_r}{(EI)_d(\kappa GA)_d} + \frac{k_n k_r}{(EI)_d(\kappa GA)_s}\right] \tag{3.16}$$

This is a fourth-order linear differential equation. And, the general solution for the transverse displacement, w_d, will be

$$w_d(x) = (w_d)_I + (w_d)_{II} \tag{3.17}$$

where, $(w_d)_I$ is the general solution from the homogeneous part of Equation 3.15 and $(w_d)_{II}$ is the particular solution from the non-homogeneous part. Solving the homogeneous part, we get the solution as:

$$\begin{aligned}(w_d)_I = c_{1d}\cosh k_1 x \cos k_2 x + c_{2d}\sinh k_1 x \cos k_2 x + c_{3d}\cosh k_1 x \sin k_2 x + \\ + c_{4d}\sinh k_1 x \sin k_2 x\end{aligned} \tag{3.18}$$

where,

$$k_1 = real\left(\frac{\sqrt{A-\sqrt{A^2-4B}}}{\sqrt{2}}\right); \quad k_2 = im\left(\frac{\sqrt{A+\sqrt{A^2-4B}}}{\sqrt{2}}\right) \tag{3.19}$$

The non-homogeneous part of Equation 3.15 is linear in terms of x and hence the particular solution will also be linear in x:

$$(w_d)_{II} = c_{p_1}x + c_{p_2} \tag{3.20}$$

Substituting Equation 3.20 in the left hand side of Equation 3.15 and comparing the terms on both sides, we get

$$c_{p_1} = -\frac{k_r(q_2-q_1)}{EI_d(\kappa GA)_s(a+l)B}\ ; \qquad c_{p_2} = -\frac{k_r(q_2a+q_1l)}{EI_d(\kappa GA)_s(a+l)B} \tag{3.21}$$

Hence, the general solution for the transverse displacement of the top face sheet in the bonded section is:

$$\begin{aligned} w_d(x) = c_{1d}\cosh k_1x\cos k_2x + c_{2d}\sinh k_1x\cos k_2x + c_{3d}\cosh k_1x\sin k_2x + \\ + c_{4d}\sinh k_1x\sin k_2x + c_{p_1}x + c_{p_2} \end{aligned} \tag{3.22}$$

From Equation 3.16, we know that

$$\frac{d\phi_d}{dx} = \frac{d^2w_d}{dx^2} - \frac{k_n}{(\kappa GA)_d}w_d \tag{3.23}$$

Substituting w_d in the above equation and then integrating, we get

$$\begin{aligned}\phi_d =& \frac{1}{(k_1^2+k_2^2)(\kappa GA)_d}\Bigg[\\ &\left(k_n(-c_{2d}k_1+c_{3d}k_2)+(c_{2d}k_1+c_{3d}k_2)(k_1^2+k_2^2)(\kappa GA)_d\right)\cosh(k_1x)\cos(k_2x)+ \\ &+\left(k_n(-c_{1d}k_1+c_{4d}k_2)+(c_{1d}k_1+c_{4d}k_2)(k_1^2+k_2^2)(\kappa GA)_d\right)\sinh(k_1x)\cos(k_2x)+ \\ &+\left(-k_n(c_{4d}k_1+c_{1d}k_2)+(c_{4d}k_1-c_{1d}k_2)(k_1^2+k_2^2)(\kappa GA)_d\right)\cosh(k_1x)\sin(k_2x)+ \\ &+\left(-k_n(c_{3d}k_1+c_{2d}k_2)+(c_{3d}k_1-c_{2d}k_2)(k_1^2+k_2^2)(\kappa GA)_d\right)\sinh(k_1x)\sin(k_2x)\Bigg]- \\ &-\frac{k_n}{2(\kappa GA)_d}(2c_{p_2}x+c_{p_1}x^2)+c_{\phi_d} \end{aligned} \tag{3.24}$$

From Equation 3.12, we get the section rotation in the substrate

$$\begin{aligned}\phi_s =& -\frac{k_n}{(\kappa GA)_s(k_1^2+k_2^2)}\Big[(c_{2d}k_1-c_{3d}k_2)(\cosh(k_1x)\cos(k_2x)-1) \\ &+(c_{1d}k_1-c_{4d}k_2)\sinh(k_1x)\cos(k_2x)+c_{4d}k_1+c_{1d}k_2)\cosh(k_1x)\sin(k_2x)+ \\ &+(c_{3d}k_1+c_{2d}k_2)\sinh(k_1x)\sin(k_2x)\Big]-\frac{k_n}{2(\kappa GA)_s}(2c_{p_2}x+c_{p_1}x^2)- \\ &-\frac{(a+x)(2lq_1+a(q_1+q_2)+(-q_1+q_2)x)}{2(a+l)(\kappa GA)_s} \end{aligned} \tag{3.25}$$

From these general solutions (Equation 3.23,Equation 3.24 & Equation 3.25), we have 5 unknown coefficients c_{1d}, c_{2d}, c_{3d}, c_{4d} and c_{ϕ_d}

3.2.2 Debonded Section of the beam: -a ≤ x ≤ 0

In the debonded section of the beam, there is no elastic foundation between the debonded face and the substrate. Using Timoshenko beam theory, we get the governing equations for the debonded top face are:

$$EI_d\phi_d'''+(\kappa GA)_d(w_d''-\phi_d')=0\,; \qquad (\kappa GA)_d(w_d''-\phi_d')=0 \tag{3.26}$$

From the above equations

$$\phi_d''' = 0 \tag{3.27}$$

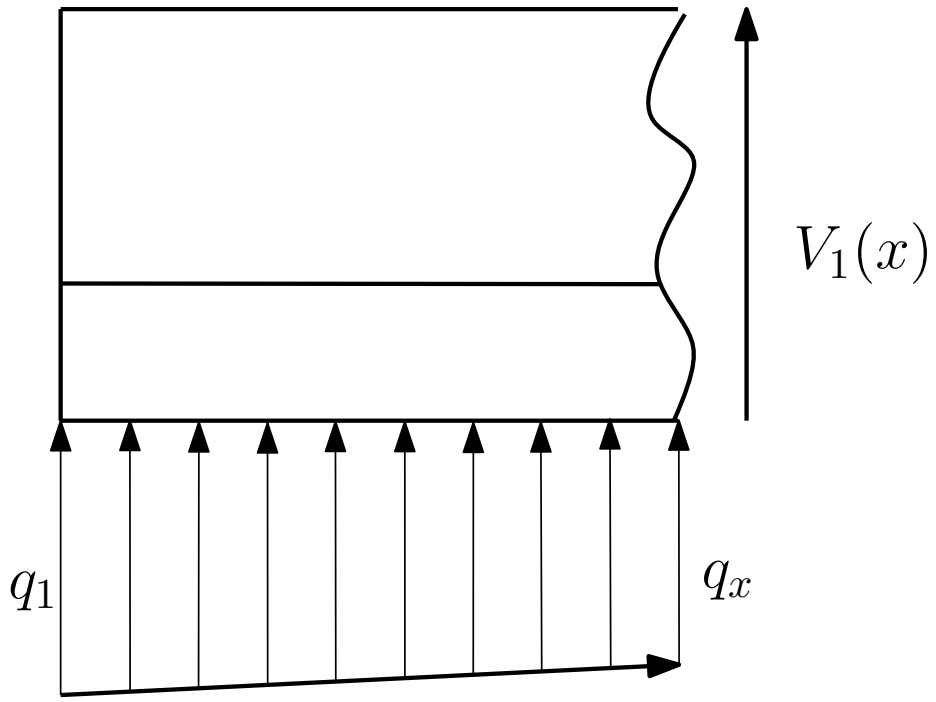

Figure 3.4: Shear distribution in the Substrate: Debonded section SCB

In the substrate of the debonded section, there is no transverse displacement and we are only interested in the transverse shear in the substrate. We can take the shear equilibrium in the substrate (using Figure 3.4) to get:

$$V_s + \int_{-a}^{x} q_x dx = 0 \tag{3.28}$$

From the above equations, we obtain the displacement and section rotations in the debonded top face and the substrate:

$$w_d = e_{1d}x^3 + e_{2d}x^2 + e_{3d}x + e_{4d}\ ; \qquad \phi_d = 3e_{1d}x^2 + 2e_{2d}x + e_{\phi_d} \tag{3.29}$$

And from Equation 3.28, we get

$$\phi_s = -\frac{(a+x)(2lq_1 + a(q_1+q_2) + (-q_1+q_2)x)}{2(a+l)(\kappa GA)_s} \tag{3.30}$$

It is important to note that in the general solutions (Equation 3.29 & Equation 3.30) there are 5 more unknown coefficients, namely, the e_{id}, i =1,2,3,4; and the e_{ϕ_d}. We need to solve for these unknown coefficients in order to determine the complete displacements and rotations of the beam sections. In total, we have 10 unknown coefficients from general solutions in the debonded and bonded section of the beam.

3.3 Boundary Conditions

In the Single Cantilever Beam (SCB) specimen, the debonded top face sheet is under external bending moment and shear force as shown in Figure. At the left end, x = -a, the bending moment and the shear forces on the top face sheet are

$$V_d = -(\kappa GA)_d(w_d' - \phi_d)|_{-a} = -(\kappa GA)_d(e_{3d} - e_{\phi_d}) \tag{3.31}$$

$$M_d = EI_d\phi_d'|_{-a} = EI_d(-6e_{1d}a + 2e_{2d}) \tag{3.32}$$

At the crack tip, x = 0, the bending moment on the debonded part is

$$M_d + V_d a = EI_d\phi_d'|_0 = EI_d 2e_{2d} \tag{3.33}$$

At the crack tip, $x = 0$, we also have continuity conditions on the top face sheet across the debonded section and the bonded section of the beam. *Displacement continuity*:

$$e_{4d} = c_{1d} + c_{p_2} \tag{3.34}$$

Beam rotation continuity:

$$e_{\phi_d} = \frac{1}{(k_1^2 + k_2^2)(\kappa GA)_d}\left[k_n(-c_{2d}k_1 + c_{3d}k_2) + (c_{2d}k_1 + c_{3d}k_2)(k_1^2 + k_2^2)(\kappa GA)_d\right] + c_{\phi_d} \tag{3.35}$$

Bending moment continuity:

$$2e_{2d} = 2c_{4d}k_1k_2 + c_{1d}(k_1^2 - k_2^2) - c_{1d}\frac{k_n}{(\kappa GA)_d} - k_n\frac{c_{p_2}}{(\kappa GA)_d} \tag{3.36}$$

Shear force continuity:

$$\begin{aligned} e_{3d} - e_{\phi_d} = &- \frac{1}{(k_1^2 + k_2^2)(\kappa GA)_d}\left[k_n(-c_{2d}k_1 + c_{3d}k_2) + (c_{2d}k_1 + c_{3d}k_2)(k_1^2 + k_2^2)(\kappa GA)_d\right] + \\ &+ c_{2d}k_1 + c_{3d}k_2 + c_{p_1} - c_{\phi_d} \end{aligned} \tag{3.37}$$

At the right end, x = l, we have free end conditions. The shear force and bending moment on the top face sheet is zero.

$$\begin{aligned}
\phi_d'(l) =& \left(2c_{4d}k_1k_2 + c_{1d}(k_1^2 - k_2^2) - c_{1d}\frac{k_n}{(\kappa GA)_d}\right)\cosh(k_1l)\cos(k_2l) + \\
&+ \left(2c_{3d}k_1k_2 + c_{2d}(k_1^2 - k_2^2) - c_{2d}\frac{k_n}{(\kappa GA)_d}\right)\sinh(k_1l)\cos(k_2l) + \\
&+ \left(-2c_{2d}k_1k_2 + c_{3d}(k_1^2 - k_2^2) - c_{3d}\frac{k_n}{(\kappa GA)_d}\right)\cosh(k_1l)\sin(k_2l) + \\
&+ \left(-2c_{1d}k_1k_2 + c_{4d}(k_1^2 - k_2^2) - c_{4d}\frac{k_n}{(\kappa GA)_d}\right)\sinh(k_1l)\sin(k_2l) - \\
&- \frac{k_n}{(\kappa GA)_d}(c_{p_1}l + c_{p_2}) = 0 \qquad (3.38)
\end{aligned}$$

$$\begin{aligned}
(w_d' - \phi_d)(l) =& \frac{k_n}{(\kappa GA)_d(k_1^2 + k_2^2)}\Big[(c_{2d}k_1 - c_{3d}k_2)\cosh(k_1l)\cos(k_2l) + \\
&+ (c_{1d}k_1 - c_{4d}k_2)\sinh(k_1l)\cos(k_2l) + \\
&+ (c_{4d}k_1 + c_{1d}k_2)\cosh(k_1l)\sin(k_2l) + \\
&+ (c_{3d}k_1 + c_{2d}k_2)\sinh(k_1l)\sin(k_2l)\Big] \\
&+ c_{p_1} - c_{\phi_d} + \frac{(2c_{p_2}k_nl + c_{p_1}k_nl^2)}{2(\kappa GA)_d} = 0 \qquad (3.39)
\end{aligned}$$

It is also important to note that the hyperbolic cosine and sine functions can quickly become very large numbers, unlike the hyperbolic tan function, and this would make the numerical solution fail, thus we divide by $\cosh k_1l$, to obtain

$$\begin{aligned}
&\left(2c_{4d}k_1k_2 + c_{1d}(k_1^2 - k_2^2) - c_{1d}\frac{k_n}{(\kappa GA)_d}\right)\cos(k_2l) + \\
&+ \left(2c_{3d}k_1k_2 + c_{2d}(k_1^2 - k_2^2) - c_{2d}\frac{k_n}{(\kappa GA)_d}\right)\tanh(k_1l) + \cos(k_2l) + \\
&+ \left(-2c_{2d}k_1k_2 + c_{3d}(k_1^2 - k_2^2) - c_{3d}\frac{k_n}{(\kappa GA)_d}\right)\sin(k_2l) + \\
&+ \left(-2c_{1d}k_1k_2 + c_{4d}(k_1^2 - k_2^2) - c_{4d}\frac{k_n}{(\kappa GA)_d}\right)\tanh(k_1l)\sin(k_2l) - \\
&- \frac{k_n}{\cosh k_1l(\kappa GA)_d}(c_{p_1}l + c_{p_2}) = 0 \qquad (3.40)
\end{aligned}$$

Further,

$$\frac{k_n}{(\kappa GA)_d(k_1^2+k_2^2)}\Big[(c_{2d}k_1-c_{3d}k_2)\cos(k_2l)+(c_{1d}k_1-c_{4d}k_2)\tanh(k_1l)\cos(k_2l)+$$
$$+(c_{4d}k_1+c_{1d}k_2)\sin(k_2l)+(c_{3d}k_1+c_{2d}k_2)\tanh(k_1l)\sin(k_2l)\Big]+$$
$$+\frac{c_{p_1}}{\cosh(k_1l)}-\frac{c_{\phi_d}}{\cosh(k_1l)}+\frac{(2c_{p_2}k_el+c_{p_1}k_el^2)}{2(\kappa GA)_d\cosh k_1l}=0 \tag{3.41}$$

In Equation 3.41, the term $\cosh(k_1l)$ is very large and close to zero for cases when k_1l is large. While solving these equations for finding the unknown coefficients, it is necessary to neglect this term to avoid numerical error. These terms are negligibly small (in the range of 10^{-20} - 10^{-50}) and almost zero for most beam lengths and material combinations that are commonly used. Hence, Equation 3.39 is simplified to:

$$\frac{k_n}{(\kappa GA)_d(k_1^2+k_2^2)}\Big[(c_{2d}k_1-c_{3d}k_2)\cos(k_2l)+(c_{1d}k_1-c_{4d}k_2)\tanh(k_1l)\cos(k_2l)+$$
$$+(c_{4d}k_1+c_{1d}k_2)\sin(k_2l)+(c_{3d}k_1+c_{2d}k_2)\tanh(k_1l)\sin(k_2l)\Big]=0 \tag{3.42}$$

We now have 9 equations (Equation 3.31-Equation 3.42), we need an additional condition to evaluate all the unknown constants. In the SCB specimen, the bottom substrate is supported and at the right end, $x=l$, we can assume that the transverse displacement is zero throughout the right end as it is far from the crack tip. So

$$w_d(l)=c_{1d}\cosh k_1x\cos k_2x+c_{2d}\sinh k_1x\cos k_2x+c_{3d}\cosh k_1x\sin k_2x+$$
$$+c_{4d}\sinh k_1x\sin k_2x+c_{p_1}l+c_{p_2}=0 \tag{3.43}$$

Again, to avoid numerical failure, we divide the above equation by $\cosh k_1l$ to get

$$c_{1d}\cos k_2x+c_{2d}\tanh k_1x\cos k_2x+c_{3d}\sin k_2x+$$
$$+c_{4d}\tanh k_1x\sin k_2x+\frac{c_{p_1}l}{\cosh k_1l}+\frac{c_{p_2}}{\cosh k_1l}=0 \tag{3.44}$$

Now, we have 10 linear algebraic equations from (Equation 3.31-Equation 3.44) and the unknown coefficients c_{id} & e_{id} (i = 1,2,3,4) of the general solutions can be solved for by solving these equations using a simple computer program.

3.4 Energy Release Rate

Once we have solved the governing equations, the displacements and the section rotations of the beam section can be used to obtain the fracture parameters. In previous chapter, we obtained the energy release rate using J-Integral.

3.4.1 J-Integral

J-Integral defined in Equation 2.96 with the integration path shown in Figure 3.5 is used to the obtain the energy release rate.

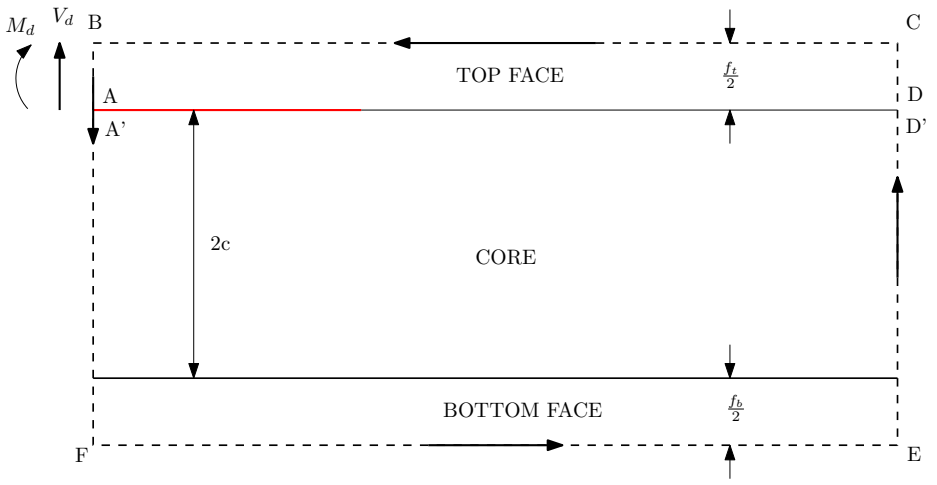

Figure 3.5: J-Integral path - SCB specimen

On both the top and bottom horizontal segments of the path, dz = 0. And on the top segment, there is no traction $\vec{T}$=0, thus J_{CB}=0. On the bottom horizontal segment (FE),

$$T_i \frac{\partial u_i}{\partial x} = -\tau_{xz}\epsilon_{xx} - \sigma_{zz}w_{,x} \tag{3.45}$$

where, w is the transverse displacement and we use "," to denote the partial derivation. In SCB specimen, the bottom horizontal segment has fixed support (zero transverse displacement, w, throughout the segment FE) which also means that $w_{,x}$=0. Moreover, since the reaction at the bottom edge is along the transverse direction only and no additional shear loads are applied, τ_{xz} can also be assumed to be zero. Thus, on the bottom horizontal segment of the path, we also have J_{EF}=0. On the vertical sides:

$$W = \frac{1}{2}(\sigma_{xx}\epsilon_{xx} + \sigma_{zz}\epsilon_{zz} + \tau_{xz}\gamma_{xz}) \tag{3.46}$$

On the vertical sides that are not loaded (AF',CD and D'E), $\vec{T}$=0, which means σ_{xx}=τ_{xz}=0 and in the case of plane stress σ_{zz}=0. For a plane strain assumption (ϵ_{zz}=0) σ_{zz}=$\nu_{xz}\sigma_{xx}$=0. Therefore, on these sides, it is also W=0. As a result, on the vertical sides A'F, ED', D'C, we have J=0. We are left with side AB and on this segment, dz==-ds

$$dJ = \left[\frac{1}{2}(\sigma_{xx}\epsilon_{xx} - \tau_{xz}\gamma_{xz}) + \tau_{xz}\phi_d)\right]ds \tag{3.47}$$

We assume that the shear load creates a shear stress τ_{xz} and a shear strain γ_{xz}=$\kappa\tau_{xz}/G_{eq}$, where G_{eq} is the equivalent shear modulus of the section and κ is the shear correction factor, which takes into account the non-uniform distribution of shear stresses due to the sandwich construction throughout the entire cross section. For the debonded part, which is homogeneous, the equivalent shear modulus is the shear modulus of the top face, G_{eq}=G_{f_t} and the shear correction factor,

$$\kappa_d = \frac{6}{5} \tag{3.48}$$

On the segment BA, where dz=-ds:

$$dJ = \frac{1}{2}(\sigma_{xx}\epsilon_{xx} + \sigma_{zz}\epsilon_{zz} + \tau_{xz}\gamma_{xz})(-ds) - (-\sigma_{xx}\epsilon_{xx} - \tau_{xz}\phi_d)(ds) \tag{3.49}$$

From plane stress assumption, σ_{zz}=0, and ϵ_{xx}=σ_{xx}/E_{ft},

$$dJ = \left[\frac{1}{2}(\sigma_{xx}\epsilon_{xx} - \tau_{xz}\gamma_{xz}) + \tau_{xz}\phi_d)\right]ds \tag{3.50}$$

$$J_{BA} = \int_{-f_t/2}^{f_t/2}\left[\frac{1}{2E_{ft}}\sigma_{xx}^2 - \frac{\kappa_d}{2G_{eq}}\tau_{xz}^2 + \tau_{xz}\phi_d|_{-a}\right]ds \tag{3.51}$$

Substituting $EI_d = E_d b f_t^3/12$ and $A_d = bf_t$, we get

$$J_{BA} = \frac{6M_d^2}{E_d f_t^3} - \frac{\kappa_d V_d^2}{2G_{eq}b^2 f_t} - \frac{V_d}{b}\phi_d|_{-a} \tag{3.52}$$

To evaluate the J-integral, we need to find $w_{d,x}|_{-a}$

$$\phi_d(-a) = 3e_{1d}a^2 - 2e_{2d} + e_{\phi_d} \tag{3.53}$$

Therefore, we obtain the J-integral as

$$J = \frac{6M_d^2}{E_d f_t^3} - \frac{\kappa_d V_d^2}{2G_{eq}b^2 f_t} - \frac{V_d}{b}\Big(3e_{1d}a^2 - 2e_{2d} + e_{\phi_d}\Big) \tag{3.54}$$

The above equation will give us the energy release release in the single cantilever sandwich beam subjected to shear force and bending moment.

3.4.2 Rate of Energy Released by the springs

Similar to DCB specimen, the energy released released during debonding can be obtained by finding the energy stored in the springs due to the deformations in the beam. Let the differential spring length be da, the energy released by the crack when it propagates by length da is the energy stored in this differential spring element. And the total energy released by the springs in the foundation is given by

$$G_{spring} = \lim_{\delta a \to 0} \frac{1}{2\delta a} \int_0^{\delta a} \sigma_{zz}(r) \Delta w(\delta a - r)\, dr \tag{3.55}$$

We can obtain expressions for the energy released using the displacements of the springs near the crack tip

$$G_{spring} = \frac{1}{2} k_e [w_d(0) - w_s(0)]^2 + \frac{1}{2} k_r [\phi_d(0) - \phi_s(0)]^2 \tag{3.56}$$

The beam rotation in the substrate at the crack tip is given by Equation 3.30

$$\phi_s(0) = -a \frac{(2lq_1 + a(q_1 + q_2))}{2(a + l)(\kappa GA)_s} \tag{3.57}$$

So, an alternate expression to find the energy released when the crack grows is

$$G_{spring} = \frac{1}{2} k_e (e_{4d})^2 + \frac{1}{2} k_r \left(e_{\phi_d} + a \frac{(2lq_1 + a(q_1 + q_2))}{2(a + l)(\kappa GA)_s} \right)^2 \tag{3.58}$$

3.5 Mode Partitioning

Here, we are using an alternate approach to obtain the mode mixity, using displacements near the crack tip. In this approach, a mode partitioning phase angle, ψ_{EF}, is defined from the relative crack flank opening and shearing displacements (δ_w and δ_u respectively).

$$\psi_{EF} = tan^{-1} \frac{\delta u}{\delta w} = tan^{-1} \left(\frac{u_{d_o} - u_{s_o}}{w_{d_o} - w_{s_o}} \right) \tag{3.59}$$

It is defined such that ψ_{EF} = 0 if only crack flank opening occurs near the crack tip and ψ_{EF} = 90 if only crack flank shearing occurs near the crack tip. Using the solutions for the

displacements, we obtain

$$\psi_{EF} = tan^{-1}\left(\frac{\frac{f_t}{2}e_{\phi_d} + c(\phi_s(0))}{e_{4d}}\right) \tag{3.60}$$

3.6 Results and Discussion

We choose a symmetrical sandwich beam with faces made out of isotropic face and core materials. The material properties used are given in Table 3.1. The geometry of the beam was chosen to have face thicknesses f_t = f_b = 2mm and the core to have a thickness of 2c = 20mm. The total length of the beam was chosen as 500mm and the debond length to be 200mm.

Table 3.1: SCB: Material Properties

Aluminium face (isotropic)	Aluminium foam core (isotropic)	H100 core(isotropic)
E = 70,000 MPa	E = 7,000 MPa	E = 130 MPa
G = 26,923 MPa	G = 2651.5 MPa	G = 50 MPa
ν = 0.30	ν = 0.32	ν = 0.30

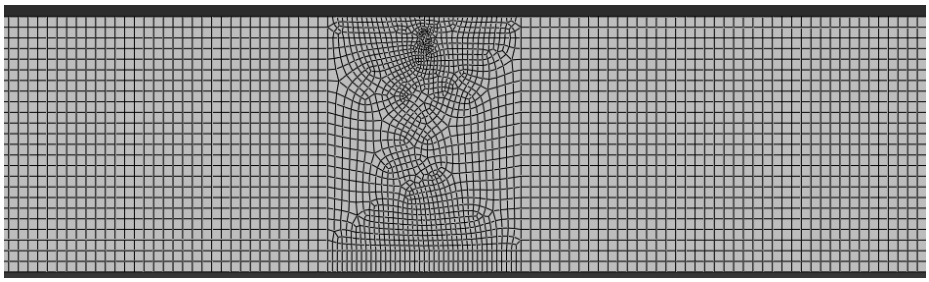

Figure 3.6: FEA Mesh - SCB Beam

We chose isotropic face and core materials because commercial finite softwares can only calculate stress intensity factors for an interfacial crack when both the face & core materials are linear elastic and isotropic. To validate the results we obtain from the elastic foundation approach, we model the Single Cantilever Beam (SCB) specimen in ABAQUS using isoparametric eight-node biquadratic plane stress (CPS8R - second order 8-noded

quad plane stress) elements. The interface crack in the SCB specimen is modeled using seam cracks. The singular elements were used near the crack tip to include stress singularity, these elements have the midpoint moved to one quarter side distance from the original midpoint position to the node. We also use 6-noded triangle plane stress elements (CPS6M) near the crack tip. And, the stress intensity factor values are evaluated using the contour integral in ABAQUS. Here, K_I and K_{II} are obtained using interaction integral method. In the FEA model, we ignore the large deformation effects and perform a linear analysis. The mode mixity from FEA is obtained using the stress intensity values

$$\psi_{FEA} = \tan^{-1}\left(\frac{K_{II}}{K_I}\right) \tag{3.61}$$

The expressions obtained for energy release rate and mode partitioning are simple. Using these expressions, we obtained results for two different core materials (Table 3.1).

Table 3.2 shows the values of energy release rates obtained using the closed form expression (subscript EF) and also the energy release rate values from ABAQUS (J_{FEA}). Here, we have obtained the values for the case of SCB sandwich with Al face and Al Foam core. In Single Cantilever beam specimen, the top face is subjected to both shear load and bending moment. We are comparing the fracture parameters for different loading conditions to see if there are any effects. It can be seen that values show excellent agreement with each other. Also, when compared with the previous values from previous elastic foundation model using Euler-Bernoulli [46] ($J_{ref_{46}}$), the values obtained using the model presented here are in better agreement with the values from FEA. In addition, J_{spring} shows the energy released by the springs and the value are comparable to the values from FEA.

We have also obtained the mode partitioning measure obtained using Timoshenko Beam theory (ψ_{EF}). It should be emphasized that in the elastic foundation approach, there is no crack tip beyond which the top face and the core are bonded and have the same axial and transverse displacements. Here, we have normal and shear springs at the interface and

thus there is a gap in the mathematical elastic foundation model. Hence, we use the mode partitioning measure values (ψ_{EF}) and they are compared with the mode mixity values FEA (ψ_{FEA}) and mode partitioning values from Euler Bernoulli model [10] $J_{ref_{46}}$. It can be seen that the J_{EF} values are in excellent agreement with the finite element results. The mode partitioning measure values from this model (J_{EF}) are consistently better than the values from the previous elastic foundation model based on Elastic Foundation model ($\psi_{ref_{46}}$).

Table 3.2: SCB: Energy release rate and mode partitioning - Al Face & Al Foam Core

V_d (N)	M_d (N-mm)	$J_{ref_{46}}$ (N/mm)	J_{EF} (N/mm)	J_{FEA} (N/mm)	G_{spring} (N/mm)	$\psi_{ref_{46}}$ (deg)	ψ_{EF} (deg)	ψ_{FEA} (deg)
0.5	0.0	0.1111	0.1102	0.1098	0.1085	-28.0	-31.3	-31.1
0.0	100	0.1071	0.1071	0.1071	0.1054	-28.3	-31.7	-31.4
0.5	100	0.4365	0.4347	0.4338	0.4276	-28.1	-31.5	-31.3

In sandwich composite beam, the core is usually made of low density materials. The main advantage of the model presented here is that this can be used for both isotropic and orthotropic materials. It can be used to quickly obtained the results for both these material types and can be adapted for plane strain case as well. Table 3.3 we obtained the energy release rate and mode partitioning values for a soft H100 core and beam with same geometry. It can be noticed that the model presented here show very good agreement with the FEA values and are better than the values obtained from Euler-Bernoulli beam model [46].

Table 3.3: SCB: Energy release rate and mode partitioning - Al Face & H100 Core

V_d (N)	M_d (N-mm)	$J_{ref_{46}}$ (N/mm)	J_{EF} (N/mm)	J_{FEA} (N/mm)	G_{spring} (N/mm)	$\psi_{ref_{46}}$ (deg)	ψ_{EF} (deg)	ψ_{FEA} (deg)
0.5	0.0	0.1183	0.1177	0.1176	0.1140	-10.9	-8.8	-9.0
0.0	100	0.1071	0.1071	0.1071	0.1033	-11.1	-10.2	-9.4
0.5	100	0.4506	0.4494	0.4491	0.4342	-11.0	-9.5	-9.2

Further, we studied the effect of core stiffness on the accuracy of the model. In Table 3.2, we looked at the beam with Aluminium faces and Aluminium core ($E_f/E_c = 10$).

In Table 3.4 & Table 3.5, we have obtained fracture parameters for various stiffness ratios (keeping same Al faces only changing the core material). We can see that J_{EF} values obtained for even soft core materials are in excellent agreement with the FEA values from ABAQUS. The mode partitioning values obtained here also follow the same trend as the values from FEA and [46]. ψ_{EF} are in better agreement with ψ_{FEA} when compared to $\psi_{ref_{10}}$. Here, we can see that for very soft core materials ($E_f/E_c > 500$), the mode partitioning values are slightly off. It is still a very good estimate, but this difference could be due to the use of first order shear deformation theory which is inadequate at these very low core stiffness.

Table 3.4: SCB: Effect of Core Stiffness for V_d=0.5 Nt, M_d=0. Debond length a=200mm

E_f/E_c	$J_{ref_{46}}$ (N/mm)	J_{EF} (N/mm)	J_{FEA} (N/mm)	$\psi_{ref_{46}}$ (deg)	ψ_{EF} (deg)	ψ_{FEA} (deg)
10	0.1110	0.1102	0.1100	-28.0	-31.3	-31.1
50	0.1130	0.1124	0.1180	-19.0	-20.3	-21.3
100	0.1140	0.1136	0.1130	-15.7	-16.6	-17.3
200	0.1150	0.1150	0.1150	-12.7	-13.3	-13.6
500	0.1180	0.1174	0.1180	-9.0	-9.2	-9.4
800	0.1190	0.1188	0.1190	-7.2	-6.9	-7.5
1000	0.1200	0.1195	0.1200	-6.3	-5.7	-6.6

Table 3.5: SCB: Effect of Core Stiffness for V_d=0.5 Nt, M_d=100Nmm. Debond length a=200mm

E_f/E_c	$J_{ref_{46}}$ (N/mm)	J_{EF} (N/mm)	J_{FEA} (N/mm)	$\psi_{ref_{46}}$ (deg)	ψ_{EF} (deg)	ψ_{FEA} (deg)
10	0.4360	0.4347	0.4340	-28.0	-31.5	-31.3
50	0.4400	0.4390	0.4380	-19.0	-20.6	-21.5
100	0.4430	0.4414	0.4400	-15.7	-16.9	-17.5
200	0.4450	0.4442	0.4430	-12.7	-13.7	-13.8
500	0.4500	0.4488	0.4490	-9.0	-9.8	-9.6
800	0.4530	0.4515	0.4520	-7.2	-7.8	-7.8
1000	0.4540	0.4529	0.4540	-6.3	-6.7	-6.8

Table 3.4 & Table 3.5 are for different loading conditions. Table 3.4 is for $V_d = 0.5N$ and $M_d = 0$ load case and Table 3.5 is for $V_d = 0.5N$ and $M_d = 100Nmm$. It is clear that the model can provide very good estimate of the fracture parameters for different loading conditions and material combinations.

Table 3.6: SCB: Results for a smaller debond length, a=20mm. Aluminium Foam (7 GPa) Core

V_d (N)	M_d (N-mm)	J_{EF} (N/mm)	J_{FEA} (N/mm)	G_{spring} (N/mm)	ψ_{EF} (deg)	ψ_{FEA} (deg)
0.5	0.0	0.0014	0.0014	0.0014	-28.6	-28.3
0.0	100	0.1071	0.1070	0.1052	-31.9	-31.4
0.5	100	0.1330	0.1330	0.1306	-31.6	-31.1

Table 3.7: SCB: Results for a smaller debond length, a=20mm. H100 (0.13 GPa) Core

V_d (N)	M_d (N-mm)	J_{EF} (N/mm)	J_{FEA} (N/mm)	G_{spring} (N/mm)	ψ_{EF} (deg)	ψ_{FEA} (deg)
0.5	0.0	0.0023	0.0023	0.0023	-7.2	-6.3
0.0	100	0.1071	0.1070	0.1028	-11.3	-9.5
0.5	100	0.1412	0.1412	0.1357	-10.7	-9.1

Next, we also obtained values for the case of a small crack (a = 20mm) for two different core materials in Table 3.6. & Table 3.7. The energy release rate values and the mode partitioning values show excellent agreement with the finite element values. It can be safely said that the results are accurate for smaller debond length.

3.7 Conclusion

Elastic foundation analysis is used to obtain closed form solutions for energy release rates and mode partitioning of face/core debonds in Single Cantilever beam specimen. The SCB specimen is divided in four parts: two along its length, namely debonded part and bonded part and two along its thickness, namely debonded face and substrate, which includes the core and the bottom face. An elastic foundation approach based on the Timoshenko beam theory is pursued to obtain the governing equations. The model pursued here is comprehensive and includes the deformation of the substrate in the governing equations. The solutions are obtained such that these solutions are valid for both isotropic and orthotropic faces and core and can be applied for a general asymmetric sandwich beam (top and bottom faces not the same). Energy release rate is obtained using J-Integral approach and it shows excellent agreement with the results from finite element analysis for various loading conditions and material combinations. A mode partitioning measure based on the relative crack flank opening and shearing displacements is here. The results show that this mode partitioning values closely follow the traditional mode mixity values from finite element analysis.

CHAPTER 4

CRACK FACE CONTACT MODEL - TENSIONLESS FOUNDATION

So far, we have have looked at mode I dominant fracture specimens. When we look at a End-Notched Flexure specimen (Figure 4.1), it is mode II dominant and in this case the effects of crack face contact can be significant. Here, we are extending the elastic foundation analysis by introducing a tensionless spring foundation in the cracked region. This is a novel approach, where tensionless springs are used to capture the compressive stresses across the interface between the debonded face sheet and the substrate. The absence of tensile stresses in the foundation is because when there is tension the debonded face sheet lifts away from the substrate. An End Notched Flexure sandwich specimen is widely used test specimen for mode II fracture. It is a simply supported beam with a shear load at the middle of the beam. The ENF sandwich beam is divided into 4 regions along its length as shown in Figure 4.2. Region I & II form the cracked portion of the beam and Region III & IV together form the bonded portion of the beam. For an ENF specimen, it has been shown in experiments that there is a significant contact zone near the end support in the cracked section. In the region of debond, the sandwich beam consists of two parts: the debonded part (debonded upper face sheet) and the substrate. In the case of Mode II/III dominated crack, there will be contact between the debonded part and the substrate. From literature, it has been shown that the contact plays a significant role in affecting the energy release rate and mode mixity.

Across the interface between crack faces, only compressive stresses are transmitted when there is contact. The absence of tensile stresses in the cracked region is because the debonded face sheet lifts away from the substrate. Tensionless spring foundation can be used to model the crack face contact. A beam of length $2L$ with a crack of length a is chosen. The beam is pinned on both the ends and has a shear load P at the middle of the

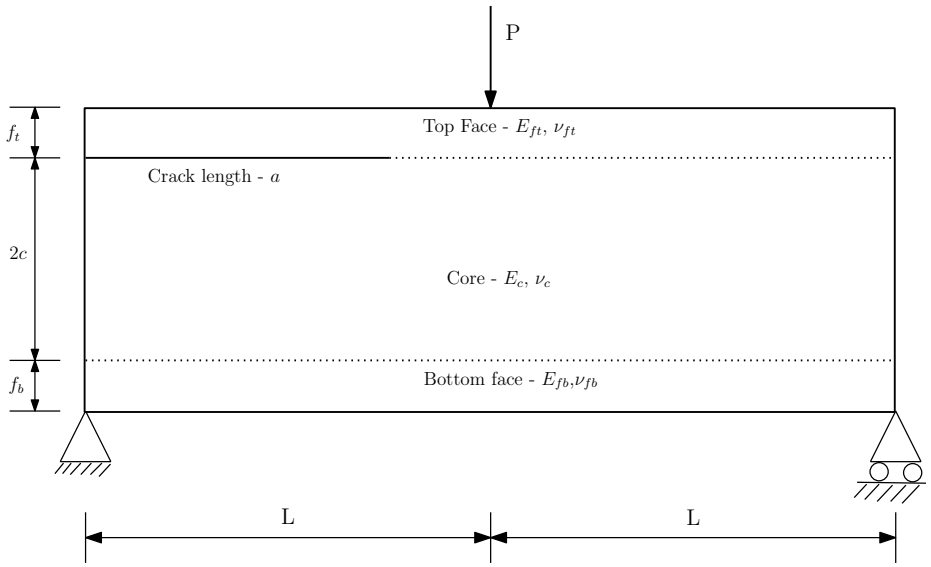

Figure 4.1: End-Notched Flexure Specimen

beam.

Here, the beam is divided into four regions Figure 4.2: Region III & IV together form the bonded section of the beam. In the bonded section of the beam, we use elastic foundation to capture the effects of crack tip deformations. Whereas in the cracked section, region I & II are the regions of contact and no-contact respectively. In region I, we introduce tensionless spring foundation to capture only the compressive stresses that are acting across the crack face contact.

4.1 Governing equations

We are using elastic foundation at the interface between top face and the core in the bonded section. The elastic foundation consists of only normal springs in the bonded section of the beam. And in the cracked section, we have two regions, Region I - we use tensionless spring foundation to model the contact region and Region II - free region in the cracked section of the beam and we use simple beam theory to obtain the governing equations in this region. This is a novel approach and we are first using Euler Bernoulli Beam theory to develop the governing equations for this case.

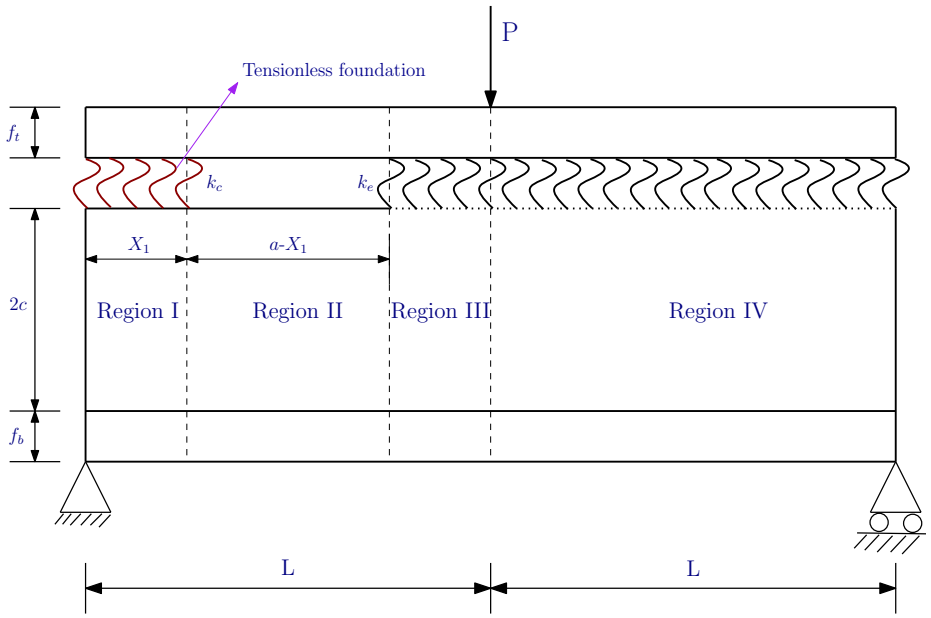

Figure 4.2: Tensionless Foundation in ENF Specimen

It should also be noted that the formulation and approach are applicable to both beams (plane stress) and wide panels (plane strain) but different moduli should be used for plane strain and plane stress problems. The solutions provided are for the plane stress case and for plane strain, E (Young's Modulus) should be replaced by $E/(1-\nu^2)$, where ν is Poisson's ratio.

4.1.1 Cracked section

In the cracked section of the beam, we are introducing tensionless spring foundation to capture the transfer of compressive stresses across the debonded top face sheet and the substrate. In the cracked portion, contact is present across the debonded face and substrate only in certain zones and they are called contact zones. In this type of specimen, we will have a contact zone near the crack tip and another contact zone near the support region. In literature, it has been shown from various experiments that the contact zone near the support is significant. This is Region I shown in Figure 4.2 and the tensionless foundation is used here to model the contact zone. The length of the contact region (Region I) is unknown. The tensionless foundation introduces a unknown contact length(X_1) in addition

to the unknown constants from the solutions of governing equations.

Weitsman [63] has worked on foundation that react in compression only. The model employed in the study involved only linear differential equations. And when a foundation is tensionless, the existence of gaps between the structure and the foundations introduces additional unknowns into the problem. It was further extended in several studies [64, 65] for beams resting on the tensionless foundation. Using this approach we extend the elastic foundation analysis to capture the compressive stresses in region I.

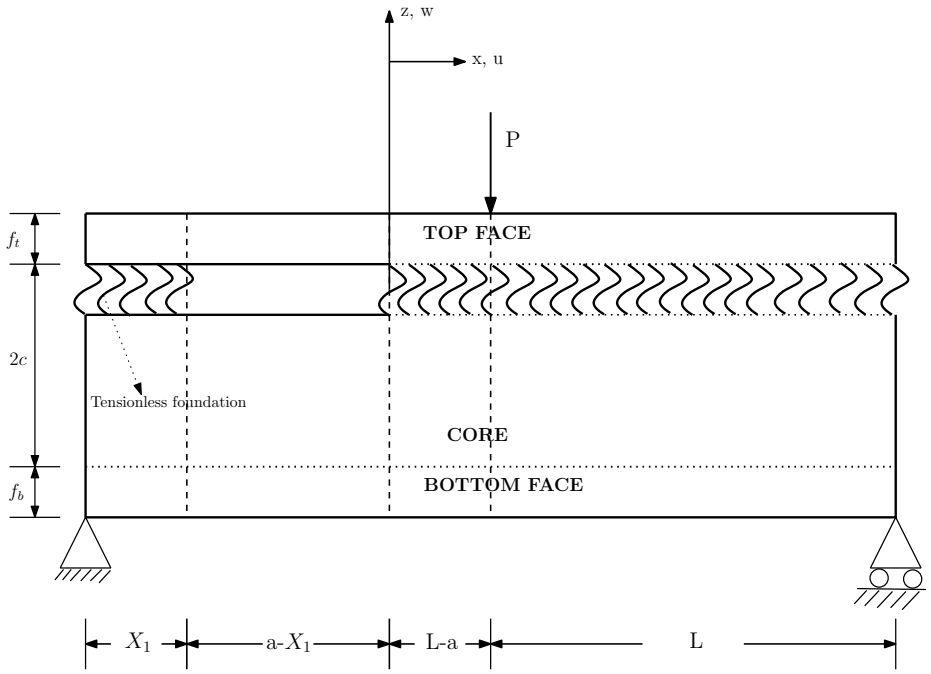

Figure 4.3: Coordinate System in the ENF specimen

The elastic foundation here is assumed only to react when there is compression and the modulus of the tensionless foundation is k_t. At the interface between debonded part and the substrate, compression occurs only when $w_d < w_s$. When $w_d > w_s$, it means the crack is open and there is no contact or transfer of stresses across the debonded top face and the substrate. The coordinate system is set so that x = 0 is at the crack tip (shown in Figure 4.3), i.e., the debond is negative for x and the intact part is for positive x. Thus, the governing

equations are:

$$EI_d \frac{d^4 w_{d_I}}{dx^4} + S(x) k_t (w_{d_I} - w_{s_I}) = 0 \qquad -a \leq x \leq 0 \tag{4.1}$$

$$EI_s \frac{d^4 w_{s_I}}{dx^4} + S(x) k_t (w_{s_I} - w_{d_I}) = 0 \qquad -a \leq x \leq 0 \tag{4.2}$$

where $k_t(w_{d_I} - w_{s_I})$ term represents the compressive force distribution and X_1 is the length of the contact zone from the left end. Also, X_1 is unknown and we will need to find its value when we solve the equations. The function S(x) is a step function allowing to separate the contact region and the non-contact region in the cracked portion of the beam. Region I and II can be separated as:

$$S(x) = \begin{cases} 1 & \text{if } -a \leq x \leq -a + X_1 \qquad \text{Region I: } w_{d_I} \leq w_{s_I} \\ 0 & \text{if } -a + X_1 \leq x \leq 0 \qquad \text{Region II: } w_{d_I} \geq w_{s_I} \end{cases} \tag{4.3}$$

In Region I:

For the crack face contact part $-a \leq x \leq -a + X_1$, $S(x) = 1$, substituting w_d from Equation 4.2 into Equation 4.1 results in

$$\frac{(EI)_s}{k_t} \frac{d^8 w_{s_I}}{dx^8} + \left[1 + \frac{(EI)_s}{(EI)_d}\right] \frac{d^4 s_I}{dx^4} = 0 \tag{4.4}$$

with

$$w_{d_I} = \frac{(EI)_s}{k_t} \frac{d^4 w_{s_I}}{dx^4} + w_{s_I} \tag{4.5}$$

Then setting,

$$\lambda_1 = k_t \frac{(EI)_d + (EI)_s}{4(EI)_d (EI)_s} \tag{4.6}$$

Equation 4.4 can be written in the form

$$\frac{d^8 w_{s_I}}{dx^8} + 4\lambda_1^4 \frac{d^4 w_{s_I}}{dx^4} = 0 \tag{4.7}$$

The tensionless spring foundation modulus (k_t) value is chosen based on the study by Kardomateas et al. [45]. This modulus value is same the modulus in the elastic foundation in region III & IV. Only difference being, foundation in region I reacts only in compression and its modulus is given by

$$k_t = \frac{c_{33}^c}{c} b \tag{4.8}$$

where

$$c_{33}^c = E_3^c \frac{(1 - \nu_{12}^c \nu_{21}^c)}{1 - (\nu_{12}^c \nu_{21}^c + \nu_{23}^c \nu_{32}^c) + \nu_{13}^c \nu_{31}^c) - (\nu_{12}^c \nu_{23}^c \nu_{31}^c + \nu_{21}^c \nu_{32}^c \nu_{13}^c)} \tag{4.9}$$

where we have adopted the convention 1 $\equiv$ x, 2 $\equiv$ y, and 3 $\equiv$ z; E_3^c is the transverse extensional modulus of the core; and the $\nu' s$ are Poisson's ratios of the core.

The general solutions for the transverse displacements from these governing equations are

$$w_{d_I} = \frac{-EI_s}{EI_d} \Big[D_1 \cosh \lambda_1 x \cos \lambda_1 x + D_2 \cosh \lambda_1 x \sin \lambda_1 x + D_3 \sinh \lambda_1 x \cos \lambda_1 x + \\ + D_4 \sinh \lambda_1 x \sin \lambda_1 x \Big] + D_5 x^3 + D_6 x^2 + D_7 x + D_8 \tag{4.10}$$

$$w_{s_I} = \Big[D_1 \cosh \lambda_1 x \cos \lambda_1 x + D_2 \cosh \lambda_1 x \sin \lambda_1 x + D_3 \sinh \lambda_1 x \cos \lambda_1 x + \\ + D_4 \sinh \lambda_1 x \sin \lambda_1 x \Big] + D_5 x^3 + D_6 x^2 + D_7 x + D_8 \tag{4.11}$$

In Region I, it can be noticed that the general solutions for the displacements have

hyperbolic functions and polynomials. There are 8 unknown coefficients in these equations.

In Region II:

In this region, there is no contact between the top debonded face and the substrate. Hence, the top debonded part and the substrate are independent and the governing equations (Equation 4.1 & Equation 4.2) are simplified to simple beam equations

$$EI_d \frac{d^4 w_{d_{II}}}{dx^4} = 0 \qquad -a + X_1 \leq x \leq 0 \tag{4.12}$$

$$EI_s \frac{d^4 w_{s_{II}}}{dx^4} = 0 \qquad -a + X_1 \leq x \leq 0 \tag{4.13}$$

And solving these equations, we get the general solutions as

$$w_{d_{II}} = e_{1d}x^3 + e_{2d}x^2 + e_{3d}x + e_{4d} \tag{4.14}$$

$$w_{s_{II}} = e_{1s}x^3 + e_{2s}x^2 + e_{3s}x + e_{4s} \tag{4.15}$$

We can the see that the general solutions for the displacements are simple polynomial equations and we have 8 unknown coefficients from this region.

4.1.2 Bonded section

We introduce an elastic foundation in the bonded region to capture the crack tip deformations. The governing equations are same in Region III and IV. There is a shear load acting between Region III & IV and both the regions have the elastic foundation with normal springs between the top face sheet and the substrate. The beam is split into two regions at $x = L - a$, where there is transverse shear load in the middle of the beam.

In Region III:

Here, the elastic foundation has a distribution of normal springs and the stiffness of the springs are k_n The governing equations in region III is given by,

$$(EI)_d \frac{d^4 w_{d_{III}}}{dx^4} + k_n(w_{d_{III}} - w_{s_{III}}) = 0 \qquad 0 \leq x \leq L - a \tag{4.16}$$

$$(EI)_s \frac{d^4 w_{s_{III}}}{dx^4} + k_n(w_{s_{III}} - w_{d_{III}}) = 0 \qquad 0 \leq x \leq L - a \tag{4.17}$$

Simplifying these equations, we get

$$\frac{(EI)_s}{k_n} \frac{d^8 w_{s_{III}}}{dx^8} + \left[1 + \frac{(EI)_s}{(EI)_d}\right] \frac{d^4 s_{III}}{dx^4} = 0 \tag{4.18}$$

with

$$w_{d_{III}} = \frac{(EI)_s}{k_n} \frac{d^4 w_{s_{III}}}{dx^4} + w_{s_{III}} \tag{4.19}$$

Then setting,

$$\lambda_2 = k_n \frac{(EI)_d + (EI)_s}{4(EI)_d(EI)_s} \tag{4.20}$$

Equation 4.4 can be written in the form

$$\frac{d^8 w_{s_{III}}}{dx^8} + 4\lambda_2^4 \frac{d^4 w_{s_{III}}}{dx^4} = 0 \tag{4.21}$$

The general solutions obtained from solving the governing equations (Equation 4.16 & Equation 4.17) are

$$w_{d_{III}} = \frac{-EI_s}{EI_d}\Big[C_1 \cosh\lambda_2 x \cos\lambda x + C_2 \cosh\lambda_2 x \sin\lambda_2 x + C_3 \sinh\lambda_2 x \cos\lambda_2 x + \\ + C_4 \sinh\lambda_2 x \sin\lambda_2 x\Big] + C_5 x^3 + C_6 x^2 + C_7 x + C_8 \tag{4.22}$$

$$w_{s_{III}} = \Big[C_1 \cosh\lambda_2 x \cos\lambda x + C_2 \cosh\lambda_2 x \sin\lambda_2 x + C_3 \sinh\lambda_2 x \cos\lambda_2 x + \\ + C_4 \sinh\lambda_2 x \sin\lambda_2 x\Big] + C_5 x^3 + C_6 x^2 + C_7 x + C_8 \tag{4.23}$$

From the general solutions, we have 8 unknown coefficients (C_i where i =1,...,8) in this region.

In Region IV:

In this region, the governing equations are similar to region III and they can be solved in the same way

$$(EI)_d \frac{d^4 w_{d_{IV}}}{dx^4} + k_n(w_{d_{IV}} - w_{s_{IV}}) = 0 \qquad L - a \le x \le 2L - a \tag{4.24}$$

$$(EI)_s \frac{d^4 w_{s_{IV}}}{dx^4} + k_n(w_{s_{IV}} - w_{d_{IV}}) = 0 \qquad L - a \le x \le 2L - a \tag{4.25}$$

Again the general solutions obtained from solving the governing equations are

$$w_{d_{IV}} = \frac{-EI_s}{EI_d}\Big[B_1 \cosh\lambda_2 x \cos\lambda_2 x + B_2 \cosh\lambda_2 x \sin\lambda_2 x + B_3 \sinh\lambda_2 x \cos\lambda_2 x + \\ + B_4 \sinh\lambda_2 x \sin\lambda_2 x\Big] + B_5 x^3 + B_6 x^2 + B_7 x + B_8 \tag{4.26}$$

$$w_{s_{IV}} = \Big[B_1 \cosh \lambda_2 x \cos \lambda_2 x + B_2 \cosh \lambda_2 x \sin \lambda_2 x + B_3 \sinh \lambda_2 x \cos \lambda_2 x + \\ + B_4 \sinh \lambda_2 x \sin \lambda_2 x \Big] + B_5 x^3 + B_6 x^2 + B_7 x + B_8 \quad (4.27)$$

From the general solutions (Equation 4.26 & Equation 4.27), we have 8 unknown coefficients (B_i where i =1,...,8).

4.2 Boundary and Continuity Conditions

From the general solutions for transverse displacements in all four regions, we have 32 unknown coefficients. In addition, we also have an unknown length of contact region (X_1). So, to find all these unknowns, we need atleast 33 equations. From the ENF specimen (shown in Figure 4.1), we have 8 boundary conditions and 24 continuity conditions (8 each from x = -a+ X_1, 0, L-a) and 1 additional condition at the end of the contact region. At the end of crack face contact, we known that the displacements of the debonded face and the substrate must be equal. This gives us an additional condition that we need to solve the unknown length of crack face contact (X_1).

In the End Notched Flexure specimen, the beam is pinned at the right end $x = 2L - a$,

so the bending moment and displacements are

$$
\begin{aligned}
&(EI)_d w''_{d_{IV}}|_{2L-a} = 0 \\
&= 2(-(EI)_s)\lambda_2^2\Big[B_4\cosh(\lambda_2(2L-a))\cos(\lambda_2(2L-a))- \\
&- B_3\cosh(\lambda_2(2L-a))\sin(\lambda_2(2L-a)) + B_2\sinh(\lambda_2(2L-a))\cos(\lambda_2(2L-a))- \\
&- B_1\sinh(\lambda_2(2L-a))\sin(\lambda_2(2L-a))\Big] + 6B_5(2L-a) + 2B_6 \qquad (4.28)
\end{aligned}
$$

$$
\begin{aligned}
&(EI)_s w''_{s_{IV}}|_{2L-a} = 0 \\
&= 2(EI)_s\lambda_2^2\Big[B_4\cosh(\lambda_2(2L-a))\cos(\lambda_2(2L-a))- \\
&- B_3\cosh(\lambda_2(2L-a))\sin(\lambda_2(2L-a)) + B_2\sinh(\lambda_2(2L-a))\cos(\lambda_2(2L-a))- \\
&- B_1\sinh(\lambda_2(2L-a))\sin(\lambda_2(2L-a))\Big] + 6B_5(2L-a) + 2B_6 \qquad (4.29)
\end{aligned}
$$

$$
\begin{aligned}
&w_{d_{IV}}|_{2L-a} = 0 \\
&= (-(EI)_s/(EI)_d)\Big[B_1\cosh(\lambda_2(2L-a))\cos(\lambda_2(2L-a))+ \\
&+ B_2\cosh(\lambda_2(2L-a))\sin(\lambda_2(2L-a)) + B_3\sinh(\lambda_2(2L-a))\cos(\lambda_2(2L-a))+ \\
&+ B_4\sinh(\lambda_2(2L-a))\sin(\lambda_2(2L-a))\Big] + B_5(2L-a)^3+ \\
&+ B_6(2L-a)^2 + B_7(2L-a) + B_8 \qquad (4.30)
\end{aligned}
$$

$$
\begin{aligned}
&w_{s_{IV}}|_{2L-a} = 0 \\
&= \Big[B_1\cosh(\lambda_2(2L-a))\cos(\lambda_2(2L-a)) + B_2\cosh(\lambda_2(2L-a))\sin(\lambda_2(2L-a)) \\
&+ B_3\sinh(\lambda_2(2L-a))\cos(\lambda_2(2L-a)) + B_4\sinh(\lambda_2(2L-a))\sin(\lambda_2(2L-a))\Big]+ \\
&+ B_5(2L-a)^3 + B_6(2L-a)^2 + B_7(2L-a) + B_8 \qquad (4.31)
\end{aligned}
$$

At the crack tip, x = 0, we have continuity conditions on the top face sheet across the cracked section and the bonded section of the beam:

Displacement continuity:

$$e_{4d} = (-(EI)_s/(EI)_d)C_1 + C_8 \tag{4.32}$$

$$e_{4s} = C_1 + C_8 \tag{4.33}$$

Slope continuity:

$$e_{3d} = (-(EI)_s/(EI)_d)\lambda_2(C_2 + C_3) + C_7 \tag{4.34}$$

$$e_{3s} = \lambda_2(C_2 + C_3) + C_7 \tag{4.35}$$

Bending moment continuity:

$$e_{2d} = (-(EI)_s/(EI)_d)\lambda_2^2 C_4 + C_6 \tag{4.36}$$

$$e_{2s} = \lambda_2^2 C_4 + C_6 \tag{4.37}$$

Shear force continuity:

$$6e_{1d} = 2\lambda_2^3(-(EI)_s/(EI)_d)(C_2 - C_3) + 6C_5 \tag{4.38}$$

$$6e_{1s} = 2\lambda_2^3(C_2 - C_3) + 6C_5 \tag{4.39}$$

At the left end, x = -a, the ENF specimen is pinned. The bending moments and displacements are

$$(EI)_d w''_{d_I}|_{-a} = 0$$
$$= 2(-(EI)_s)\lambda_1^2\Big[D_4\cosh(-\lambda_1 a)\cos(-\lambda_1 a) - D_3\cosh(-\lambda_1 a)\sin(-\lambda_1 a) +$$
$$+ D_2\sinh(-\lambda_1 a)\cos(-\lambda_1 a) - D_1\sinh(-\lambda_1 a)\sin(-\lambda_1 a)\Big] + 6D_5(-a) + 2D_6 \quad (4.40)$$

$$(EI)_s w''_{s_I}|_{-a} = 0$$
$$= 2(EI)_s\lambda_1^2\Big[D_4\cosh(-\lambda_1 a)\cos(-\lambda_1 a) - D_3\cosh(-\lambda_1 a)\sin(-\lambda_1 a) +$$
$$+ D_2\sinh(-\lambda_1 a)\cos(-\lambda_1 a) - D_1\sinh(-\lambda_1 a)\sin(-\lambda_1 a)\Big] + 6D_5(-a) + 2D_6 \quad (4.41)$$

$$w_{d_I}|_{-a} = 0$$
$$= (-(EI)_s/(EI)_d)\Big[D_1\cosh(-\lambda_1 a)\cos(-\lambda_1 a) + D_2\cosh(-\lambda_1 a)\sin(-\lambda_1 a) +$$
$$+ D_3\sinh(-\lambda_1 a)\cos(-\lambda_1 a) + D_4\sinh(-\lambda_1 a)\sin(-\lambda_1 a)\Big] +$$
$$+ D_5(-a)^3 + D_6(-a)^2 + D_7(-a) + D_8 \quad (4.42)$$

$$w_{s_I}|_{-a} = 0$$
$$= \Big[D_1\cosh(-\lambda_1 a)\cos(-\lambda_1 a) + D_2\cosh(-\lambda_1 a)\sin(-\lambda_1 a) +$$
$$+ D_3\sinh(-\lambda_1 a)\cos(-\lambda_1 a) + D_4\sinh(-\lambda_1 a)\sin(-\lambda_1 a)\Big] +$$
$$+ D_5(-a)^3 + D_6(-a)^2 + D_7(-a) + D_8 \quad (4.43)$$

We also have continuity condition at the middle of the beam, x= L-a, where there is a transverse shear load (P). Using this we can obtain the following equations:

Displacement continuity:

$$
\begin{aligned}
&w_{d_{III}}|_{L-a} = w_{d_{IV}}|_{L-a} \\
&= (-(EI)_s/(EI)_d)\Big[(C_1 - B_1)\cosh(\lambda_2(L-a))\cos(\lambda_2(L-a)) + \\
&+ (C_2 - B_2)\cosh(\lambda_2(L-a))\sin(\lambda_2(L-a)) + \\
&+ (C_3 - B_3)\sinh(\lambda_2(L-a))\cos(\lambda_2(L-a)) + \\
&+ (C_4 - B_4)\sinh(\lambda_2(L-a))\sin(\lambda_2(L-a))\Big] + (C_5 - B_5)(L-a)^3 + \\
&+ (C_6 - B_6)(L-a)^2 + (C_7 - B_7)(L-a) + (C_8 - B_8) = 0
\end{aligned} \tag{4.44}
$$

$$
\begin{aligned}
&w_{s_{III}}|_{L-a} = w_{s_{IV}}|_{L-a} \\
&= \Big[(C_1 - B_1)\cosh(\lambda_2(L-a))\cos(\lambda_2(L-a)) + \\
&+ (C_2 - B_2)\cosh(\lambda_2(L-a))\sin(\lambda_2(L-a)) + \\
&+ (C_3 - B_3)\sinh(\lambda_2(L-a))\cos(\lambda_2(L-a)) + \\
&+ (C_4 - B_4)\sinh(\lambda_2(L-a))\sin(\lambda_2(L-a))\Big] + (C_5 - B_5)(L-a)^3 + \\
&+ (C_6 - B_6)(L-a)^2 + (C_7 - B_7)(L-a) + (C_8 - B_8) = 0
\end{aligned} \tag{4.45}
$$

(4.46)

Slope continuity:

$$
\begin{aligned}
&w'_{d_{III}}|_{L-a} = w'_{d_{IV}}|_{L-a} \\
&= (-(EI)_s/(EI)_d)\lambda_2\Big[(C_2 + C_3 - B_2 - B_3)\cosh(\lambda_2(L-a))\cos(\lambda_2(L-a)) + \\
&+ (-C_1 + C_4 + B_1 - B_4)\cosh(\lambda_2(L-a))\sin(\lambda_2(L-a)) + \\
&+ (C_1 + C_4 - B_1 - B_4)\sinh(\lambda_2(L-a))\cos(\lambda_2(L-a)) + \\
&+ (C_2 - C_3 - B_2 + B_3)\sinh(\lambda_2(L-a))\sin(\lambda_2(L-a))\Big] + 3(C_5 - B_5)(L-a)^2 + \\
&+ 2(C_6 - B_6)(L-a) + (C_7 - B_7) = 0
\end{aligned} \tag{4.47}
$$

$$
\begin{aligned}
&w'_{s_{III}}|_{L-a} = w'_{s_{IV}}|_{L-a} \\
&= \lambda\Big[(C_2 + C_3 - B_2 - B_3)\cosh(\lambda_2(L-a))\cos(\lambda_2(L-a)) + \\
&+ (-C_1 + C_4 + B_1 - B_4)\cosh(\lambda_2(L-a))\sin(\lambda_2(L-a)) + \\
&+ (C_1 + C_4 - B_1 - B_4)\sinh(\lambda_2(L-a))\cos(\lambda_2(L-a)) + \\
&+ (C_2 - C_3 - B_2 + B_3)\sinh(\lambda_2(L-a))\sin(\lambda_2(L-a))\Big] + 3(C_5 - B_5)(L-a)^2 + \\
&+ 2(C_6 - B_6)(L-a) + (C_7 - B_7) = 0
\end{aligned} \tag{4.48}
$$

Bending Moment continuity:

$$
\begin{aligned}
&(EI)_d w''_{d_{III}}|_{L-a} = (EI)_d w''_{d_{IV}}|_{L-a} \\
&= 2(-(EI)_s/(EI)_d)\lambda_2^2\Big[(C_4 - B_4)\cosh(\lambda_2(L-a))\cos(\lambda_2(L-a)) - \\
&- (C_3 - B_3)\cosh(\lambda_2(L-a))\sin(\lambda_2(L-a)) + \\
&+ (C_2 - B_2)\sinh(\lambda_2(L-a))\cos(\lambda_2(L-a)) - \\
&- (C_1 - B_1)\sinh(\lambda_2(L-a))\sin(\lambda_2(L-a))\Big] + 6(C_5 - B_5)(L-a) + 2(C_6 - B_6) = 0
\end{aligned} \tag{4.49}
$$

$$
\begin{aligned}
&(EI)_s w''_{s_{III}}|_{L-a} = (EI)_s w''_{s_{IV}}|_{L-a} \\
&= 2\lambda_2^2 \Big[(C_4 - B_4)\cosh(\lambda_2(L-a))\cos(\lambda_2(L-a)) - \\
&- (C_3 - B_3)\cosh(\lambda_2(L-a))\sin(\lambda_2(L-a)) + \\
&+ (C_2 - B_2)\sinh(\lambda_2(L-a))\cos(\lambda_2(L-a)) - \\
&- (C_1 - B_1)\sinh(\lambda_2(L-a))\sin(\lambda_2(L-a)) \Big] + 6(C_5 - B_5)(L-a) + 2(C_6 - B_6) = 0
\end{aligned}
\tag{4.50}
$$

Shear Force continuity:

$$
\begin{aligned}
&[(EI)_d w'''_{d_{III}} + (EI)_s w'''_{s_{III}} - (EI)_d w'''_{d_{IV}} - (EI)_s w'''_{s_{IV}}]|_{L-a} = P \\
&6((EI)_d + (EI)_s)(C_5 - B_5) = P
\end{aligned}
\tag{4.51}
$$

In addition, we also have a shear force condition at the right end. The shear load is acting at the middle of the beam, hence the reaction at the pinned supports will be half of it,

$$
\begin{aligned}
&[(EI)_d w'''_{d_{IV}} + (EI)_s w'''_{s_{IV}}]|_{2L-a} = -P/2 \\
&6((EI)_d + (EI)_s)B_5 = -P/2
\end{aligned}
\tag{4.52}
$$

In the cracked section, between Region I and II, $x = -a + X_1$, we have continuity conditions across these two regions

Displacement continuity:

$$
\begin{aligned}
&w_{d_I}|_{-a+X_1} = w_{d_{II}}|_{-a+X_1} \\
&= (-(EI)_s/(EI)_d)\Big[D_1\cosh(\lambda_1(-a+X_1))\cos(\lambda_1(-a+X_1))+ \\
&+ D_2\cosh(\lambda_1(-a+X_1))\sin(\lambda_1(-a+X_1)) + D_3\sinh(\lambda_1(-a+X_1))\cos(\lambda_1(-a+X_1))+ \\
&+ D_4\sinh(\lambda_1(-a+X_1))\sin(\lambda_1(-a+X_1))\Big] + D_5(-a+X_1)^3 + D_6(-a+X_1)^2+ \\
&+ D_7(-a+X_1) + D_8 = W_d(-a+X_1)^3 + X_d(-a+X_1)^2 + Y_d(-a+X_1) + Z_d
\end{aligned}
\tag{4.53}
$$

$$
\begin{aligned}
&w_{s_I}|_{-a+X_1} = w_{s_{II}}|_{-a+X_1} \\
&= \Big[D_1\cosh(\lambda_1(-a+X_1))\cos(\lambda_1(-a+X_1))+ \\
&+ D_2\cosh(\lambda_1(-a+X_1))\sin(\lambda_1(-a+X_1)) + D_3\sinh(\lambda_1(-a+X_1))\cos(\lambda_1(-a+X_1))+ \\
&+ D_4\sinh(\lambda_1(-a+X_1))\sin(\lambda_1(-a+X_1))\Big] + D_5(-a+X_1)^3 + D_6(-a+X_1)^2+ \\
&+ D_7(-a+X_1) + D_8 = W_s(-a+X_1)^3 + X_s(-a+X_1)^2 + Y_s(-a+X_1) + Z_s
\end{aligned}
\tag{4.54}
$$

Slope continuity:

$$
\begin{aligned}
&w'_{d_I}|_{-a+X_1} = w'_{d_{II}}|_{-a+X_1} \\
&= (-(EI)_s/(EI)_d)\lambda_1\Big[(D_2+D_3)\cosh(\lambda_1(-a+X_1))\cos(\lambda_1(-a+X_1))+ \\
&+ (-D_1+D_4)\cosh(\lambda_1(-a+X_1))\sin(\lambda_1(-a+X_1))+ \\
&+ (D_1+D_4)\sinh(\lambda_1(-a+X_1))\cos(\lambda_1(-a+X_1))+ \\
&+ (D_2-D_3)\sinh(\lambda_1(-a+X_1))\sin(\lambda_1(-a+X_1))\Big] + 3D_5(-a+X_1)^2+ \\
&+ 2D_6(-a+X_1) + D_7 = 3W_d(-a+X_1)^2 + 2X_d(-a+X_1) + Y_d
\end{aligned}
\tag{4.55}
$$

$$
\begin{aligned}
&w'_{s_I}|_{-a+X_1} = w'_{s_{II}}|_{-a+X_1} \\
&= \lambda_1 \Big[(D_2 + D_3)\cosh(\lambda_1(-a+X_1))\cos(\lambda_1(-a+X_1)) + \\
&+ (-D_1 + D_4)\cosh(\lambda_1(-a+X_1))\sin(\lambda_1(-a+X_1)) + \\
&+ (D_1 + D_4)\sinh(\lambda_1(-a+X_1))\cos(\lambda_1(-a+X_1)) + \\
&+ (D_2 - D_3)\sinh(\lambda_1(-a+X_1))\sin(\lambda_1(-a+X_1)) \Big] + 3D_5(-a+X_1)^2 + \\
&+ 2D_6(-a+X_1) + D_7 = 3W_s(-a+X_1)^2 + 2X_s(-a+X_1) + Y_s
\end{aligned} \tag{4.56}
$$

Bending Moment continuity:

$$
\begin{aligned}
&(EI)_d w''_{d_I}|_{-a+X_1} = (EI)_d w''_{d_{II}}|_{-a+X_1} \\
&= 2(-(EI)_s/(EI)_d)\lambda_1^2 \Big[D_4\cosh(\lambda_1(-a+X_1))\cos(\lambda_1(-a+X_1)) - \\
&- D_3\cosh(\lambda_1(-a+X_1))\sin(\lambda_1(-a+X_1)) + D_2\sinh(\lambda_1(-a+X_1))\cos(\lambda_1(-a+X_1)) - \\
&- D_1\sinh(\lambda_1(-a+X_1))\sin(\lambda_1(-a+X_1)) \Big] + 6D_5(-a+X_1) + \\
&+ 2D_6 = 6W_d(-a+X_1) + 2X_d
\end{aligned} \tag{4.57}
$$

$$
\begin{aligned}
&(EI)_s w''_{s_I}|_{-a+X_1} = (EI)_s w''_{s_{II}}|_{-a+X_1} \\
&= 2\lambda_1^2 \Big[D_4\cosh(\lambda_1(-a+X_1))\cos(\lambda_1(-a+X_1)) - \\
&- D_3\cosh(\lambda_1(-a+X_1))\sin(\lambda_1(-a+X_1)) + D_2\sinh(\lambda_1(-a+X_1))\cos(\lambda_1(-a+X_1)) - \\
&- D_1\sinh(\lambda_1(-a+X_1))\sin(\lambda_1(-a+X_1)) \Big] + 6D_5(-a+X_1) + \\
&+ 2D_6 = 6W_s(-a+X_1) + 2X_s
\end{aligned} \tag{4.58}
$$

Shear Force continuity:

$$
\begin{aligned}
&(EI)_d w'''_{d_I}|_{-a+X_1} = (EI)_d w'''_{d_{II}}|_{-a+X_1} \\
&= 2(-(EI)_s/(EI)_d)\lambda_1^3 \Big[(D_2 - D_3)\cosh(\lambda_1(-a+X_1))\cos(\lambda_1(-a+X_1)) - \\
&- (D_1 + D_4)\cosh(\lambda_1(-a+X_1))\sin(\lambda_1(-a+X_1)) + \\
&+ (-D_1 + D_4)\sinh(\lambda_1(-a+X_1))\cos(\lambda_1(-a+X_1)) - \\
&- (D_2 + D_3)\sinh(\lambda_1(-a+X_1))\sin(\lambda_1(-a+X_1)) \Big] + 6D_5 = 6W_d
\end{aligned} \tag{4.59}
$$

$$
\begin{aligned}
&(EI)_s w'''_{s_I}|_{-a+X_1} = (EI)_s w'''_{s_{II}}|_{-a+X_1} \\
&= 2\lambda_1^3 \Big[(D_2 - D_3)\cosh(\lambda_1(-a+X_1))\cos(\lambda_1(-a+X_1)) - \\
&- (D_1 + D_4)\cosh(\lambda_1(-a+X_1))\sin(\lambda_1(-a+X_1)) + \\
&+ (-D_1 + D_4)\sinh(\lambda_1(-a+X_1))\cos(\lambda_1(-a+X_1)) - \\
&- (D_2 + D_3)\sinh(\lambda_1(-a+X_1))\sin(\lambda_1(-a+X_1)) \Big] + 6D_5 = 6W_s
\end{aligned} \tag{4.60}
$$

From these boundary conditions and continuity conditions (Equation 4.28 - Equation 4.60), we have 32 equations to solve for the unknown coefficients in the general solutions. We still need one more equation to solve all the 33 unknown coefficients. The additional equations comes from the condition at the interface between Region I & II, we know that the contact between the crack faces are lost at that interface. Hence, the transverse displacement of the top debonded face and the substrate should be the same at the interface between Region I & II ($x = -a + X_1$). This gives us

$$
\begin{aligned}
&w_{d_{II}}|_{-a+X_1} = w_{s_{II}}|_{-a+X_1} \\
&W_d(-a+X_1)^3 + X_d(-a+X_1)^2 + Y_d(-a+X_1) + Z_d = \\
&\qquad W_s(-a+X_1)^3 + X_s(-a+X_1)^2 + Y_s(-a+X_1) + Z_s
\end{aligned} \tag{4.61}
$$

With all these conditions, we obtain a system of non-linear equations(Equation 4.28-Equation 4.61)

and we can write a computer code to solve the numerical equations numerically.

4.3 Energy Release Rate

We have the general solutions for the transverse displacements of the beam section and they can be used to find the energy release rates. J-Integral provides a way to calculate the strain energy release rate. The ENF specimen is a standard beam for the measurement of the mode-II toughness of composites. The J-integral was developed in 1968 by Rice to characterize the strain concentration around cracks and notches.

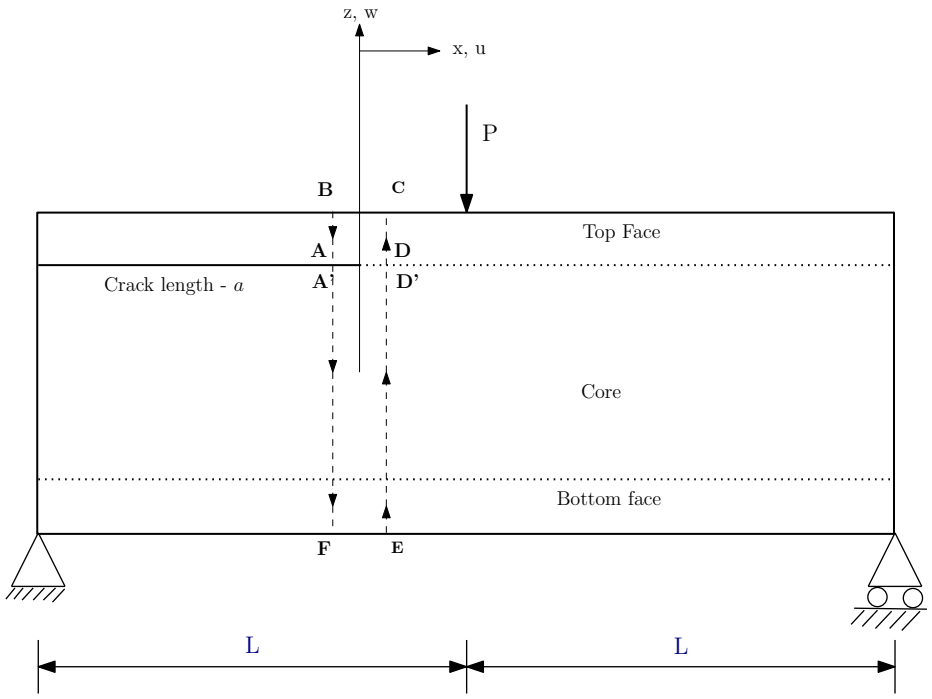

Figure 4.4: Zero-area path for J-Integral Calculation - ENF

The original definition of the integral is:

$$J = \int_{\Gamma} W dz - T_i \frac{\partial u_i}{\partial x} ds \tag{4.62}$$

For the calculation we define a zero-area path [97][98] around the crack tip. The dashed lines show the stress and displacement fields on both sides of the tip. For the calculation,

we define a zero-area path around the crack tip (Γ = BAA'FEDD'C) as shown in Figure 5.4.

The strain energy density on along the path can be written as:

$$W = \frac{1}{2}(\sigma_{xx}\epsilon_{xx} + \sigma_{zz}\epsilon_{zz} + \tau_{xz}\gamma_{xz}) \tag{4.63}$$

And, the second term in Equation 4.62 can be written as

$$T_i \frac{\partial u_i}{\partial x} = -\sigma_{xx}\epsilon_{xx} - \tau_{xz}w_{,x} \tag{4.64}$$

The equivalent shear modulus for the section should be derived by assuming the constituent sections are "springs in parallel", as shown in Kardomateas and Simitses[45].
For the debonded part, which is homogeneous, the equivalent shear modulus is:

$$G_d \ = \ G_{f_t} \tag{4.65}$$

For the substrate part which consists of the core and the bottom face:

$$\frac{2c + f_b}{G_s} = \frac{2c}{G_c} + \frac{f_b}{G_{f_b}} \tag{4.66}$$

For the base part

$$\frac{f_t + 2c + f_b}{G_b} = \frac{f_t}{G_{f_t}} + \frac{2c}{G_c} + \frac{f_b}{G_{f_b}} \tag{4.67}$$

Regarding the shear correction factor, for a homogeneous section, κ = 6/5. Thus, for the debonded part:

$$\kappa_d \ = \ \frac{6}{5} \tag{4.68}$$

The shear correction factor for the substrate part can be found using the general asymmetric

section formula in [96],

$$\kappa_s \;=\; \frac{G_s b^2(2c+f_b)}{4(EI)_s^2}\left(\frac{E_c^2}{G_c}q_2 - \frac{E_{f_b}^2}{G_- f_b}q_1\right), \tag{4.69}$$

where

$$\begin{aligned} q_1 \;=\; & f_b(c-e_s+f_b)^4 + \frac{1}{5}[(c-e_s+f_b)^5 - (c-e_s)^5] - \\ & - \frac{2}{3}(c-e_s+f_b)^2[(c-e_s+f_b)^3 - (c-e_s)^3]; \end{aligned} \tag{4.70}$$

$$q_2 \;=\; 2c(c+e_s)^4 + \frac{1}{5}[(c+e_s)^5 - (c-e_s)^5] - \frac{2}{3}(c+e_s)^2[(c-e_s)^3 - (c-e_s)^3] \tag{4.71}$$

The shear correction factor for the base part can again be taken from Huang and Kardomateas [96] formula for a general asymmetric sandwich section:

$$a_t \;=\; e_b + c + f_t; \qquad b_t \;=\; e_b + c; \qquad c_t \;=\; e_b + c + \frac{f_t}{2} \tag{4.72}$$

$$a_b \;=\; -e_b + c + f_b; \qquad b_b \;=\; -e_b + c; \qquad c_b \;=\; -e_b + c + \frac{f_b}{2} \tag{4.73}$$

and

$$d_i = \frac{E_{fi}^2}{E_c} f_i^2 c_i^2 + E_{fi} f_i c_i b_i^2 + \frac{E_c}{4} b_i^4 \tag{4.74}$$

then the shear correction formula for the base part is given from:

$$\kappa_b = \frac{b^2(f_b + 2c + f_t)G_b}{EI_{eq}^2}(a_f + a_c) \tag{4.75}$$

where

$$a_f = \sum_{i=t,b} \frac{E_{fi}^2}{4G_i}\left[a_i^4 f_i - \frac{2}{3}a_i^2(a_i^3 - b_i^3) + \frac{1}{5}(a_i^5 - b_i^5)\right] \tag{4.76}$$

$$a_c = \frac{E_c}{G_c}\sum_{i=t,b} \frac{E_c}{20}(b_i^5 - e_b^5) - \left(E_c\frac{b_i^2}{2} + E_{fi}f_i c_i\right)\frac{1}{3}(b_i^3 - e_b^3) + d_i c\Bigg] \tag{4.77}$$

From a plane stress assumption, $\sigma_{zz} = 0$, and $\epsilon_{xx} = \sigma_{xx}/E$,thus

When dz = -ds,

$$dJ = \frac{1}{2}\left(\sigma_{xx}\epsilon_{xx} + \sigma_{zz}\epsilon_{zz} + \tau_{xz}\gamma_{xz}\right)(-ds) - \left(-\sigma_{xx}\epsilon_{xx} - \tau_{xz}w_{i,x}\right)ds \tag{4.78}$$

$$dJ = \frac{1}{2}\left(\frac{\sigma_{xx}^2}{E} - \kappa\frac{\tau_{xz}^2}{G_{eq}} + 2\tau_{xz}w_{i,x}\right)ds \tag{4.79}$$

Similarly, when dz = ds,

$$dJ = \frac{1}{2}\left(-\frac{\sigma_{xx}^2}{E} + \kappa\frac{\tau_{xz}^2}{G_{eq}} - 2\tau_{xz}w_{i,x}\right)ds \tag{4.80}$$

Here,

$$\sigma_{xx} = E_i\frac{M_i s}{(EI)_{eq}}; \qquad \tau_{xz} = \frac{-V_i}{A}; \qquad i = d, s, b \tag{4.81}$$

where E_i refers to $E_i = E_c$ if it is in the core, $E_i = E_f t$ if in the top face etc. Also, $(EI)_{eq}$ is the equivalent bending rigidity of the section, for example, for the substrate part, $(EI)_{eq} = (EI)_s$, and for the base part, $(EI)_{eq} = (EI)_b$.

Notice that for a plane strain assumption, ϵ_{zz} = 0, we would have $\sigma_{zz} = \nu_{xz}\sigma_{xx}$, there, $\epsilon_{xx} = (\sigma_{xx} - \nu_{zx}\sigma_{zz})/E = (1 - \nu_{zx}\nu xz)\sigma_{xx}/E$.

In the zero-area path for J-Integral, we evaluate the stresses and slopes at the crack tip (x=0). Therefore, again for a plane stress assumption,

On BA: dz = -ds

$$J_{BA} = \int_{-\frac{f_t}{2}}^{\frac{f_t}{2}} \left(\frac{1}{2E_d}\sigma_{xx}^2 - \frac{\kappa_d}{2G_{eq}}\tau_{xz}^2 + \tau_{xz} w_{i,x}|_0 \right) ds \tag{4.82}$$

$$\tag{4.83}$$

$$= \int_{-\frac{f_t}{2}}^{\frac{f_t}{2}} \left(\frac{1}{2}E_d \frac{M_d^2 s^2}{(EI)_d^2} - \frac{\kappa_d}{2G_{eq}} \frac{V_d^2}{A_d^2} - \frac{V_d}{A_d} w_{d,x}|_0 \right) ds \tag{4.84}$$

$$J_{BA} = \frac{1}{2b^2} \left(\frac{12M_d^2}{E_d f_t^3} - \frac{\kappa_d V_d^2}{G_d f_t} - 2V_d b(e_{3d}) \right) \tag{4.85}$$

Here, M_d & V_d are the bending moment and shear force on the debonded part at the crack tip (x=0) are given by

$$M_d = (EI)_d(2e_{2d}); \qquad V_d = (EI)_d(6e_{1d}) \tag{4.86}$$

On A'F: dz = -ds

$$J_{A'F} = \int_{A'F} \left(\frac{1}{2}E_s \frac{M_s^2 s^2}{(EI)_s^2} - \frac{\kappa_s V_s^2}{2G_s A_s^2} - \frac{V_s}{A_s} w_{s,x}|_0 \right) ds \tag{4.87}$$

$$\begin{aligned} J_{A'F} = {} & \frac{M_s^2}{2(EI)_s^2} \left[E_{f_b} f_b \left[(c - e_s)(c - e_s + f_b) + \frac{f_b^2}{3} \right] + 2E_c c \left(\frac{c^2}{3} + e_s^2 \right) \right] - \\ & - \frac{k_s V_s^2}{2G_s b^2 (2c + f_b)} - \frac{V_s}{b}(e_{3s}) \end{aligned} \tag{4.88}$$

Here, M_s & V_s are the bending moment and shear force on the substrate part at the crack tip (x=0) are given by

$$M_s = (EI)_s(2e_{2s}); \qquad V_s = (EI)_s(6e_{1s}) \tag{4.89}$$

On the right side, EC, we can assume that the bonded section (actual beam structure) is

used. This "base" beam will have its neutral axis at a distance "e_b" from the mid-core line, which is given by

$$e_b[E_{f_t}f_t + E_c(2c) + E_{f_b}f_b] = E_{f_b}f_b\left(\frac{f_b}{2} + c\right) - E_{f_t}f_t\left(\frac{f_t}{2} + c\right) \tag{4.90}$$

and its flexural rigidity will be

$$\begin{aligned}(EI)_b \ = b\Bigg[E_{f_t}\frac{f_t^3}{12} + E_{f_t}f_t\left(\frac{f_t}{2} + c + e_b\right)^2 + E_c\frac{2c^3}{3} + E_c(2c)e_b^2 + \\ + E_{f_b}\frac{f_b^3}{12} + E_{f_b}f_b\left(\frac{f_b}{2} + c - e_b\right)^2\Bigg]\end{aligned} \tag{4.91}$$

On EC: dz = ds

$$J_{EC} = \int_{CE}\left(- E_b\frac{M_b^2 s^2}{2(EI)_b^2} + \frac{\kappa_b V_b^2}{2G_b A_b^2} + \frac{V_b}{A_b}w_{b,x}|_0\right)ds \tag{4.92}$$

$$\begin{aligned}= &- \frac{M_b^2}{2(EI)_b^2}\left(E_{f_b}\int_{e_b-c-f_b}^{e_b-c} s^2 ds + E_c\int_{e_b-c}^{e_b+c} s^2 ds + E_{f_t}\int_{e_b+c}^{e_b+c+f_t} s^2 ds\right) + \\ &+ \frac{\kappa_b V_b}{2G_b A_b^2}\int_{e_b-c-f_b}^{e_b+c+f_t} ds + \frac{V_b}{A_b}w_{b,x}|_0\int_{e_b-c-f_b}^{e_b+c+f_t} ds\end{aligned} \tag{4.93}$$

Simplifying the above equation we get

$$\begin{aligned}J_{EC} = -\frac{M_b^2}{2(EI)_b^2}\Bigg\{&E_{f_b}f_b\left[(e_b - c)(e_b - c - f_b) + \frac{f_b^2}{3}\right] + 2E_c c(\frac{c^2}{3} + e_b^2) + \\ &+ E_{f_t}f_t\left[(e_b + c)(e_b + c + f_t) + \frac{f_t^2}{3}\right]\Bigg\} + \left(\frac{\kappa_b V_b^2}{2G_b A_b^2}\right)(2c + f_t + f_b) - \\ &- \frac{V_b}{A_b}w_{b,x}|_0(f_t + 2c + f_b)\end{aligned} \tag{4.94}$$

M_b & V_b are the bending moment and shear force on the base part at the crack tip (x=0) are given by

$$M_b = (EI)_d(2e_{2d}) + (EI)_s(2e_{2s}); \qquad V_b = (EI)_d(6e_{1d}) + (EI)_s(6e_{1s}) \tag{4.95}$$

Finally, the strain energy release rate is the sum of these individual contributions (J_{BA},$J_{A'F}$,J_{EC}).

$$J \;=\; J_{BA} \;+\; J_{A'F} \;+\; J_{EC} \tag{4.96}$$

Hence, the energy release rate of the end-notched flexure sandwich specimen can be obtained using the following expression

$$\begin{aligned}
J \;=&\frac{1}{2b^2}\left(\frac{12((EI)_d(2e_{2d}))^2}{E_d f_t^3} - \frac{\kappa_d((EI)_d(6e_{1d}))^2}{G_d f_t} - 2((EI)_d(6e_{1d}))b(e_{3d})\right)+\\
&+\frac{((EI)_s(2e_{2s}))^2}{2(EI)_s^2}\left[E_{f_b}f_b\left[(c-e_s)(c-e_s+f_b)+\frac{f_b^2}{3}\right]+2E_c c\left(\frac{c^2}{3}+e_s^2\right)\right]-\\
&-\frac{k_s((EI)_s(6e_{1s}))^2}{2G_s b^2(2c+f_b)} - \frac{((EI)_s(6e_{1s}))}{b}(e_{3s}) - \frac{((EI)_d(2e_{2d})+(EI)_s(2e_{2s}))^2}{2(EI)_b^2}\Bigg\{\\
&E_{f_b}f_b\left[(e_b-c)(e_b-c-f_b)+\frac{f_b^2}{3}\right]+2E_c c(\frac{c^2}{3}+e_b^2)+\\
&+E_{f_t}f_t\left[(e_b+c)(e_b+c+f_t)+\frac{f_t^2}{3}\right]\Bigg\}+\left(\frac{\kappa_b((EI)_d(6e_{1d})+(EI)_s(6e_{1s}))^2}{2bG_bA_b}\right)-\\
&-\frac{((EI)_d(6e_{1d})+(EI)_s(6e_{1s}))}{b}w_{b,x}|_0
\end{aligned} \tag{4.97}$$

4.4 Mode Partitioning

The goal in this thesis is to provide a closed/near-closed form solution. Hence, we use mode partitioning approach, which makes use of the displacements. Notice that displacements as an alternative approach to determine mode mixity have been used in bimaterial fracture mechanics by Berggreen et al. [36]. However, the latter is based on the fracture mechanics singular field and thus it is conceptually different and this mode partitioning approach was introduced by Kardomateas et al. [43].

According to the Euler-Bernoulli beam theory, the displacements of the debonded part

in the limit are

$$w_{d_0} = \lim_{x\to 0} w_d(x) = e_{4d} \tag{4.98}$$

$$u_{d_0} = \frac{f_t}{2} \lim_{x\to 0} w_{d,x}(x) = \frac{f_t}{2} e_{3d} \tag{4.99}$$

and the corresponding ones for the substrate part in the limit are

$$w_{s_0} = \lim_{x\to 0} w_s(x) = e_{4s} \tag{4.100}$$

$$u_{s_0} = -\left(e_s + c\right) \lim_{x\to 0} w_{d,x}(x) = -(e_s + c) e_{3s} \tag{4.101}$$

We can also account for the effect of transverse shear in an approximate way by including the shear strain $\gamma = \kappa V/(G_{eq}A)$ in the slope. Notice that, a positive shear would create a clockwise slope. Thus, the axial displacements at the face/core interface due to the shear, to be added to the u_{d_0} and u_{s_0}, respectively, are

$$u_{d_\gamma} = -\frac{f_t}{2} \frac{\kappa_d V_d}{(G_d b f_t)}; \qquad u_{s_\gamma} = (e_s + c) \frac{\kappa_s V_s}{[G_s b(2c + f_b)]} \tag{4.102}$$

A mode partitioning phase angle, ψ_{TEF}, based on the elastic foundation approach, is defined from the relative crack flank opening and shearing displacements, δ_w and δ_u, respectively, at the tip; it is defined so that $\psi_{TEF} = 0$ if only transverse (opening) displacement occurs at the beginning of the springs, x = 0 (pure mode I) and $\psi_{TEF} = 90^0$ if only axial (shearing) displacement occurs at $x = 0$ (pure mode II)

$$\psi_{TEF} = \tan^{-1}\left(\frac{\delta_u}{\delta_w}\right) = \tan^{-1} \frac{(u_{d_0} + u_{d_\gamma}) - (u_{s_0} + u_{s_\gamma})}{(w_{d_0} - w_{s_0})} \tag{4.103}$$

After substituting

$$\psi_{TEF} = \tan^{-1} \frac{\left(\frac{f_t}{2} e_{3d} - \frac{f_t}{2} \frac{\kappa_d V_d}{(G_d b f_t)} \right) - \left(-(e_s + c) e_{3s} + (e_s + c) \frac{\kappa_s V_s}{[G_s b (2c + f_b)]} \right)}{(e_{4d} - e_{4s})} \quad (4.104)$$

It should be noted that in the elastic foundation model, a crack does not exist, instead we have beams connected by elastic springs. Therefore, this mode partitioning approach is not the same as the mode mixity in a bimaterial crack, which is based on the stress intensity factors from a fracture mechanics approach.

4.5 Results and Discussion

A symmetric sandwich configuration with faces made of isotropic aluminium with Young's modulus $E_f = 70$GPa and Poisson's ratio $\nu_f = 0.3$ is chosen. The core material is isotropic aluminium foam with Young's modulus $E_c = 7$GPa and Poisson's ratio $\nu_c = 0.32$. We chose isotropic faces and core because we are comparing our results with the commercial finite element ANSYS, and most finite element softwares can only calculate the stress intensity factor, $K_{I,II}$, for an interfacial crack when the two materials are both isotropic and linear elastic.

In all cases, the faces had a thickness of f_t=f_b=2 mm and the core had a thickness of 2c = 20mm. The total length of the beam was L=500 mm. A debond of length a = 200 mm is introduced between the top face and the core.

For verification, we modeled the End-Notched Flexure sandwich specimen into ANSYS (Figure 4.5). Here, the crack tip singularity was introduced using Pre-Meshed Crack and a frictionless surface-to-surface contact was also introduced between the two crack faces. We then obtained the Energy release rate values using J-Integral and Virtual Crack Closure technique. We also obtained the mode mixity values from the stress intensity factor values using the expression given below:

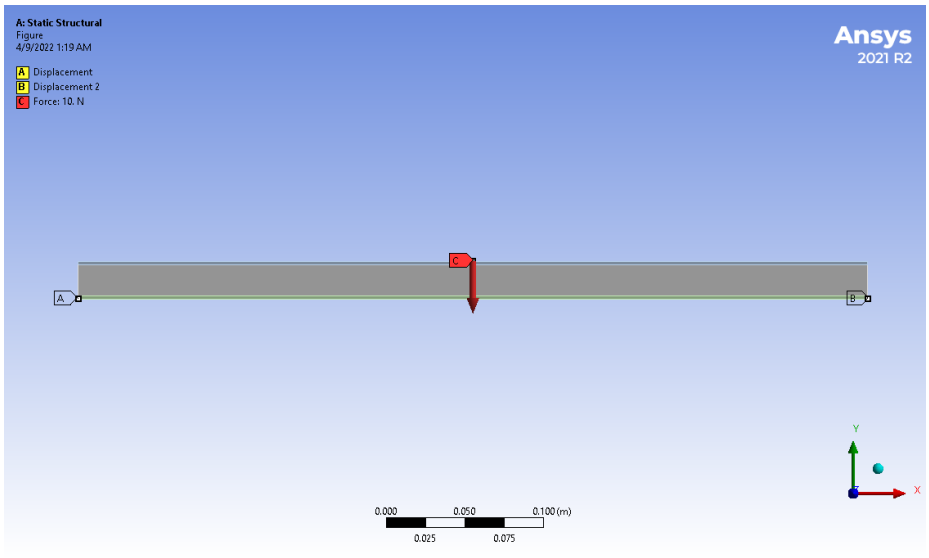

Figure 4.5: ENF sandwich specimen with pre-meshed crack

$$\psi = \tan^{-1}\left(\frac{K_{II}}{K_I}\right) \tag{4.105}$$

Table 4.1 shows the energy release rate values from the closed form expression (Equation 4.97) from the tensionless foundation analysis, J_{TEF} in comparison with the one computed from the finite element analysis, ERR_{FEA} for a range of load values. We have used the subscript TEF to denote results from the tensionless elastic foundation approach and FEA to denote results from the finite element code ANSYS. It can be seen that the energy release rate values (J_{TEF}) show very good agreement with the energy release rate value from FEA (ERR_{FEA}). In addition, by solving the unknown equations using boundary conditions, it is interesting to note that we are able to find the crack face contact length (X_1) for each load case. We can see that there is a significant contact region from the left support as we expected.

Table 4.1: ENF: Energy Release Rate Values - Al Foam Core

P (N_t)	J_{TEF} (N_t/mm) Tensionless Foundation	ERR_{FEA} (N_t/mm) VCCT	Contact Length mm Region I
10	0.0248	0.023141	129.07
15	0.0558	0.0521	160.12
20	0.0993	0.0926	160.12
40	0.3970	0.3706	157.65
60	0.8934	0.8331	157.65
100	2.4816	2.3141	157.65
150	5.5836	5.2068	157.65
250	15.5100	14.463	157.65
400	39.7055	37.026	157.65
750	139.5897	130.17	157.65
1000	248.1595	231.41	183.10

Next, we chose a soft core isotropic material with Young's modulus $E_c = 0.35$GPa and Poisson's ratio $\nu_c = 0.32$. Table 4.2 shows the energy release values (J_{TEF}) compared with the finite element analysis (ERR_{FEA}). Even for this soft core case, we can see that the tensionless elastic foundation approach gives a very good estimation of the energy release rate values. Also, in the soft core case, it can be noticed that the crack face contact length X_1 is significantly large.

Table 4.2: ENF: Energy Release Rate Values - Soft Core

P (N_t)	J_{TEF} (N_t/mm) Tensionless Foundation	ERR_{FEA} (N_t/mm) VCCT	Contact Length mm Region I
10	0.4263	0.4054	160.12
15	0.9592	0.9122	160.12
20	1.7053	1.6216	160.12
40	6.8210	6.4865	160.12
60	15.3474	14.5950	160.12
100	42.6316	40.5410	160.12
150	95.9210	91.2160	160.12
250	266.4474	253.3800	157.65
400	682.1055	648.6500	183.10
750	2398.0270	2280.4000	183.10
1000	4263.1592	4054.1000	183.10

The mode partitioning phase angles defined in the context of the tensionless elastic foundation analysis, ψ_{TEF}, gives $\psi_{TEF} = 90^0$ for all the load cases and both the material combination. This is very accurate as we know that the ENF specimen is a pure mode II specimen and the mode mixity phase angle for the pure mode II case should be 90^0. We also obtained the mixity values from ANSYS stress intensity factor values and they also shows that the specimen is in pure mode II fracture.

It is interesting to note that in Table 4.1 & Table 4.2, there is slight difference in the energy release rate values obtained using the tensionless foundation theory and the FEA

values. This is expected since our elastic foundation analysis uses Euler-Bernoulli beam theory. A Timoshenko-based, first order shear analysis or high-order shear theory could lead to better accuracy.

4.6 Conclusion

Semi-Closed form expressions for the energy release rate and mode partitioning of End-Notched Flexure sandwich specimen are obtained. An elastic foundation approach using Euler-Bernoulli beam theory is used in the bonded section of the beam. In the debonded part, crack face contact is usually neglected in literature for analytical approaches. Here, the crack face contact is modelled using tensionless spring foundation approach. The tensionless spring foundation captures the transfer of compressive stress across the crack faces. In this approach, in addition to the transverse displacements in the debonded part and the substrate, we also obtain the length of the crack face contact region. The model presented here is applicable for both isotropic and orthotropic face and core materials and can also be done for the general asymmetric sandwich beam construction. J-Integral is used to derive a closed form expression for energy release rate and the J-Integral values shows excellent agreement with the corresponding values from the finite element analysis. The transverse and axial displacements at the beginning of the elastic foundation are used to define a mode partitioning measure values. It shows that the ENF specimen undergoes pure mode II fracture.

CHAPTER 5

CRACK FACE CONTACT MODEL - WITH FRICTION

In mode II fracture specimen, when there is crack face contact, we will have friction in the contact region. Analytical approaches usually neglect the crack face contact and friction forces. Here, we are extending the elastic foundation analysis with tensionless spring foundation to also capture the friction between the crack faces. The same ENF sandwich specimen is used here to include friction in the contact region. In Figure 5.1, Region I is the contact region in the debonded portion of the beam. Here, we will introduce the effects of crack face contact friction.

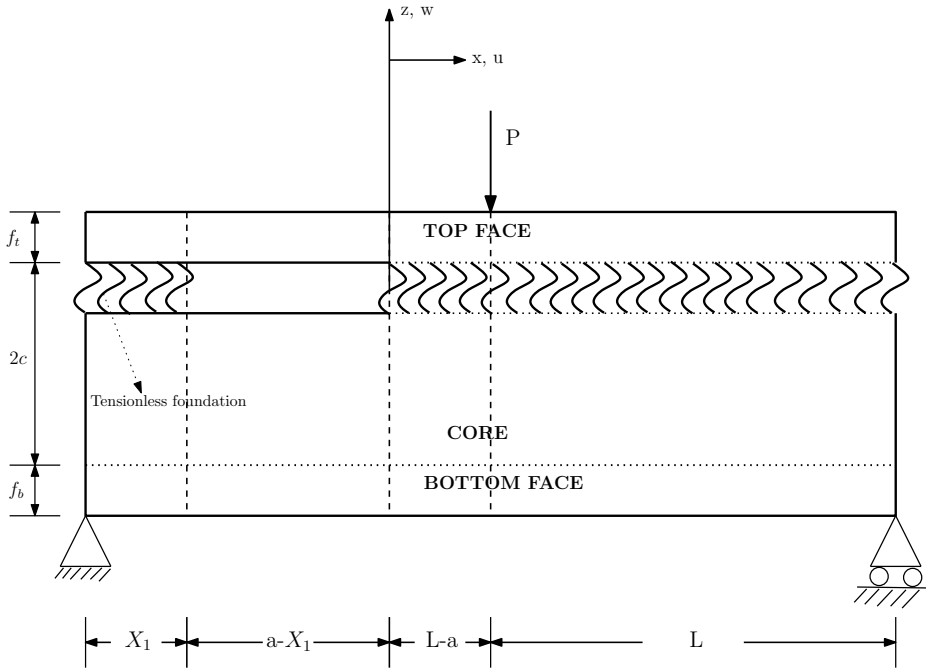

Figure 5.1: Tensionless Foundation with crack face friction in ENF Specimen

5.1 Governing Equations

We are extending the elastic foundation approach with tensionless foundation in the contact region to also include the friction in the contact region. In Region I, we are using tensionless spring foundation to capture the compressive stresses across the interface between debonded top face and the substrate. Region II is the free region in the cracked section of the beam and we simple beam theory to obtain the governing equations in this region. Region III and IV form the bonded section of the beam, elastic foundation with normal springs are used to capture the interaction between the face and the substrate in this region. In this model, we are using Euler-Bernoulli beam theory to develop the governing equations in all these regions.

It should again be noted that the formulation and approach are applicable to both beams (plane stress) and wide panels (plane strain) but different moduli should be used for plane stress and plane strain problems. The solutions derived here are for the plane stress case and for plane strain, E (Young's Modulus) should be replaced by $E/(1-\nu^2)$, where ν is Poisson's ratio.

5.1.1 Cracked section

In the cracked section of the beam, we have two regions, Region I is the crack face contact region with tensionless spring foundation and friction. The tensionless spring foundation here is assumed only to react when there is compression and the modulus of the tensionless foundation is k_t. At the interface between debonded part and the substrate, compression occurs only when $w_d < w_s$. When $w_d > w_s$, it means the crack is open and there is no contact or transfer of stresses across the debonded top face and the substrate. The coordinate system is set so that x = 0 is at the crack tip (shown in Figure 4.3), i.e., the debond is negative for x and the intact part is for positive x.

Region I: $(-a \leq x \leq -a + X_1)$

The beam element of the top debonded face shear is shown in Figure 5.2. Using the equi-

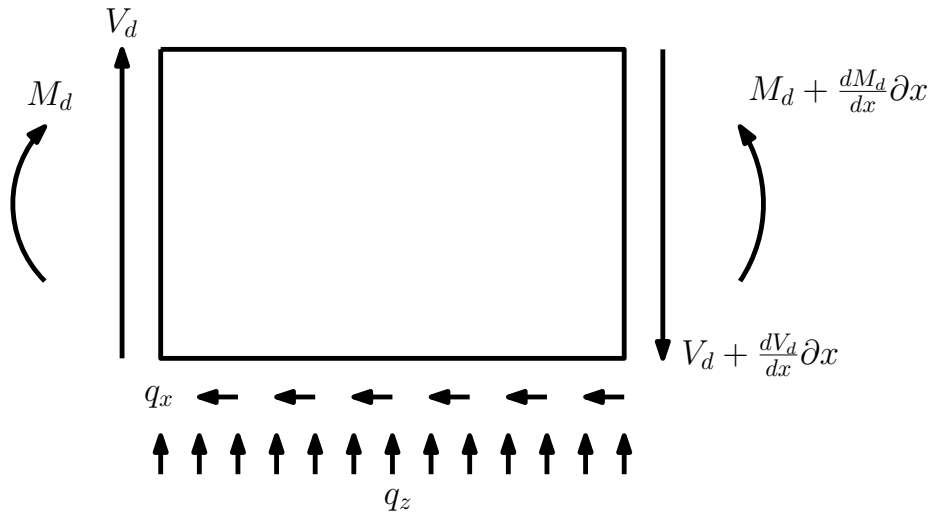

Figure 5.2: Beam Element in the Debonded Face - Region I

librium equations of the beam element, we get

$$\frac{dM_d}{dx} = V_d + q_x \frac{f_t}{2} \tag{5.1}$$

$$\frac{dV_d}{dx} = q_z \tag{5.2}$$

where, q_z is the force distribution from the tensionless spring foundation and q_x is the frictional force distribution from the crack face contact. And similarly, the beam element of the substrate part is shown in Figure 5.3 and if we solve the equilibrium equations, we get

$$\frac{dM_s}{dx} = V_s + q_x(e_s + c) \tag{5.3}$$

$$\frac{dV_s}{dx} = -q_z \tag{5.4}$$

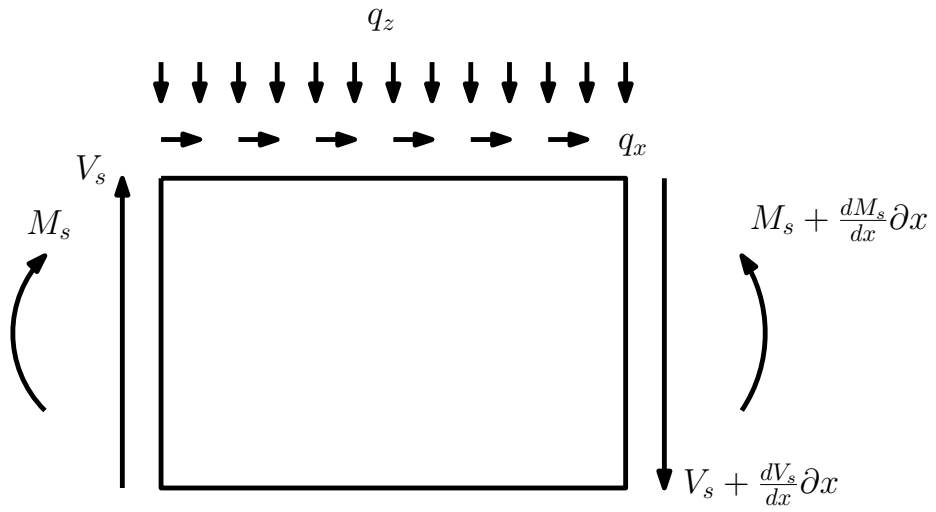

Figure 5.3: Beam Element in the Substrate - Region I

The force distribution from the tensionless spring foundation (q_z) can be written as

$$q_z = -k_t(w_d - w_s) \tag{5.5}$$

where, w_d and w_s are the transverse displacements in the top debonded part and the substrate respectively. k_t is the elastic modulus of the tensionless spring foundation and the elastic modulus value is obtained using the same expression for the modulus of normal springs in the elastic foundation. The only difference is that the springs in the tensionless foundation only reacts for compressive forces. μ is the friction coefficient between the crack faces. The friction force distribution (q_x) between the crack faces is proportional to the normal force distribution and can be written as:

$$q_x = -\mu k_t(w_d - w_s) \tag{5.6}$$

Using Equation 5.5 & Equation 5.6 in the equilibrium equations for the debonded part and the substrate, we get

$$(EI)_d \frac{d^3 w_d}{dx^3} = V_d - \mu k_t (w_d - w_s) \frac{f_t}{2} \tag{5.7}$$

$$\frac{dV_d}{dx} = -k_t (w_d - w_s) \tag{5.8}$$

$$(EI)_s \frac{d^3 w_s}{dx^3} = V_s - \mu k_t (e_s + c)(w_d - w_s) \tag{5.9}$$

$$\frac{dV_s}{dx} = k_t (w_d - w_s) \tag{5.10}$$

Simplifying this further, we get the governing equations in the Region I as

$$(EI)_d \frac{d^4 w_d}{dx} + k_t (w_d - w_s) + \mu k_t \frac{f_t}{2} \left(\frac{dw_d}{dx} - \frac{dw_s}{dx}\right) = 0 \tag{5.11}$$

$$(EI)_s \frac{d^4 w_s}{dx} + k_t (w_s - w_d) + \mu k_t (e_s + c) \left(\frac{dw_d}{dx} - \frac{dw_s}{dx}\right) = 0 \tag{5.12}$$

The governing equations are linear fourth order coupled differential equations and are in terms of the transverse displacements of the debonded part and the substrate. These equations can be solved by taking laplace transform

$$s^4 (EI)_d W_d(s) + k_t (W_d(s) - W_s(s)) + \mu k_t \frac{f_t}{2} s (W_d(s) - W_s(s)) = 0 \tag{5.13}$$

$$s^4 (EI)_s W_s(s) + k_t (W_s(s) - W_d(s)) + \mu k_t (e_s + c) s (W_d(s) - W_s(s)) = 0 \tag{5.14}$$

Solving Equation 5.13, we can obtain $W_s(s)$ in terms of $W_d(s)$,

$$W_s(s) = \frac{2k_t + f_t k_t \mu s + 2(EI)_d s^4}{k_t (2 + \mu f_t s)} W_d(s) \tag{5.15}$$

Substituting this into Equation 5.14 and simplifying, we get

$$s^8 w_d - \frac{k_t \mu}{(EI)_d (EI)_s}[(EI)_d (c + e_s) - (EI)_s \frac{f_t}{2}] s^5 w_d + \frac{k_e((EI)_d + (EI)_s)}{(EI)_d (EI)_s} s^4 w_d = 0 \tag{5.16}$$

Now taking inverse Laplace transform of the above equation results in

$$w_d'''''''' - 2\lambda_1^2 w_d'''' + \lambda_2^4 w_d'''' = 0 \tag{5.17}$$

where

$$\lambda_1^2 = \frac{k_t \mu}{2(EI)_d (EI)_s}[(EI)_d (c + e_s) - (EI)_s \frac{f_t}{2}] \tag{5.18}$$

$$\lambda_2^4 = \frac{k_t((EI)_d + (EI)_s)}{(EI)_d (EI)_s} \tag{5.19}$$

This is a linear eight-order homogeneous differential equation. Assuming a solution of the form e^{rx}, results in the following equation:

$$r^8 - 2\lambda_1^2 r^5 + \lambda_2^4 r^4 = 0; \quad or \quad r^4(r^4 - 2\lambda_1^2 r + \lambda_2^4) = 0 \tag{5.20}$$

The solution for the above characteristic equation is of the form

$$r_{1,2} = -k_1 \pm ik_2 \qquad r_{3,4} \qquad = -k_1 \pm ik_3 \qquad r_{5,6,7,8} = 0 \tag{5.21}$$

So, the general solutions for the governing equations are

$$w_{d_I} = D_{1d}e^{-k_1 x}\cos(k_2 x) + D_{2d}e^{-k_1 x}\sin(k_2 x) + D_{3d}e^{k_1 x}\cos(k_3 x) + D_{4d}e^{k_1 x}\sin(k_3 x) + \\ + D_{5d}x^3 + D_{6d}x^2 + D_{7d}x + D_{8d} \tag{5.22}$$

$$w_{s_I} = D_{1s}e^{-k_1 x}\cos(k_2 x) + D_{2s}e^{-k_1 x}\sin(k_2 x) + D_{3s}e^{k_1 x}\cos(k_3 x) + D_{4s}e^{k_1 x}\sin(k_3 x) + \\ + D_{5s}x^3 + D_{6s}x^2 + D_{7s}x + D_{8s} \tag{5.23}$$

From Equation 5.11, we get

$$(EI)_d w_d'''' + k_t w_d + \mu k_t \frac{f_t}{2} w_d' = k_t w_s + \mu k_t \frac{f_t}{2} w_s' \tag{5.24}$$

Using the above equation, substituting the general solutions (Equation 5.22 & Equation 5.23) and comparing the coefficients on the left sides of the equation and right side of the equation, we get

$$D_{1s} = \frac{2D_{1d}F_1 + 2D_{2d}F_2 - (D_{1d}F_1 + D_{2d}F_2)f_t k_1 \mu + (D_{1d}F_2 - D_{2d}F_1)f_t k_2 \mu}{k_t(4 - 4f_t k_1 \mu + f_t^2 k_1^2 \mu^2 + f_t^2 k_2^2 \mu^2)} \tag{5.25}$$

$$D_{2s} = \frac{2D_{2d}F_1 - 2D_{1d}F_2 - (D_{2d}F_1 - D_{1d}F_2)f_t k_1 \mu + (D_{1d}F_1 + D_{2d}F_2)f_t k_2 \mu}{k_t(4 - 4f_t k_1 \mu + f_t^2 k_1^2 \mu^2 + f_t^2 k_2^2 \mu^2)} \tag{5.26}$$

$$D_{3s} = \frac{2D_{3d}F_3 - 2D_{4d}F_4 + (D_{3d}F_3 - D_{4d}F_4)f_t k_1 \mu - (D_{4d}F_3 + D_{3d}F_4)f_t k_3 \mu}{k_t(4 + 4f_t k_1 \mu + f_t^2 k_1^2 \mu^2 + f_t^2 k_3^2 \mu^2)} \tag{5.27}$$

$$D_{4s} = \frac{2D_{3d}F_3 + 2D_{4d}F_4 + (D_{4d}F_3 + D_{3d}F_4)f_t k_1 \mu + (D_{3d}F_3 - D_{4d}F_4)f_t k_3 \mu}{k_t(4 + 4f_t k_1 \mu + f_t^2 k_1^2 \mu^2 + f_t^2 k_3^2 \mu^2)} \tag{5.28}$$

$$D_{is} = D_{id}\ ; \qquad i = 5, 6, 7, 8 \tag{5.29}$$

where

$$F_1 = 2k_t + 2(EI)_d(k_1^4 - 6k_1^2k_2^2 + k_2^4) - f_t k_t k_1 \mu \tag{5.30}$$

$$F_2 = -8(EI)_d k_1 k_2 (k_1^2 - k_2^2) + f_t k_t k_2 \mu \tag{5.31}$$

$$F_3 = 2k_t + 2(EI)_d(k_1^4 - 6k_1^2k_3^2 + k_3^4) - f_t k_t k_1 \mu \tag{5.32}$$

$$F_4 = -8(EI)_d k_1 k_3 (k_1^2 - k_3^2) + f_t k_t k_3 \mu \tag{5.33}$$

In Region I, there is a slight difference in the general solutions for the case with friction. With the crack face contact friction, we have exponential functions and polynomials in the general solutions for the transverse displacements of the debonded part and the substrate. There are 8 unknown coefficients in these equations.

Region II: $(-a + X_1 \leq x \leq 0)$

In this region, there is no contact between the top debonded face and the substrate. Hence, the top debonded part and the substrate are independent and the governing equations are same and the solutions for transverse displacements are also the same as the ones in the case of tensionless foundation with friction.

$$w_{d_{II}} = e_{1d}x^3 + e_{2d}x^2 + e_{3d}x + e_{4d} \tag{5.34}$$

$$w_{s_{II}} = e_{1s}x^3 + e_{2s}x^2 + e_{3s}x + e_{4s} \tag{5.35}$$

We can the see that the general solutions for the displacements are simple polynomial equations and we have 8 unknown coefficients from this region.

5.1.2 Bonded section

The bonded section of the beam has the elastic foundation to capture the interaction between the top face and the substrate. The governing equations in the bonded section (both

in Region III & IV) are the same as in previous chapter.

Region III: $(0 \leq x \leq L - a)$

Here, the elastic foundation has a distribution of normal springs and the stiffness of the springs are k_n. The general solutions for the transverse displacements in the top debonded part and the substrate are

$$w_{d_{III}} = \frac{-EI_s}{EI_d}\Big[C_1 \cosh \lambda_2 x \cos \lambda x + C_2 \cosh \lambda_2 x \sin \lambda_2 x + C_3 \sinh \lambda_2 x \cos \lambda_2 x + \\ + C_4 \sinh \lambda_2 x \sin \lambda_2 x\Big] + C_5 x^3 + C_6 x^2 + C_7 x + C_8 \tag{5.36}$$

$$w_{s_{III}} = \Big[C_1 \cosh \lambda_2 x \cos \lambda x + C_2 \cosh \lambda_2 x \sin \lambda_2 x + C_3 \sinh \lambda_2 x \cos \lambda_2 x + \\ + C_4 \sinh \lambda_2 x \sin \lambda_2 x\Big] + C_5 x^3 + C_6 x^2 + C_7 x + C_8 \tag{5.37}$$

From the general solutions, we have 8 unknown coefficients (C_i where i =1,...,8) in this region.

Region IV: $(L - a \leq x \leq 2L - a)$

Here, we obtain general solutions similar to Region III

$$w_{d_{IV}} = \frac{-EI_s}{EI_d}\Big[B_1 \cosh \lambda_2 x \cos \lambda_2 x + B_2 \cosh \lambda_2 x \sin \lambda_2 x + B_3 \sinh \lambda_2 x \cos \lambda_2 x + \\ + B_4 \sinh \lambda_2 x \sin \lambda_2 x\Big] + B_5 x^3 + B_6 x^2 + B_7 x + B_8 \tag{5.38}$$

$$w_{s_{IV}} = \Big[B_1 \cosh \lambda_2 x \cos \lambda_2 x + B_2 \cosh \lambda_2 x \sin \lambda_2 x + B_3 \sinh \lambda_2 x \cos \lambda_2 x + \\ + B_4 \sinh \lambda_2 x \sin \lambda_2 x\Big] + B_5 x^3 + B_6 x^2 + B_7 x + B_8 \tag{5.39}$$

Similar to Region III, we have 8 unknown coefficients (B_i where i =1,...,8) in this region.

5.2 Boundary Conditions

From the general solutions in all the regions, we have 32 constant coefficients. The crack face contact length, X_1, is already found in the case without friction and we can use that value. From the ENF specimen (shown in Figure 4.1), we have 8 boundary conditions and 24 continuity conditions (8 each from x = -a+ X_1, 0, L-a)

In the End Notched Flexure specimen, the beam is pinned at the right end $x = 2L - a$, so the bending moment and displacements are

$$(EI)_d w''_{d_{IV}}|_{2L-a} = 0$$

$$= 2(-(EI)_s)\lambda_2^2\Big[B_4\cosh(\lambda_2(2L-a))\cos(\lambda_2(2L-a))-$$

$$- B_3\cosh(\lambda_2(2L-a))\sin(\lambda_2(2L-a)) + B_2\sinh(\lambda_2(2L-a))\cos(\lambda_2(2L-a))-$$

$$- B_1\sinh(\lambda_2(2L-a))\sin(\lambda_2(2L-a))\Big] + 6B_5(2L-a) + 2B_6 \tag{5.40}$$

$$(EI)_s w''_{s_{IV}}|_{2L-a} = 0$$

$$= 2(EI)_s\lambda_2^2\Big[B_4\cosh(\lambda_2(2L-a))\cos(\lambda_2(2L-a))-$$

$$- B_3\cosh(\lambda_2(2L-a))\sin(\lambda_2(2L-a)) + B_2\sinh(\lambda_2(2L-a))\cos(\lambda_2(2L-a))-$$

$$- B_1\sinh(\lambda_2(2L-a))\sin(\lambda_2(2L-a))\Big] + 6B_5(2L-a) + 2B_6 \tag{5.41}$$

$$w_{d_{IV}}|_{2L-a} = 0$$

$$= (-(EI)_s/(EI)_d)\Big[B_1\cosh(\lambda_2(2L-a))\cos(\lambda_2(2L-a))+$$

$$+ B_2\cosh(\lambda_2(2L-a))\sin(\lambda_2(2L-a)) + B_3\sinh(\lambda_2(2L-a))\cos(\lambda_2(2L-a))+$$

$$+ B_4\sinh(\lambda_2(2L-a))\sin(\lambda_2(2L-a))\Big] + B_5(2L-a)^3+$$

$$+ B_6(2L-a)^2 + B_7(2L-a) + B_8 \tag{5.42}$$

$$w_{s_{IV}}|_{2L-a} = 0$$

$$= \Big[B_1\cosh(\lambda_2(2L-a))\cos(\lambda_2(2L-a)) + B_2\cosh(\lambda_2(2L-a))\sin(\lambda_2(2L-a))$$

$$+ B_3\sinh(\lambda_2(2L-a))\cos(\lambda_2(2L-a)) + B_4\sinh(\lambda_2(2L-a))\sin(\lambda_2(2L-a))\Big]+$$

$$+ B_5(2L-a)^3 + B_6(2L-a)^2 + B_7(2L-a) + B_8 \tag{5.43}$$

At the crack tip, x = 0, we have continuity conditions on the top face sheet across the cracked section and the bonded section of the beam:

Displacement continuity:

$$e_{4d} = (-(EI)_s/(EI)_d)C_1 + C_8 \tag{5.44}$$

$$e_{4s} = C_1 + C_8 \tag{5.45}$$

Slope continuity:

$$e_{3d} = (-(EI)_s/(EI)_d)\lambda_2(C_2 + C_3) + C_7 \tag{5.46}$$

$$e_{3s} = \lambda_2(C_2 + C_3) + C_7 \tag{5.47}$$

Bending moment continuity:

$$e_{2d} = (-(EI)_s/(EI)_d)\lambda_2^2 C_4 + C_6 \tag{5.48}$$

$$e_{2s} = \lambda_2^2 C_4 + C_6 \tag{5.49}$$

Shear force continuity:

$$6e_{1d} = 2\lambda_2^3(-(EI)_s/(EI)_d)(C_2 - C_3) + 6C_5 \tag{5.50}$$

$$6e_{1s} = 2\lambda_2^3(C_2 - C_3) + 6C_5 \tag{5.51}$$

At the left end, x = -a, the ENF specimen is pinned. The bending moments and displacements are

$$
\begin{aligned}
&(EI)_d w''_{d_I}|_{-a} = 0 \\
&= (D_{1d}(k_1^2 - k_2^2) - 2D_{2d}k_1k_2)e^{k_1 a}\cos(-k_2 a) + \\
&+ (D_{2d}(k_1^2 - k_2^2) + 2D_{1d}k_1k_2)e^{k_1 a}\sin(-k_2 a) + \\
&+ (D_{3d}(k_1^2 - k_3^2) + 2D_{4d}k_1k_3)e^{-k_1 a}\cos(-k_3 a) + \\
&+ (D_{4d}(k_1^2 - k_3^2) - 2D_{3d}k_1k_3)e^{-k_1 a}\sin(-k_3 a) + \\
&+ 6D_{5d}(-a) + 2D_{6d} \qquad (5.52)
\end{aligned}
$$

$$
\begin{aligned}
&(EI)_s w''_{s_I}|_{-a} = 0 \\
&= (D_{1s}(k_1^2 - k_2^2) - 2D_{2s}k_1k_2)e^{k_1 a}\cos(-k_2 a) + \\
&+ (D_{2s}(k_1^2 - k_2^2) + 2D_{1s}k_1k_2)e^{k_1 a}\sin(-k_2 a) + \\
&+ (D_{3s}(k_1^2 - k_3^2) + 2D_{4s}k_1k_3)e^{-k_1 a}\cos(-k_3 a) + \\
&+ (D_{4s}(k_1^2 - k_3^2) - 2D_{3s}k_1k_3)e^{-k_1 a}\sin(-k_3 a) + \\
&+ 6D_{5s}(-a) + 2D_{6s} \qquad (5.53)
\end{aligned}
$$

$$
\begin{aligned}
&w_{d_I}|_{-a} = 0 \\
&= D_{1d}e^{k_1 a}\cos(-k_2 a) + D_{2d}e^{k_1 a}\sin(-k_2 a) + D_{3d}e^{-k_1 a}\cos(-k_3 a) + \\
&+ D_{4d}e^{-k_1 a}\sin(-k_3 a) + D_{5d}(-a)^3 + D_{6d}(-a)^2 + D_{7d}(-a) + D_{8d} \qquad (5.54)
\end{aligned}
$$

$$
\begin{aligned}
&w_{s_I}|_{-a} = 0 \\
&= D_{1s}e^{k_1 a}\cos(-k_2 a) + D_{2s}e^{k_1 a}\sin(-k_2 a) + D_{3s}e^{-k_1 a}\cos(-k_3 a) + \\
&+ D_{4s}e^{-k_1 a}\sin(-k_3 a) + D_{5s}(-a)^3 + D_{6s}(-a)^2 + D_{7s}(-a) + D_{8s} \qquad (5.55)
\end{aligned}
$$

We also have continuity condition at the middle of the beam, x= L-a, where there is a transverse shear load (P). Using this we can obtain the following equations:

Displacement continuity:

$$
\begin{aligned}
&w_{d_{III}}|_{L-a} = w_{d_{IV}}|_{L-a} \\
&= (-(EI)_s/(EI)_d)\Big[(C_1 - B_1)\cosh(\lambda_2(L-a))\cos(\lambda_2(L-a)) + \\
&+ (C_2 - B_2)\cosh(\lambda_2(L-a))\sin(\lambda_2(L-a)) + \\
&+ (C_3 - B_3)\sinh(\lambda_2(L-a))\cos(\lambda_2(L-a)) + \\
&+ (C_4 - B_4)\sinh(\lambda_2(L-a))\sin(\lambda_2(L-a))\Big] + (C_5 - B_5)(L-a)^3 + \\
&+ (C_6 - B_6)(L-a)^2 + (C_7 - B_7)(L-a) + (C_8 - B_8) = 0
\end{aligned} \tag{5.56}
$$

$$
\begin{aligned}
&w_{s_{III}}|_{L-a} = w_{s_{IV}}|_{L-a} \\
&= \Big[(C_1 - B_1)\cosh(\lambda_2(L-a))\cos(\lambda_2(L-a)) + \\
&+ (C_2 - B_2)\cosh(\lambda_2(L-a))\sin(\lambda_2(L-a)) + \\
&+ (C_3 - B_3)\sinh(\lambda_2(L-a))\cos(\lambda_2(L-a)) + \\
&+ (C_4 - B_4)\sinh(\lambda_2(L-a))\sin(\lambda_2(L-a))\Big] + (C_5 - B_5)(L-a)^3 + \\
&+ (C_6 - B_6)(L-a)^2 + (C_7 - B_7)(L-a) + (C_8 - B_8) = 0
\end{aligned} \tag{5.57}
$$

(5.58)

Slope continuity:

$$
\begin{aligned}
&w'_{d_{III}}|_{L-a} = w'_{d_{IV}}|_{L-a} \\
&= (-(EI)_s/(EI)_d)\lambda_2 \Big[(C_2 + C_3 - B_2 - B_3)\cosh(\lambda_2(L-a))\cos(\lambda_2(L-a)) + \\
&+ (-C_1 + C_4 + B_1 - B_4)\cosh(\lambda_2(L-a))\sin(\lambda_2(L-a)) + \\
&+ (C_1 + C_4 - B_1 - B_4)\sinh(\lambda_2(L-a))\cos(\lambda_2(L-a)) + \\
&+ (C_2 - C_3 - B_2 + B_3)\sinh(\lambda_2(L-a))\sin(\lambda_2(L-a)) \Big] + 3(C_5 - B_5)(L-a)^2 + \\
&+ 2(C_6 - B_6)(L-a) + (C_7 - B_7) = 0
\end{aligned} \tag{5.59}
$$

$$
\begin{aligned}
&w'_{s_{III}}|_{L-a} = w'_{s_{IV}}|_{L-a} \\
&= \lambda \Big[(C_2 + C_3 - B_2 - B_3)\cosh(\lambda_2(L-a))\cos(\lambda_2(L-a)) + \\
&+ (-C_1 + C_4 + B_1 - B_4)\cosh(\lambda_2(L-a))\sin(\lambda_2(L-a)) + \\
&+ (C_1 + C_4 - B_1 - B_4)\sinh(\lambda_2(L-a))\cos(\lambda_2(L-a)) + \\
&+ (C_2 - C_3 - B_2 + B_3)\sinh(\lambda_2(L-a))\sin(\lambda_2(L-a)) \Big] + 3(C_5 - B_5)(L-a)^2 + \\
&+ 2(C_6 - B_6)(L-a) + (C_7 - B_7) = 0
\end{aligned} \tag{5.60}
$$

Bending Moment continuity:

$$
\begin{aligned}
&(EI)_d w''_{d_{III}}|_{L-a} = (EI)_d w''_{d_{IV}}|_{L-a} \\
&= 2(-(EI)_s/(EI)_d)\lambda_2^2 \Big[(C_4 - B_4)\cosh(\lambda_2(L-a))\cos(\lambda_2(L-a)) - \\
&- (C_3 - B_3)\cosh(\lambda_2(L-a))\sin(\lambda_2(L-a)) + \\
&+ (C_2 - B_2)\sinh(\lambda_2(L-a))\cos(\lambda_2(L-a)) - \\
&- (C_1 - B_1)\sinh(\lambda_2(L-a))\sin(\lambda_2(L-a)) \Big] + 6(C_5 - B_5)(L-a) + 2(C_6 - B_6) = 0
\end{aligned} \tag{5.61}
$$

$$
\begin{aligned}
&(EI)_s w''_{s_{III}}|_{L-a} = (EI)_s w''_{s_{IV}}|_{L-a} \\
&= 2\lambda_2^2 \Big[(C_4 - B_4)\cosh(\lambda_2(L-a))\cos(\lambda_2(L-a)) - \\
&- (C_3 - B_3)\cosh(\lambda_2(L-a))\sin(\lambda_2(L-a)) + \\
&+ (C_2 - B_2)\sinh(\lambda_2(L-a))\cos(\lambda_2(L-a)) - \\
&- (C_1 - B_1)\sinh(\lambda_2(L-a))\sin(\lambda_2(L-a)) \Big] + 6(C_5 - B_5)(L-a) + 2(C_6 - B_6) = 0
\end{aligned}
\tag{5.62}
$$

Shear Force continuity:

$$
\begin{aligned}
&[(EI)_d w'''_{d_{III}} + (EI)_s w'''_{s_{III}} - (EI)_d w'''_{d_{IV}} - (EI)_s w'''_{s_{IV}}]|_{L-a} = P \\
&6((EI)_d + (EI)_s)(C_5 - B_5) = P
\end{aligned}
\tag{5.63}
$$

In addition, we also have a shear force condition at the right end. The shear load is acting at the middle of the beam, hence the reaction at the pinned supports will be half of it,

$$
\begin{aligned}
&[(EI)_d w'''_{d_{IV}} + (EI)_s w'''_{s_{IV}}]|_{2L-a} = -P/2 \\
&6((EI)_d + (EI)_s)B_5 = -P/2
\end{aligned}
\tag{5.64}
$$

In the cracked section, between Region I and II, $x = -a + X_1$, we have continuity conditions across these two regions

Displacement continuity:

$$
\begin{aligned}
& w_{d_I}|_{-a+X_1} = w_{d_{II}}|_{-a+X_1} \\
=& D_{1d}e^{-k_1(-a+X_1)}\cos(k_2(-a+X_1)) + D_{2d}e^{-k_1(-a+X_1)}\sin(k_2(-a+X_1)) \\
& + D_{3d}e^{k_1(-a+X_1)}\cos(k_3(-a+X_1)) + D_{4d}e^{k_1(-a+X_1)}\sin(k_3(-a+X_1))+ \\
& + D_{5d}(-a+X_1)^3 + D_{6d}(-a+X_1)^2 + D_{7d}(-a+X_1) \\
& + D_{8d} = W_d(-a+X_1)^3 + X_d(-a+X_1)^2 + Y_d(-a+X_1) + Z_d
\end{aligned} \tag{5.65}
$$

$$
\begin{aligned}
& w_{s_I}|_{-a+X_1} = w_{s_{II}}|_{-a+X_1} \\
=& D_{1s}e^{-k_1(-a+X_1)}\cos(k_2(-a+X_1)) + D_{2s}e^{-k_1(-a+X_1)}\sin(k_2(-a+X_1)) \\
& + D_{3s}e^{k_1(-a+X_1)}\cos(k_3(-a+X_1)) + D_{4s}e^{k_1(-a+X_1)}\sin(k_3(-a+X_1))+ \\
& + D_{5s}(-a+X_1)^3 + D_{6s}(-a+X_1)^2 + D_{7s}(-a+X_1) \\
& + D_{8s} = W_s(-a+X_1)^3 + X_s(-a+X_1)^2 + Y_s(-a+X_1) + Z_s
\end{aligned} \tag{5.66}
$$

Slope continuity:

$$
\begin{aligned}
& w'_{d_I}|_{-a+X_1} = w'_{d_{II}}|_{-a+X_1} \\
=& (-D_{1d}k_1 + D_{2d}k_2)e^{-k_1(-a+X_1)}\cos(k_2(-a+X_1))+ \\
& + (D_{2d}k_1 + D_{1d}k_2)e^{-k_1(-a+X_1)}\sin(k_2(-a+X_1))+ \\
& + (D_{3d}k_1 + D_{4d}k_3)e^{k_1(-a+X_1)}\cos(k_3(-a+X_1))+ \\
& + (D_{4d}k_1 - D_{3d}k_3)e^{k_1(-a+X_1)}\sin(k_3(-a+X_1))+ \\
& + 3D_{5d}(-a+X_1)^2 + 2D_{6d}(-a+X_1) + D_{7d} = 3W_d(-a+X_1)^2 + 2X_d(-a+X_1) + Y_d
\end{aligned} \tag{5.67}
$$

$$
\begin{aligned}
&w'_{s_I}|_{-a+X_1} = w'_{s_{II}}|_{-a+X_1} \\
=&(-D_{1s}k_1 + D_{2s}k_2)e^{-k_1(-a+X_1)}\cos(k_2(-a+X_1))+ \\
&+ (D_{2s}k_1 + D_{1s}k_2)e^{-k_1(-a+X_1)}\sin(k_2(-a+X_1))+ \\
&+ (D_{3s}k_1 + D_{4s}k_3)e^{k_1(-a+X_1)}\cos(k_3(-a+X_1))+ \\
&+ (D_{4s}k_1 - D_{3s}k_3)e^{k_1(-a+X_1)}\sin(k_3(-a+X_1))+ \\
&+ 3D_{5s}(-a+X_1)^2 + 2D_{6s}(-a+X_1) + D_{7s} = 3W_s(-a+X_1)^2 + 2X_s(-a+X_1) + Y_s
\end{aligned}
\tag{5.68}
$$

Bending Moment continuity:

$$
\begin{aligned}
&(EI)_d w''_{d_I}|_{-a+X_1} = (EI)_d w''_{d_{II}}|_{-a+X_1} \\
=&(D_{1d}(k_1^2 - k_2^2) - 2D_{2d}k_1k_2)e^{-k_1(-a+X_1)}\cos(k_2(-a+X_1))+ \\
&+ (D_{2d}(k_1^2 - k_2^2) + 2D_{1d}k_1k_2)e^{-k_1(-a+X_1)}\sin(k_2(-a+X_1))+ \\
&+ (D_{3d}(k_1^2 - k_3^2) + 2D_{4d}k_1k_3)e^{k_1(-a+X_1)}\cos(k_3(-a+X_1))+ \\
&+ (D_{4d}(k_1^2 - k_3^2) - 2D_{3d}k_1k_3)e^{k_1(-a+X_1)}\sin(k_3(-a+X_1))+ \\
&+ 6D_{5d}(-a+X_1) + 2D_{6d} = 6W_d(-a+X_1) + 2X_d
\end{aligned}
\tag{5.69}
$$

$$
\begin{aligned}
&(EI)_s w''_{s_I}|_{-a+X_1} = (EI)_s w''_{s_{II}}|_{-a+X_1} \\
=&(D_{1s}(k_1^2 - k_2^2) - 2D_{2s}k_1k_2)e^{-k_1(-a+X_1)}\cos(k_2(-a+X_1))+ \\
&+ (D_{2s}(k_1^2 - k_2^2) + 2D_{1s}k_1k_2)e^{-k_1(-a+X_1)}\sin(k_2(-a+X_1))+ \\
&+ (D_{3s}(k_1^2 - k_3^2) + 2D_{4s}k_1k_3)e^{k_1(-a+X_1)}\cos(k_3(-a+X_1))+ \\
&+ (D_{4s}(k_1^2 - k_3^2) - 2D_{3s}k_1k_3)e^{k_1(-a+X_1)}\sin(k_3(-a+X_1))+ \\
&+ 6D_{5s}(-a+X_1) + 2D_{6s} = 6W_s(-a+X_1) + 2X_s
\end{aligned}
\tag{5.70}
$$

Shear Force continuity:

$$
\begin{aligned}
&(EI)_d w'''_{d_I}|_{-a+X_1} = (EI)_d w'''_{d_{II}}|_{-a+X_1} \\
=&(3D_{2d}k_1^2k_2 - D_{2d}k_2^3 - D_{1d}k_1^3 + 3D_{1d}k_1k_2^2)e^{-k_1(-a+X_1)}\cos(k_2(-a+X_1))+ \\
&+(-3D_{1d}k_1^2k_2 + D_{1d}k_2^3 - D_{2d}k_1^3 + 3D_{2d}k_1k_2^2)e^{-k_1(-a+X_1)}\sin(k_2(-a+X_1))+ \\
&+(3D_{4d}k_1^2k_3 - D_{4d}k_3^3 + D_{3d}k_1^3 - 3D_{3d}k_1k_3^2)e^{k_1(-a+X_1)}\cos(k_3(-a+X_1))+ \\
&+(-3D_{3d}k_1^2k_3 + D_{3d}k_3^3 + D_{4d}k_1^3 - 3D_{4d}k_1k_3^2)e^{k_1(-a+X_1)}\sin(k_3(-a+X_1))+ \\
&+6D_{5d} = 6W_d
\end{aligned} \tag{5.71}
$$

$$
\begin{aligned}
&(EI)_s w'''_{s_I}|_{-a+X_1} = (EI)_s w'''_{s_{II}}|_{-a+X_1} \\
=&(3D_{2s}k_1^2k_2 - D_{2s}k_2^3 - D_{1s}k_1^3 + 3D_{1s}k_1k_2^2)e^{-k_1(-a+X_1)}\cos(k_2(-a+X_1))+ \\
&+(-3D_{1s}k_1^2k_2 + D_{1s}k_2^3 - D_{2s}k_1^3 + 3D_{2s}k_1k_2^2)e^{-k_1(-a+X_1)}\sin(k_2(-a+X_1))+ \\
&+(3D_{4s}k_1^2k_3 - D_{4s}k_3^3 + D_{3s}k_1^3 - 3D_{3s}k_1k_3^2)e^{k_1(-a+X_1)}\cos(k_3(-a+X_1))+ \\
&+(-3D_{3s}k_1^2k_3 + D_{3s}k_3^3 + D_{4s}k_1^3 - 3D_{4s}k_1k_3^2)e^{k_1(-a+X_1)}\sin(k_3(-a+X_1))+ \\
&+6D_{5s} = 6W_s
\end{aligned} \tag{5.72}
$$

From these boundary conditions and continuity conditions (Equation 5.40 - Equation 5.72), we have 32 equations to solve for the unknown coefficients in the general solutions. In addition, we can use the crack face contact length from the crack face contact without friction analysis. With all these conditions, we obtain a system of linear equations(Equation 5.40-Equation 5.72) and we can write a computer code to solve the equations.

5.3 Energy Release Rate

We have the general solutions for the transverse displacements of the beam section and they can be used to find the energy release rates. J-Integral provides a way to calculate the strain energy release rate. The J- Integral expression for the End-Notched Flexure specimen is obtained in the previous chapter using the zero-area path approach. For the calculation we

define a zero-area path [97][98] ((Γ = BAA'FEDD'C)) around the crack tip.

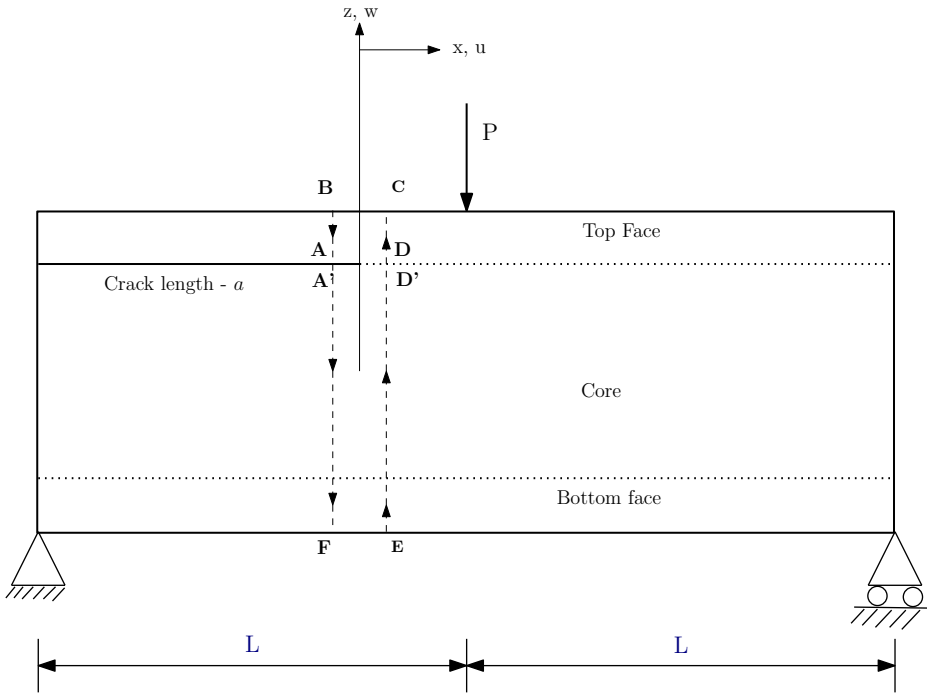

Figure 5.4: Zero-area path for J-Integral Calculation - ENF

Around the zero-area path, we have the J-Integral contributions from each section from Equation 4.85,Equation 4.88 & Equation 4.94

$$J_{BA} = \frac{1}{2b^2}\left(\frac{12M_d^2}{E_d f_t^3} - \frac{\kappa_d V_d^2}{G_d f_t} - 2V_d b(e_{3d})\right) \tag{5.73}$$

$$J_{A'F} = \frac{M_s^2}{2(EI)_s^2}\left[E_{f_b} f_b\left[(c-e_s)(c-e_s+f_b) + \frac{f_b^2}{3}\right] + 2E_c c\left(\frac{c^2}{3} + e_s^2\right)\right] - \\ - \frac{k_s V_s^2}{2G_s b^2(2c+f_b)} - \frac{V_s}{b}(e_{3s}) \tag{5.74}$$

$$J_{EC} = -\frac{M_b^2}{2(EI)_b^2}\left\{E_{f_b} f_b\left[(e_b-c)(e_b-c-f_b) + \frac{f_b^2}{3}\right] + 2E_c c(\frac{c^2}{3} + e_b^2) + \right. \\ \left. + E_{f_t} f_t\left[(e_b+c)(e_b+c+f_t) + \frac{f_t^2}{3}\right]\right\} + \left(\frac{\kappa_b V_b^2}{2G_b A_b^2}\right)(2c+f_t+f_b) - \\ - \frac{V_b}{A_b} w_{b,x}|_0 (f_t + 2c + f_b) \tag{5.75}$$

In addition, we also know that the energy release rate value reduces due to the friction be-

tween the crack faces. The J-Integral modified with a contour integral to account for the energy lost due to friction tractions by Palmer and Rice [99]. The definition of the modified J-Integral [100][101][102][103] is

$$J = \int_{\Omega} \left[\left(\sigma_{ij} \frac{\partial u_j}{\partial x_1} - W \delta_{1i} \right) \right] d\Omega - \int_{\Gamma_s} T_i \frac{\partial u_i}{\partial x_1} d\Gamma \tag{5.76}$$

where, T_i is the traction vector on the crack faces, $T_i = \sigma_{ji} n_j$, and $\Gamma_s = \Gamma_{top} \cup \Gamma_{bottom}$ is the portion of the crack faces where the contour integral is performed (where crack faces are in contact). The rest of terms are defined as customary.

When the crack face traction T_i are originated by frictional contact forces, the second integral in Equation 5.76 can be interpreted as the dissipated energy per unit area due to friction. The second integral is defined here as J_p

$$J_p = \int_{\Gamma_s} T_i \frac{\partial u_i}{\partial x_1} d\Gamma = \int_{-a+X_1}^{-a} \tau_{xz_d} \frac{\partial U_d}{\partial x_1} - \tau_{xz_s} \frac{\partial U_s}{\partial x_1} dx_1 \tag{5.77}$$

where, ΔU is relative tangential displacement between corresponding points at both crack faces. The frictional force on both the surfaces will be the same ($\mu k_t (w_{d_I} - w_{s_I})$)

$$J_p = \int_{-a+X_1}^{-a} \frac{\mu k_t (w_{d_I} - w_{s_I})}{X_1 G_d} \left(\frac{-f_t}{2} w_{d,xx_I} \right) - \frac{\mu k_t (w_{d_I} - w_{s_I})}{X_1 G_s} \left((e_s + c) w_{s,xx_I} \right) dx \tag{5.78}$$

where, w_{d_I} & w_{s_I} are the transverse displacements of the debonded part and the substrate in Region I. w_{d,xx_I} & w_{s,xx_I} are the second differentiation of the transverse displacements of the debonded part and the substrate in Region I.

Finally, by account for the energy lost due to friction tractions, we get the total strain

release rate as

$$J \;=\; J_{BA} \;+\; J_{A'F} \;+\; J_{EC} \;-\; J_p \tag{5.79}$$

5.4 Mode Partitioning

The mode partitioning partitioning phase angle can be obtained using the same expression we used in the previous chapter. The expression for the mode partitioning is not affected by the inclusion of friction

$$\psi_{TEF} = \tan^{-1} \frac{\left(\frac{f_t}{2} e_{3d} - \frac{f_t}{2} \frac{\kappa_d V_d}{(G_d b f_t)}\right) - \left(-(e_s + c) e_{3s} + (e_s + c) \frac{\kappa_s V_s}{[G_s b (2c + f_b)]}\right)}{(e_{4d} - e_{4s})} \tag{5.80}$$

5.5 Results and Discussion

The same ENF sandwich beam specimen (from previous chapter) made of isotropic aluminium with Young's modulus $E_f = 70$GPa and Poisson's ratio $\nu_f = 0.3$ is chosen. The core material is isotropic aluminium foam with Young's modulus $E_c = 7$GPa and Poisson's ratio $\nu_c = 0.32$. The face thicknesses were f_t=f_b=2 mm and the core had a thickness of 2c = 20mm. The total length of the beam was L=500 mm. A debond of length a = 200 mm was introduced between the top face and the core.

The End-Notched Flexure sandwich beam specimen is again modeled in ANSYS finite element software. In ANSYS, the debond was modeled using Pre-Meshed crack and a surface-to-surface contact of frictional contact was also introduced between the crack faces. Friction coefficient of $\mu = 0.1$ was to have a look at the results from the J- Integral expression obtained in this model and compare it with results from finite element analysis.

Table 5.1: ENF friction: Energy Release Rate Values - Al Foam Core

P (N_t)	J_{TEFF} (N_t/mm) Friction	ERR_{FEA} (N_t/mm) VCCT - friction
10	0.0248	0.02298
15	0.0558	0.0517
20	0.0993	0.0919
40	0.3970	0.3677
60	0.8934	0.8274
100	2.4816	2.2983
150	5.5836	5.1711
250	15.5100	14.3640
400	39.7055	36.7720
750	139.5897	129.2800
1000	248.1595	229.8300

In Table 5.1, we have the energy release values (J_{TEFF}) compared with the finite element analysis (ERR_{FEA}). It is interesting to notice that the energy release rate values obtained using finite element analysis have not changed much by including the effect of friction. The ERR_{FEA} values have reduced much less than 1% when compared to the frictionless contact case, which indicates that the crack face contact friction does not significantly affect the energy release rate values. The extended tensionless spring foundation solutions (J_{TEFF}) also predicts that the friction does not affect the energy release rate values much. The extended tensionless spring foundation approach can be very useful for cases where

crack face contact effects can be very significant to be quick and useful solutions. The tensionless spring foundation approach can further be extended to include the transverse shear effects by using Timoshenko beam theory or High-Order shear deformation theories to obtain the governing equations.

5.6 Conclusion

Semi-Closed form expressions for the energy release rate and mode partitioning of End-Notched Flexure sandwich specimen including friction in the crack face contact region are obtained. Friction effects are usually neglected in most analytical models. Here, the governing equations in the crack face contact region are obtain by including the effect of friction between the crack faces. In this approach, the crack face contact length obtained from the previous chapter with friction is used. The model presented here is again applicable for both isotropic and orthotropic face and core materials and can also be done for the general asymmetric sandwich beam construction. The J-Integral approach is modified with a contour integral to account for the energy lost due to friction tractions. Finite element model with frictional contact between the crack faces are chosen for comparison. The transverse and axial displacements at the beginning of the elastic foundation are used to define a mode partitioning measure values.

CHAPTER 6
CONCLUSIONS AND FUTURE WORK

6.1 Conclusions

Closed-form solutions for displacements, section rotations and fracture parameters are derived and presented for the sandwich beam specimen. The approach presented here can be used for studying the face/core debonds in sandwich structures. To analyze the face/core debonds and obtain closed-form solutions, elastic foundation approach is used. Sandwich beam construction have large transverse due to the presence of weak core and the modeled presented here is based on Timoshenko beam theory (first-order shear theory) to capture these shear effects.

The elastic foundation model proposed here is comprehensive, it includes the deformation of the substrate part in the sandwich beam, which was usually neglected in previous models in literature. In literature, previous elastic foundation analyses, the substrate was assumed to be rigid and the effects of the end fixity at the bonded segment were not included. In this model, the elastic foundation in the ”bonded” section is used to model the interaction between the top face and the substrate using both normal springs and rotational shear springs to account for transverse displacements and section rotations of the beam.

The normal and shear spring modulus are very important in the case of elastic foundation approach. The spring modulus values are obtained using expressions derived from elasticity solution and the extended-high order sandwich panel theory. With the elastic foundation force and shear distribution, Timoshenko beam theory is used to obtain the governing equations in terms of transverse displacement and section rotations. The obtained governing equations are linear second order coupled differential equations. These equations are then solved to obtain the general solutions for transverse displacements and

section rotations of the top face and the substrate part of the beam. A Double Cantilever Beam specimen with shear and bending loads is chosen. It is common test specimen for studying mode I fracture parameters. The constant coefficients in the general solutions are obtained using the appropriate boundary conditions and continuity conditions.

The J-Integral is used to derive a closed form expression for the energy release rate. In addition, it is also interesting to notice that the energy release rate is very close to the differential energy stored in the springs at the beginning of the elastic foundation, i.e., the energy released by the ”broken” differential spring element as the debond propagates. The energy release rate values obtained using J-Integral show excellent agreement with the values obtained from finite element analysis where the debond is considered as interface crack. The transverse and axial displacements at the beginning of the elastic foundation are used to define a mode partitioning measure in the context of this elastic foundation approach. A comparison with finite element results shows that this mode partitioning measure values are close to traditional mode mixity values of the corresponding interfacial cracks. The energy release rate values and the mode partitioning values showed improvement and better captured transverse shear when compared to a previous study based on Euler-Bernoulli beam theory.

Single Cantilever Beam specimen has gained attention as one of the best candidates for evaluating debond fracture toughness in mode I loading. The existence of the applied shear loading complicates the problem, as traditional approaches based on fracture mechanics cannot lead to closed form relations. The elastic foundation approach with the Timoshenko beam theory is extended in the model presented for the case of SCB sandwich specimen. In the SCB specimen the substrate part is restricted in the transverse displacement. The model presented also accounts for the transverse shear in the substrate by considering the reaction on the fixed bottom edge as linearly distributed force distribution. The governing equations for the debonded part are obtained in terms of transverse displacements and section rotations, they are linear second order coupled differential equations. These gov-

erning equations are then solved to obtain the general solutions. Appropriate boundary and continuity conditions for the Single Cantilever Beam specimen is used to get the constant coeffiecients in the general solutions for traverse displacements and section rotations. The solutions obtained for both the cases - Double Cantilever Beam specimen and Double Cantilever Beam specimen are valid for both isotropic and orthotropic face and core materials. These solutions are applicable for asymmetric sandwich beam with different face materials or thicknesses.

Again, the J-Integral approach is used to obtained closed form expression for energy release rate. The energy release rate values obtained using these expressions show excellent agreement with the results from finite element analysis for various loading conditions and material combination. It is interesting to note that the solutions obtained show good agreement with the finite element solutions even for soft core materials. In addition, the energy released by the ”broken” differntial spring element is in very good agreement with the energy release rate values. Mode partitioning measure values obtained using relative crack flank opening and shear displacements closely matches the traditional mode mixity values from finite element analysis. The proposed model for both the DCB and SCB specimens provide excellent results for beam models even with small crack lengths. The elastic foundation model presented can be used to obtain consistent results for face/core debonds in sandwich beams.

In mode II fracture, crack face contact plays a significant role and leads to poor reproducibility of fracture toughness values. The elastic foundation approach is extended with tensionless spring foundation to capture the crack face contact effects. The tensionless spring foundation for crack face contact modeling is a novel approach and it is used to capture the compressive forces across the top debonded face and the substrate of the sandwich beam specimen.

An End-Notched Flexure sandwich specimen with shear load in the middle of the beam is used in this model. In the bonded section of the beam, an elastic foundation with normal

springs is used to model the interaction between the top face and the substrate. Euler Bernoulli beam theory is used to derive governing equations for the all the regions of the beam. The elastic modulus of the tensionless spring is taken to be the same as the modulus of the normal springs in the elastic foundation, difference between that the tensionless springs only react under compressive loads. The governing equations in the crack face contact region and the bonded region are linear fourth-order coupled differential equations. General solutions for transverse displacements are obtained by solving these differential equations. In addition to contact coefficients, the crack face contact length is also unknown.

Boundary conditions and continuity conditions are used to get a system of non-linear equations. This system of non-linear equations are numerically solved to obtain the constant coefficients and the unknown crack face contact length. The energy release rate values are obtained using J-Integral approach and a zero-area path around the crack is used obtain a closed form expression for the energy release rate. The ENF sandwich beam specimen is modeled in ANSYS with frictionless contact between the crack faces. The J-integral values obtained using the model presented here show very good agreement with the energy release rate values from the finite element analysis for various shear loads. The mode partitioning measure values are in agreement that this ENF beam specimen is in pure mode II fracture.

Further, the tensionless spring foundation approach is further extended to include the frictional tractions between the crack faces. This makes the elastic foundation approach comprehensive by capturing all the crack face contact effects. Euler-Bernoulli beam theory is used to derive the governing equations in all the regions of the beam. By including the crack face friction, only the governing equations in Region I is modified. The governing equations in Region I are linear fourth-order coupled differential equations and they are solved to obtain general solutions of the transverse displacements. Using the boundary conditions, continuity conditions and crack face contact length from frictionless case, the constant coefficients in the general solutions are obtained.

The J-Integral is modified to account for the energy lost due to frition tractions. The

End-Notched Flexure sandwich beam specimen with frictional crack face contact is modeled in finite element software. It can be noticed that the frictional tractions have no significant impact on the energy release rate values in this case and the comprehensive elastic foundation approach can be used for different test specimens to obtain closed/semi-closed form solutions for face/core debonds in sandwich composite beams.

6.2 Future Work

It is seen that the elastic foundation analysis proves to be a very promising in providing closed/near-closed solutions for obtaining fracture parameters in the case of sandwich composite beams. The elastic foundation model presented here is applicable for linear elastic materials, but it can further be extended for non-linear materials or hyperelastic material models. We can also extend the elastic foundation model using micropolar beam formulation to account for the gradient in stress values in the core. In the case of mode II fracture, the tensionless spring foundation method can be further extended to capture the effects of transverse shear by using Timoshenko beam theory or high-order shear deformation theories, which can be significant in the case of sandwich composite beam. The tensionless foundation model can also be applied for Mode III (out-of-plane shearing) case. The elastic foundation approach can also be extended to capture the thermal or environmental effects. There are many more applications to which the elastic foundation model presented here can be extended to.

REFERENCES

[1] H. G. Allen, *Analysis and Design of Structural Sandwich Panels*. Pergamon Press, 1969, ISBN: 9781483159041.

[2] L. A. Carlsson and G. A. Kardomateas, *Structural and Failure Mechanics of Sandwich Composites*. Springer, 2011, ISBN: 978-1-4020-3224-0.

[3] D. Zenkert, *An Introduction to Sandwich Structures*. Oxford, 1995.

[4] J. R. Vinson, *The Behavior of Sandwich Structures of Isotropic and Composite Materials*. CRC Press, 1999.

[5] S. Prasad and L. A. Carlsson, "Debonding and crack kinking in foam core sandwich beams - ii. experimental investigation," *Engineering Fracture Mechanics*, vol. 47, pp. 825–841, 1994.

[6] A. Biel and U. Stigh, "An analysis of the evaluation of the fracture energy using the dcb - specimen," *Archives of Mechanics*, vol. 59, pp. 311–327, 2007.

[7] R. Moslemian, C. Berggreen, L. A. Carlsson, and F. Aviles, "Failure investigation of debonded sandwich columns: An experimental and numerical study," *Journal of Mechanics of Materials and Structures*, vol. 4, no. 7-8, pp. 1469–1487, 2009.

[8] J. R. Reeder and J. H. Crews Jr., "Mixed mode bending method for delamination testing," *AIAA Journal*, vol. 28, pp. 1270–1276, 1990.

[9] A. C. Balaban and K. F. Tee, "Strain energy release rate of sandwich composite beams for different densities and geometry parameters," *Theoretical and Applied Fracture Mechanics*, vol. 101, pp. 191–199, 2019.

[10] D. Zenkert, "Strength of sandwich beams with interface debondings," *Composite Structures*, vol. 17, pp. 331–350, 1991.

[11] W. L. Yin and J. T. S. Wang, "The energy release rate in the growth of a one-dimensional delamination," *Journal of Applied Mechanics*, vol. 51, no. 4, pp. 939–941, 1984.

[12] Z. Suo and J. W. Hutchinson, "Interface crack between two elastic layers," *International Journal of Fracture*, vol. 43, no. 1, pp. 1–18, 1990.

[13] G. A. Kardomateas, C. Berggreen, and L. A. Carlsson, "Energy release rate and mode mixity of face core debonds in sandwich beams," *AIAA Journal*, vol. 51, no. 4, pp. 301–316, 2013.

[14] R. C. Ostergaard and R. F. Sorensen, "Interface crack in sandwich specimen," *International Journal of Fracture*, vol. 143, pp. 301–316, 2007.

[15] V. Saseendran, C. Berggreen, and L. A. Carlsson, "Fracture mechanics analysis of reinforced dcb sandwich debond specimen loaded by moments," *AIAA Journal*, 2017.

[16] L. A. Carlsson, R. C. Matteson, F. Aviles, and D. C. Loup, "Crack path in foam cored dcb sandwich fracture specimens," *Composites Science and Technology*, vol. 65, pp. 2612–2621, 2005.

[17] J. G. Ratcliffe and J. R. Reeder, "Sizing a single cantilever beam specimen for characterizing facesheet-core debonding in sandwich structure," *Journal of Composite Materials*, vol. 45, pp. 2669–2684, 2011.

[18] B. F. Sorensen, K. Jorgensen, T. K. Jacobsen, and R. C. Ostergaard, "Dcb-specimen loaded with uneven bending moments," *International Journal of Fracture*, vol. 141, pp. 163–176, 2006.

[19] V. Saseendran, L. A. Carlsson, C. Berggreen, and W. Seneviratne, "Crack length correction and root rotation angle in a sandwich single cantilever beam (scb) fracture specimen," *International Journal of Lightweight Materials and Manufacture*, vol. 3, pp. 426–434, 2020.

[20] H. C. Cao and A. G. Evans, "An experimental study of the fracture resistance of bimaterial interfaces," *Mechanics of Materials*, pp. 295–304, 1989.

[21] J. S. Wang and Z. Suo, "Experimental determination of interfacial toughness curves using brazil-nut-sandwiches," *Acta Metall Mater*, vol. 38, pp. 1279–1290, 1990.

[22] A. Szekrényes, "J-integral for delaminated beam and plate models," *Periodica Polytechnica, Mechanical Engineering*, vol. 56, pp. 63–71, 2012.

[23] G. M. Andrews and R. Massabo, "The effects of shear and near tip deformations on energy release rate and mode mixity of edge-cracked orthotropic layers," *Engineering Fracture Mechanics*, vol. 74, pp. 2700–2720, 2007.

[24] M. D. Thouless, "The effects of transverse shear on the delamination of edge-notch flexure and 3-point bend geometries," *Composites: Part B*, vol. 40, pp. 305–312, 2009.

[25] A. B. de Morais and A. B. Pereira, "Mixed mode i+ii interlaminar fracture of glass/epoxy multidirectional laminates - part 1: Analysis," *Composites Science and Technology*, vol. 66, pp. 1889–1895, 2006.

[26] J. Wang and P. Qiao, "Fracture analysis of shear deformable bi-material interface," *Journal of Engineering Mechanics*, vol. 132, 2006.

[27] ——, "Interface crack between two shear deformable elastic layer," *Journal of the Mechanics and Physics of Solids*, vol. 52, pp. 891–905, 2004.

[28] P. Qiao and J. Wang, "Mechanics and fracture of crack tip deformable bi-material interface," *International Journal of Solids and Structures*, vol. 41, pp. 7423–7444, 2004.

[29] S. Li, J. Wang, and M. D. Thouless, "The effects of shear on delamination in layered materials," *Journal of the Mechanics of Physics and Solids*, vol. 52, no. 1, pp. 193–214, 2004.

[30] L. Barbieri, R. Massabo, and C. Berggreen, "The effects of shear and near tip deformations on interface fracture of symmetric sandwich beams," *Engineering Fracture Mechanics*, vol. 201, pp. 298–321, 2018.

[31] C. T. Sun and R. K. Pandey, "Improved method for calculating strain energy release rate based on beam theory," *AIAA Journal*, vol. 32, pp. 184–189, 1994.

[32] Y. Frostig, M. Baruch, and O. Vilnay, "High-order theory for sandwich-beam behavior with transversely flexible core," *Journal of Engineering Mechanics*, vol. 118, pp. 1026–1043, 1992.

[33] C. N. Phan, Y. Frostig, and G. A. Kardomateas, "Analysis of sandwich beam with a compliant core and with in-plane rigidity-extended high-order sandwich panel theory versus elasticity," *Journal of Applied Mechanics*, vol. 79, pp. 041001-1 - 041001–11, 2012.

[34] I. Odessa, Y. Frostig, and O. Rabinovitch, "Modeling of interfacial debonding propagation in sandwich panels," *International Journal of Solids and Structures*, vol. 148-149, pp. 67–78, 2018.

[35] ——, "Dynamic interfacial debonding in sandwich panels," *Composites Part B*, vol. 185, 2020.

[36] C. Berggreen, K. Simonsen, and K. K. Borum, "Experimental and numerical study of interface crack propagation in foam-cored sandwich beams," *Journal of Composite Materials*, 2007.

[37] A. Barut, E. Madenci, and A. Tessler, "A refined zigzag theory for laminated composite and sandwich plates incorporating thickness stretch deformation," *53rd AIAA/ASME/ASCE/AHS/ASC Structures, Structural Dynamics and Materials Conference*, 2012.

[38] L. Iurlaro, M. Gherlone, and M. Di Sciuva, "A mixed cubic zigzag model for multilayered composite and sandwich plates including transverse normal deformability," *Proceedings of the 11th World Congress on Computational Mechanics*, 2014.

[39] M. F. Kanninen, "An augmented double cantilever beam model for studying crack propagation and arrest," *International Journal of Fracture*, vol. 9, pp. 83–92, 1973.

[40] J. G. Williams, "End corrections for orthotropic dcb specimens," *Composites Science and Technology*, vol. 35, pp. 367–376, 1989.

[41] K. S. Alfredsson, "On the instantaneous energy release rate of the end-notch flexure adhesive joint specimen," *International Journal of Solids and Structures*, vol. 41, pp. 4787–4807, 2004.

[42] X. Li and L. A. Carlsson, "Elastic foundation analysis of tilted sandwich debond (tsd) specimen," *Journal of Sandwich Structures and Materials*, vol. 2, pp. 2–32, 2000.

[43] G. A. Kardomateas, N. Pichler, and Z. Yuan, "Elastic foundation solution for the energy release rate and mode partitioning of face/core debonds in sandwich composites," *Journal of Applied Mechanics*, vol. 86, 2019.

[44] V. Saseendran, L. A. Carlsson, and C. Berggreen, "Shear and foundation effects on crack root rotation and mode-mixity in moment-and force-loaded single cantilever beam sandwich specimen," *Journal of Composite Materials*, vol. 52, pp. 2537–2547, 2018.

[45] G. A. Kardomateas, Z. Yuan, and L. A. Carlsson, "Elastic foundation constant for sandwich composites," *AIAA Journal*, vol. 56, no. 10, pp. 4169–4179, 2018.

[46] G. A. Kardomateas, N. Pichler, and Z. Yuan, "Closed form solution for the energy release rate and mode partitioning of the single cantilever beam sandwich debond from an elastic foundation analysis," *Journal of Sandwich Structures and Materials*, 2020.

[47] N. J. Pagano and R. B. Pipes, "The influence of stacking sequence on laminate strength," *Journal of Composite Materials*, vol. 5, p. 50, 1971.

[48] ——, "Some observations on the interlaminar strength of composite laminates," *International Journal of Mechanical Sciences*, vol. 15, pp. 679–686, 1973.

[49] D. J. Wilkins, J. R. Eisenmann, R. A. Camin, W. S. Margolis, and R. A. Benson, "Characterizing delamination growth in graphite-epoxy," *Damage in Composite Materials*, vol. 15, p. 168, 1982.

[50] D. F. Devitt, R. A. Schapery, and W. L. Bradley, "A method for determining the mode i delamination fracture toughness of elastic and viscoelastic materials," *Journal of Composite Materials*, vol. 14, p. 270, 1980.

[51] R. B. Pipes, B. E. Kaminski, and N. J. Pagano, "Influence of the free-edge upon the strength of angle-ply laminates," *Analysis of the Test Methods for High Modulus-Fibers and Composites*, vol. 14, p. 218, 1973.

[52] K. Kageyama, M. Kikuchi, and N. Yanagisawa, "Stabilized end notched flexure test: Characterization of mode ii interlaminar crack growth," *Composite Materials Fatigue and Fracture*, vol. 3, pp. 210–225, 1991.

[53] L. A. Carlsson, J. W. Gillespie, and R. B. Pipes, "On the analysis and design of the end notched flexure (enf) specimen for mode ii testing," *Journal of Composite Materials*, pp. 594–604, 1986.

[54] C. R. Corleto and A. H. Hogen, "Energy release rates for the enf specimen using a beam on an elastic foundation," *Journal of Composite Materials*, 1995.

[55] T. J. Lu, Z. C. Xia, and J. W. Hutchinson, "Delamination of beams under transverse shear and bending," *Material Science and Engineering*, pp. 103–112, 1994.

[56] L. A. Carlsson, L. S. Sendlein, and S. L. Merry, "Characterization of face sheet/core shear fracture of composite sandwich beams," *Journal of Composite Materials*, 2017.

[57] M. Rinker, M. John, P. C. Zahlen, and R. Schauble, "Face sheet debonding in cfrp/pmi sandwich structures under quasi-static and fatigue loading considering residual thermal stress," *Engineering Fracture Mechanics*, vol. 78, pp. 2835–2847, 2011.

[58] C. D. Chen and W. L. Dai, "The analysis of mode ii strain energy release rate in a cracked sandwich beam based on the refined zigzag theory," *Theoretical and Applied Fracture Mechanics*, vol. 107, no. 102504, 1998.

[59] F. Odzil and L. A. Carlsson, "Characterization of mixed mode delamination growth in glass/epoxy composite cylinders," *Journal of Composite Materials*, vol. 34, pp. 420–440, 2000.

[60] F. Dharmawan, G. Simpson, I. Herszberg, and S. John, *Composite Structures*, vol. 75, pp. 328–338, 2006.

[61] A. Quispitupa, C. Berggreen, and L. A. Carlsson, "On the analysis of a mixed mode bending sandwich specimen for debond fracture characterization," *Engineering Fracture Mechanics*, vol. 76, pp. 594–613, 2009.

[62] M. Manca, A. Quispitupa, C. Berggreen, and L. A. Carlsson, "Face/core debond fatigue crack growth characterization using the sandwich mixed mode bending specimen," *Composites: Part A*, vol. 43, pp. 2120–2127, 2012.

[63] Y. Weitsman, "On foundations that react in compression only," *Journal of Applied Mechanics*, vol. 37, pp. 1019–1030, 1970.

[64] Y. Zhang, "Tensionless contact of a finite beam resting on reissner foundation," *International Journal of Mechanical Sciences*, vol. 50, pp. 1035–1041, 2008.

[65] X. Ma, J. W. Butterworth, and G. C. Clifton, "Response of an infinite beam resting on a tensionless elastic foundation subjected to arbitrarily complex transverse loads," *Mechanics Research Communications*, vol. 36, pp. 818–825, 2009.

[66] ——, "Static analysis of an infinite beam resting on a tensionless pasternak foundation," *European Journal of Mechanics A/Solids*, vol. 28, pp. 697–703, 2009.

[67] M. Comninou and J. Dundurs, "Effect of friction on the interface crack loaded in shear," *Journal of Elasticity*, vol. 10, pp. 203–212, 1980.

[68] V. Mantic, L. Tavara, A. Blazquez, E. Graciani, and F. Paris, "A linear elastic-brittle interface model: Application for the onset and propagation of a fibre-matrix interface crack under biaxial transverse loads," *International Journal of Fracture*, vol. 195, pp. 15–38, 2015.

[69] P. Davies *et al.*, "Comparison of test configurations for determination of mode ii interlaminar fracture toughness results from international collaborative test programme," *Plastic Rubber Composite*, vol. 28, pp. 432–437, 1999.

[70] A. J. Russell and K. N. Street, "Factors affecting the interlaminar fracture energy of graphite/epoxy laminates," *ICCM -IV*, 1982.

[71] B. D. Davidson and X. Sun, "Effects of friction, geometry and fixture compliance on the perceived toughness from three and four point bended notched flexure tests," *Journal of Reinforced Plastic Composites*, vol. 4, pp. 1611–1628, 2005.

[72] B. D. Davidson, X. Sun, and A. Vinciquerra, "Influences of friction, geometric nonlinearities, and fixture compliance on experimentally observed toughnesses from three and four-point bend end-notched flexure tests," *Journal of Composite Materials*, vol. 41, pp. 1177–1196, 2007.

[73] L. C. Bian, Z. Fawaz, and K. Behdinan, "A mixed mode crack growth model taking account of fracture surface contact and friction," *International Journal of Fracture*, vol. 139, pp. 39–58, 2006.

[74] T. S. Gross and D. A. Mendelsohn, "On the effect of crack face contact and friction due to fracture surface roughness in edge cracks subjected to external shear," *Engineering Fracture Mechanics*, vol. 31, pp. 405–420, 1988.

[75] S. Suresh and R. O. Ritchie, "A geometric model for fatigue crack closure induced by fracture surface roughness," *Metallurgical Transactions A*, vol. 13, pp. 1627–1631, 1982.

[76] G. I. Barenblatt, "The formation of equilibrium crack during brittle fracture. general idea and hypothesis. axisymmetrical cracks.," *Journal of Applied Mathematics and Mechanics*, vol. 23, pp. 622–636, 1959.

[77] D. S. Dugdale, "Yielding of steel sheets containing slits," *Journal of the Mechanics and Physics of Solids*, vol. 8, pp. 100–104, 1960.

[78] A. Needleman, "An analysis of tensile decohesion along an interface," *Journal of Applied Mechanics*, vol. 38, pp. 289–324, 1990.

[79] V. Tvergaard and J. W. Hutchinson, "The relation between crack growth resistance and fracture process parameters in elastic-plastic solids," *Journal of the Mechanics and Physics of Solids*, pp. 1377–1397, 1992.

[80] J. H. Rose, J. R. Smith, and J. Ferrante, "Universal features of bonding in metals," *Physical Review B*, vol. 28, pp. 1835–1845, 1983.

[81] A. Hillerborg, M. Modeer, and P. E. Petersson, "Analysis of crack formation and crack growth in concrete by means of fracture mechanics and finite elements," *Cement and Concrete Research*, vol. 6, pp. 773–782, 1976.

[82] X. P. Xu and A. Needleman, "Void nucleation by inclusion debonding in a crystal matrix," *Modeling and Simulation in Materials Science and Engineering*, vol. 1, pp. 111–132, 1993.

[83] A. J. Kinloch, C. C. Lau, and J. G. Williams, "The peeling of flexible laminates," *International Journal of Fracture*, vol. 66, pp. 45–70, 1994.

[84] G. T. Camacho and M. Ortiz, "Computational modeling of impact damage in brittle materials," *International Journal of Solids and Structures*, vol. 33, pp. 2899–2938, 1996.

[85] J. G. Williams and H. Hadavinia, "Analytical solutions for cohesive zone models," *Journal of the Mechanics and Physics of Solid*, vol. 40, pp. 809–825, 2002.

[86] P. H. Geubelle and J. S. Baylor, "The impact-induced delamination of laminated composites: A 2d simulation," *Composites Part B: Engineering*, vol. 29, pp. 589–602, 1998.

[87] J. W. Hutchinson and A. G. Evans, "Mechanics of materials: Top-down approaches to fracture," *Acta Materialia*, vol. 48, pp. 125–135, 2000.

[88] Z. Ouyang and G. Li, "Nonlinear interface shear fracture of end notched flexure specimens," *International Journal of Solids and Structures*, vol. 46, pp. 2659–2668, 2009.

[89] O. Rabinovitch, "An extended high order cohesive interface approach to the debonding analysis of frp strengthened beams," *International Journal of Mechanical Sciences*, vol. 81, pp. 1–16, 2014.

[90] A. Biel and U. Stigh, "Comparison of j-integral methods to experimentally determine cohesive laws in shear for adhesives," *International Journal of Adhesion and Adhesives*, vol. 94, pp. 64–75, 2019.

[91] C. A. Lundsgaard, C. Berggreen, and L. A. Carlsson, "Tailoring sandwich face/core interfaces for improved damage tolerance - part i: Finite element analysis," *Applied Composite Materials*, pp. 609–619, 2010.

[92] S. Mall and N. K. Kochhar, "Finite-element analysis of end-notch flexure specimens," *International Journal of Solids and Structures*, vol. 46, pp. 2659–2668, 2009.

[93] J. W. Gillespie, L. A. Carlsson, and R. B. Pipes, "Finite element analysis of the end notched flexure specimen for measuring mode ii fracture toughness," *Composite Science and Technology*, vol. 27, pp. 177–197, 1986.

[94] L. A. Carlsson and S. Prasad, "Interfacial fracture of sandwich beams," *Engineering Fracture Mechanics*, vol. 44, pp. 581–590, 1993.

[95] G. A. Kardomateas and G. J. Simitses, "Buckling of long sandwich cylindrical shells under external pressure," *Journal of Applied Mechanics*, vol. 72, pp. 493–499, 2004.

[96] H. Huang and G. A. Kardomateas, "Buckling and initial postbuckling behavior of sandwich beams including transverse shear," *AIAA Journal*, vol. 40, pp. 2331–2335, 2002.

[97] B. Sankar and V. Sonik, "Pointwise energy release rate in delaminated plates," *AIAA journal*, vol. 33, no. 7, pp. 1312–1318, 1995.

[98] A. Szekrényes, "J-integral for delaminated beam and plate models," *Periodica Polytechnica Mechanical Engineering*, vol. 56, no. 1, pp. 63–71, 2012.

[99] A. C. Palmer and J. R. Rice, "The growth of slip surfaces in the progressive failure of over-consolidated clay," *Proceedings of the Royal Society of London. A. Mathematical and Physical Sciences*, vol. 332, no. 1591, pp. 527–548, 1973.

[100] E. Giner, M. Sabsabi, and F. Fuenmayor, "Calculation of kii in crack face contacts using x-fem. application to fretting fatigue," *Engineering Fracture Mechanics*, vol. 78, no. 2, pp. 428–445, 2011.

[101] A. Dorogoy and L. Banks-Sills, "Shear loaded interface crack under the influence of friction: A finite difference solution," *International Journal for Numerical Methods in Engineering*, vol. 59, no. 13, pp. 1749–1780, 2004.

[102] D. Xiaomin, "An asymptotic analysis of stationary and moving cracks with frictional contact along bimaterial interfaces and in homogeneous solids," *International Journal of Solids and Structures*, vol. 31, no. 17, pp. 2407–2429, 1994.

[103] H. D. Bui and A. Oueslati, "The sliding interface crack with friction between elastic and rigid bodies," *Journal of the Mechanics and Physics of Solids*, vol. 53, no. 6, pp. 1397–1421, 2005.